Parametric Emission Prediction Model in Gas Turbines with Exhaust Gas Recirculation

Vaibhav Prakash

Technische Universiteit Delft

TU Delft Delft University of Technology

Challenge the future

Parametric Emission Prediction Model in Gas Turbines with Exhaust Gas Recirculation

by

Vaibhav Prakash

to obtain the degree of

Master of Science
in Mechanical Engineering

at the Delft University of Technology,
to be defended publicly on Friday August 25, 2017 at 9:30 AM.

Supervisor:	Prof. dr. ir. S. A. Klein,	TU Delft
Thesis committee:	Prof. dr. D. J. E. M. Roekaerts,	TU Delft
	Prof. dr. ir. B. J. Boersma,	TU Delft
	Dr. ir. A. Gangoli Rao,	TU Delft
	Dr. ir. J. S. Steimes,	TU Delft

TU Delft Delft University of Technology

Acknowledgements

I would like to first convey my heartfelt thanks to my supervisors Professor Dr.ir. Sikke Klein, Professor dr. Dirk Roekaerts and Dr. ir. Johan Steimes, for their excellent support and encouragement during the course of my thesis. I also thank Professor dr.ir. Bendiks Jan Boersma and Dr. ir. Arvind Gangoli Rao for accepting to be part of the thesis committee. My wholehearted gratitude goes to Andre Perpignan for his valuable guidance and advice. In addition, I wish to thank my family and friends for being there with me as a pillar of support throughout my masters. Overall, it has been a splendid research experience over the course of 9 months working on this thesis. I have certainly learned a lot of personal and professional lessons during my cherishable 2 years at TU Delft.

Summary

One of the challenges in gas turbines is in the reduction of NO_x and CO emissions due to simultaneous dependence on stringent emission norms and subsequent demand for change in operating conditions. To cater the volatile demand of power supply, most of the gas turbines have to be flexible to changing loads. Closer the load is to full load, more is the impact on gas turbine emissions. In order to mitigate the effects of emission rise, a shift towards emission reduction techniques are being adopted. Of the available options, Exhaust Gas Recirculation (EGR) is a promising option for good part load performance and emission reduction. EGR is a technique to reduce the flame temperature by recirculating the products of combustion into air intake and replacing part of the oxygen content with inert constituents such as CO_2. This leads to reduced NO_x emissions and increased CO_2 content at the exhaust for effective carbon capture. Despite these advantages, the introduction of an oxygen-depleted oxidizer leads to changes in combustion behaviour giving rise to flame stability issues.

In this thesis, a chemical kinetic model to predict emissions in a lean premixed combustor coupled with EGR, is built using chemical reactor networks (CRN). A CRN model was developed by splitting the whole combustor volume approximately in half before and after the recirculation zone. The first half was further partitioned into the flame reactor and the recirculation reactor. The flame reactor volume is set based on the chemical time scale approach. This approach quantifies the flame zone volume based on the difference in reaction kinetics for different oxidizers. The model was also validated with results from the literature for various flame cases with similar flow fields and was in good agreement with the data. Various chemical mechanisms and their emission prediction ability are investigated. GRI-Mech 3.0 is found to accurately predict the emissions for a given set of operating conditions.

The effect of change in oxidizer composition with different amounts of CO_2 is investigated. As a consequence of O_2 starvation in the oxidizer, NO_x formation is inhibited and CO levels are escalated. At the same flame temperature, NO_x levels reduced by a maximum of 40%, whereas the CO levels rose simultaneously as hgh as 50%. A parametric study on varying the combustor pressure indicated a rise in NO_x levels and drop in CO levels with increase in pressure. The pressure rise augmented the NO_x formed through thermal pathway and lead to the rise in NO_x beyond 1800 K. On the other hand, CO_2 dissociation to CO is suppressed by the rise of pressure, hence decreasing its magnitude.

The impact of using wet EGR is investigated and compared with results of dry EGR. It is observed that NO_x reduction is enhanced by 5-10%. Whereas the CO levels is escalated by 10-20%. The combined kinetic effect of CO_2 and thermal effect of H_2O is found to be reason for the change in emissions. This indicates an enhancement in combustion reactivity. Hydrogen injection raised the NOx levels by 5-10% and the CO levels dropped by a maximum of 12.5%. CO level suppression was a clear indication of the augmented flame stability and was found to be achieved with a slight compromise on NOx levels. Additionally, the effect of premixer efficiency is tested by discretizing the volume as parallel reactors with varying equivalence ratio inputs. Due to decreased premixing, unmixedness leads to various rich and lean pockets inside the combustor. This is a reason evident rise in both NO_x and CO levels with decreasing premixer efficiency.

Contents

List of Figures

List of Tables

Acronyms

CFD Chemical Reactor Network

CRN Computational Fluid Dynamics

EGR Exhaust Gas Recirculation

LPM Lean Premixed

NRC National Research Council

PFR Plug Flow Reactor

PSR Perfectly Stirred Reactor

TIT Turbine Inlet Temperature

UHC Unburnt Hydrocarbons

1

Introduction

1.1. Emissions and the Environmental impact

In the era of rapidly growing technology, the bane of pollution has been a part and parcel of everyday human life. Rapid industrialization along with elevated standards of living has led to large scale amounts of environmental pollution. The repercussions of human ignorance has been evident in the past few years through climate change. National Research Council (NRC) [1] has stated this fact in a very straight-forward and hard-hitting manner, that future human activities will largely decide the evolution of the Earth's climate.

The European Commission has put forward emission regulations from stationary industrial sources such as gas turbines, as a part of the Clean Air Package. A new directive for Medium Combustion Plant (MCP) aims to reduce the NO_x emissions by 50% - 60%. The existing MCP NO_x limit for natural gas fired gas turbines is set at 150 mg/Nm^3 and targets to bring down to 50 mg/Nm^3 by 2025 [2]. We can thus infer that emission reduction techniques adopted today will have an impact in the coming years. The focus of this research work will be on natural gas combustion, which is the key source of emissions in natural gas fired power plants. In order to keep pace with the stricter laws, newer combustion technologies have been developed.

1.2. Part load operation

The power plants commissioned during the past 2 decades were mostly designed for full load operation. Due to the increasing role of renewables in the grid, necessity to operate the gas turbine at part load arises due to lesser power demand. However, gas turbine based combined cycles have been reported to have relatively poor part load efficiency, as shown in figure 1.1 [3].

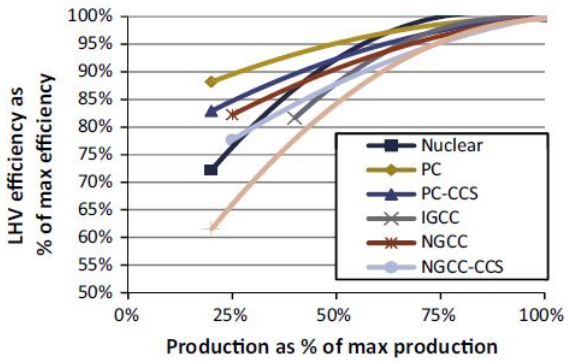

Figure 1.1: Part Load Efficiency curves for different technologies [3]

The reduction in efficiency of Natural Gas Combined Cycle (NGCC), Integrated Gasification Combined Cycle (IGCC) at part load is because of the lower flame temperature. The steam cycle efficiency is unaffected due to a constant exhaust gas temperature from the gas turbine. Hence, the gas turbine efficiency reduction is the major contributor for the poor performance in part load. Figure 1.2 summarizes the different part load control techniques. Variable guide vanes directly control the mass flow in the compressor. This decreases the air flow rate, thereby reducing the GT power output. Decreasing the turbine inlet temperature can be directly controlled by decreasing the fuel flow into the combustor, thereby reducing the power output. Air preheating and Exhaust Gas Recirculation (EGR) follow the same principle of decreasing the mass flow of the oxidizer by reducing the density of the working fluid [4]. Utamura et al. [5] have stated that exhaust gas recirculation can relatively improve part load performance of the gas turbine. They state that the combustion temperature is held constant at EGR, thereby improving its part load behaviour. Out of the existing part load techniques, a wise choice has to be made based on the benefits on both the power and emissions.

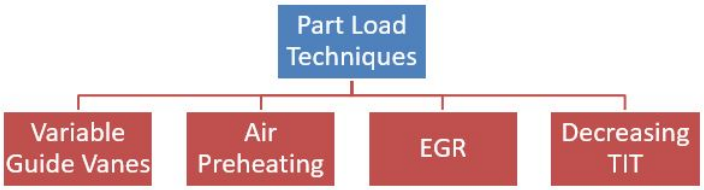

Figure 1.2: Part Load control techniques in gas turbines [4]

1.2.1. Exhaust Gas Recirculation

Lefebvre and Ballal [6] define EGR as a means to reduce the flame temperature by recirculating the products of combustion into air intake. This in turn dilutes the oxidizer, increasing the heat capacity of the resulting mixture. The inlet temperature of the oxidizer increases and part of oxygen is replaced with inerts such as CO_2. Thus, the EGR oxidizer is "oxygen-depleted air". This leads to reduced NO_x emissions and increased CO_2 content at the exhaust, helpful for effective carbon capture. Despite these advantages, the introduction of an oxygen-depleted oxidizer leads to changes in combustion behaviour giving rise to flame stability issues. A schematic of EGR implementation in gas turbine is presented in figure 1.3.

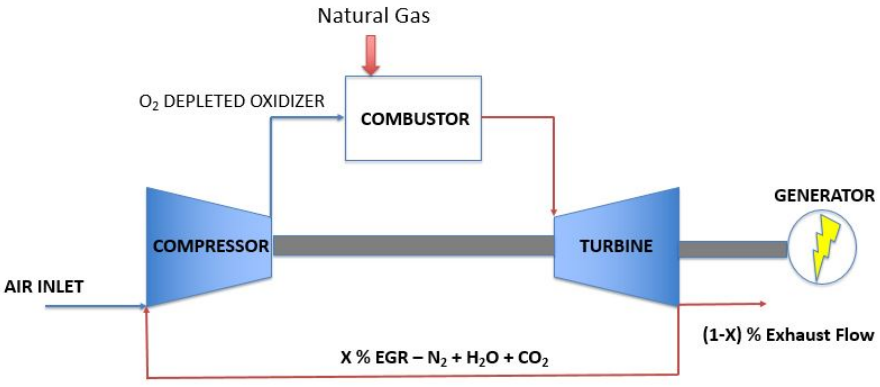

Figure 1.3: Schematic layout of EGR system: Exhaust gas is fed into the compressor inlet

Dry and Wet EGR

Depending on the moisture content of the exhaust gas, EGR can be classified into dry EGR and wet EGR. If the wet exhaust gas is directly used without intermediate condensation of vapor, then this type is called wet EGR. If the vapor content of the exhaust gas is condensed out before mixing with the air intake, then it is called dry EGR. The pollutant formation is affected due to the difference in kinetic and thermal effects between the dry and wet exhaust gas.

1.3. Motivation of the Thesis

One of the challenges in gas turbines is in the reduction of NO_x and CO emissions due to simultaneous dependence on stringent emission norms and subsequent demand for change in operating conditions. Power plants commissioned before the 1990's were built on non-premixed or diffusion type combustors, that always burnt in a stoichiometric flame front. This causes higher flame temperatures and consequently higher emissions. The scope of lean premixed combustion (LPM) to reduce these emissions to a larger extent is due to homogeneous mixing of fuel and air. Leaner equivalence ratios can be achieved, thus avoiding stoichiometric flame interfaces and reducing emissions. To cater the volatile demand of power supply due to the increased role of renewables, most of the gas turbines have to be flexible to changing loads. Out of the available options, for efficient carbon capture with overall reduced emissions, Exhaust Gas Recirculation (EGR) is a viable and promising solution [7–10].

Nature of emissions in inert atmosphere (CO_2 and N_2 due to recirculated gas stream) in gas turbine operating conditions has not been extensively studied except for companies like General Electric and ALSTOM [9, 11]. A combination of lean premixed combustion with EGR can have additional emission reduction. By building emission models with EGR in Dry Lean NO_x (DLN) combustors, emissions in this new operating regime can be analyzed in detail. Hence, the core topic of the research will be to model emissions in gas turbines under EGR operating conditions. A summary of the contributing factors in favour of EGR is shown in figure 1.4.

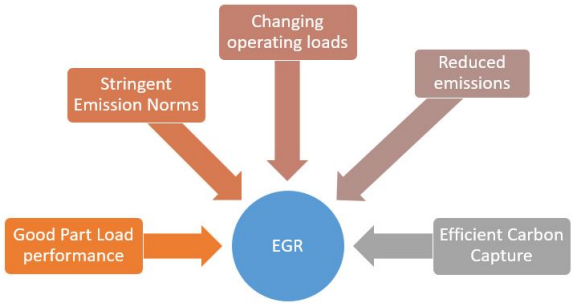

Figure 1.4: Contributing factors for EGR as a promising emission reduction technology

1.4. Approaches to Emission Modeling

Combustion is inherently governed by the complexity of turbulence-chemistry interaction. Poinsot and Veynante [12] explain this in great detail in their book. In brief, there is a two way mechanism to understand the interaction:

1. **Flame interaction with turbulent flow -** When the flame interacts with flow inside a combustor, the phenomena of turbulence is modified by virtue of heat release through the flame front, leading to highly accelerated flow. Fundamental changes such as modification of kinematic viscosity happens due to large temperature changes. This is called as "flame-generated turbulence" [12].

2. **Turbulence interaction with the flame -** On the other hand, turbulence directly affects the flame structure. In addition, turbulence enhances the chemical reaction rates, but too much turbulence can even quench the flame. This can lead to wrinkling of flames and change in flame structure.

On the whole, turbulence-chemistry interaction leads to increase in the flame surface area, conversion rate and wrinkling of the flame front. All these factors in turn affect the temperature levels and consequent emission levels. It is important to assess the modeling methodologies that account for the real physics of the problem.

As stated by Rosati [13] in his masters thesis, two common computational approaches to model emissions are Computational Fluid Dynamics (CFD) and Chemical Reactor Networks (CRN). Extensive research has been carried out by various research groups, where combination of both processes are employed to model emissions. To cite a few, Stagni et al. [14], Lebedev et al. [15] and Monaghan et al. [16] present approaches to build the reactor networks based on the flow field results from CFD. In order to make a choice, one has to ultimately weigh out the pros and cons of both the processes independently. If emission models are to be developed for combustors with similar flow fields, the mean flow can be simplified and preference can be given to the chemical modeling. In case of studying the flame shape characteristics and its effect on the emissions, CFD approach should be chosen with reduced chemistry.

Approach	Pros	Cons
CFD	Accurate solving of flow field and turbulence	High Computational Cost and Time
	Works well when combined with chemical sub-models	Reduced Chemistry (Independent Use)
CRN	Simplified flow field and turbulence	Turbulence-chemistry interaction neglected
	Very less computational time; Quick Results	Requires data from CFD/experiments

Table 1.1: Comparison between emission modelling approaches

CFD is very accurate in predicting flow fields and turbulence effects to the flow. Various turbulence models existent in literature can be used to solve the flow field. The downside of this method is that the solver takes reduced chemistry into account. Efficient use of CFD solvers for solving chemical equations is not possible due to this global chemistry assumption and the inherent stiffness problems in the reaction mechanisms [17]. Emissions are not only driven by temperature but also by chemistry. Hence, a refined mechanism leads to an approximate solution rather than an accurate one. Another disadvantage of CFD is high computational time and cost for simulating the process. In addition, inherent errors in the turbulent models can cause difference in flow predictions.

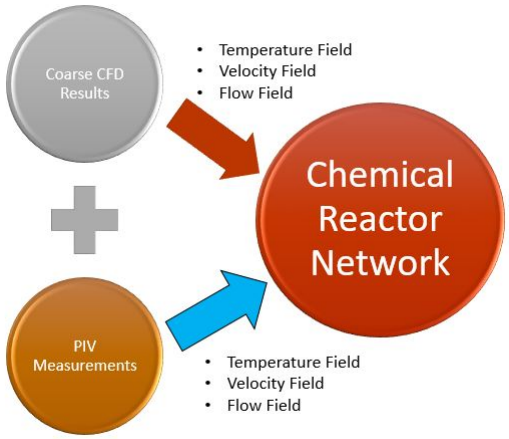

Figure 1.5: Pre-requisites for CRN model development

On the other hand, the methodology followed in CRN modeling is about spatially discretizing a combustor as a chain of chemical reactors connected in series [13]. The position of these reactors and its type is determined by having an idea of the flow field using PIV (Particle Image Velocimetry) experiments or prior CFD simulations.

The combustor volume is split into homogeneous zones and treated as individual 0D chemical reactors, which is solved through descriptive reaction mechanisms. Therefore, in this method the flow field is simplified and importance is given to the chemical kinetics of the combustion reaction.

The advantage of CRN is that it takes less computational time and results can be obtained very quickly. If the idea is to develop a predictive model to be installed on-line, then this approach will be most suitable for faster results. The overview of the necessary inputs for CRN models is described in figure 1.5. Despite the advantages, the simplification of the overall mean flow field to build CRNs without considering the local flow field can affect the accuracy of the solution. Based on the CFD solution of each mesh cell such as temperature, species concentration and velocity, a CRN can be built as an ensemble of interconnected zones [18].

Obviously, the combination of both methodologies would produce the best results. Hybrid CFD-CRN models represents the complete modeling of combustion. An intermediate approach to account for both the chemistry and flow effects can be through Flamelet Generated Manifold (FGM) technique. This is a reduction technique taking into account the important aspects of chemistry and flame structure and formulating lookup tables. Instead of a complete combustion study, the number of variables are reduced based on steady state assumptions and flamelet models. Thus, the results of the CRN can provide essential chemical input to the FGM for proper emission prediction [12].

However, due to the large computational time gap between the two methods, CRN approach has been chosen for this research work. Various chemical kinetic software like Cantera [19] and CHEMKIN [20] are used to model CRNs.

1.5. Research Objective

As already stated, not many models have been developed to predict emission trends in gas turbines operating under EGR conditions. Hence, the main objective of this thesis is to build a predictive emission model for lean premixed gas turbine combustors operating with EGR, using chemical reactor networks.

The model would include a chemical reaction sub-model that would consider different reaction mechanisms for natural gas combustion. Parametric dependence on emissions due to the change in the following parameters will be analyzed:

- EGR emission prediction ability of various chemical reaction mechanisms
- Oxidizer Composition - Comparison of Air with EGR oxidizer containing different amounts of inerts: N_2, CO_2, H_2O
- Effect of CO_2 content in the oxidizer
- Change in Combustor Pressure
- Comparison of effects of dry and wet EGR
- Effect of Hydrogen injection in the fuel and behaviour in EGR environment
- Effect of Unmixedness/ Degree of Premixing

Furthermore, the results of this investigation will be validated with existing results or trends from the literature.

1.6. Report Outline

This report will be further continued with the literature review and theoretical background in the 2nd chapter. Chapter 3 deals with the CRN architecture followed to build the model, along with assumptions and validation. Chapter 4 presents the results of the parametric study performed on the model and followed by discussions. Chapter 5 and 6 deal with the conclusions from the study and recommendations for future work.

2

Literature Survey & Theoretical Background

As the focus of the thesis is on the emission characteristics of natural gas fired gas turbine combustors, it is important to present the fundamental theory governing the phenomena involved in combustion. This chapter will cover the gas turbine cycle, basics of gas turbine combustion, types of pollutants and its formation mechanisms, relevant combustion time scales and Exhaust Gas Recirculation. In addition, existing CRN models for natural gas combustion will be discussed.

2.1. Gas Turbine Cycle

Figure 2.1 shows the schematic outline of a gas turbine cycle. Ambient air enters the compressor, where it is compressed to an elevated pressure along with an increase in temperature. The pressurized and heated air then enters the combustor with simultaneous injection of fuel. The fuel-air mixture is combusted and the chemical energy of the fuel is converted to heat energy.

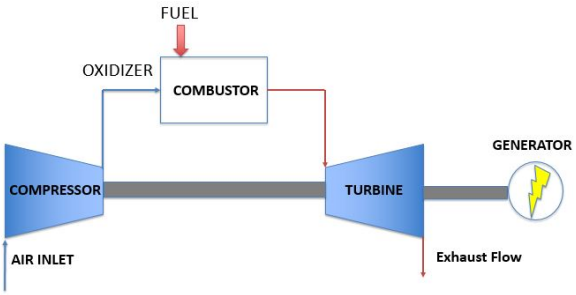

Figure 2.1: Schematic of Gas Turbine Cycle

Combustion is an exothermic reaction in which the fuel oxidizes in the presence of an oxidizer like air, accompanied with large heat release and chemical conversion of reactants to products. The pressurized hot products exit the combustor and further expand in a turbine. Heat energy is then converted to mechanical energy through rotational momentum of the turbine. After expansion, the stack gases are either released to the atmosphere or coupled to a combined Rankine cycle to extract the heat of the exhaust gas.

The temperature at which the gases enter the turbine is called the Turbine Inlet Temperature (TIT) or the firing temperature. From equation 2.1 and 2.2, higher value of TIT implies larger power output and consequently higher thermodynamic efficiency. Additionally, higher the TIT, higher is the combustion temperature. This causes higher temperature levels and a negative impact on the pollution front.

Hence, a trade-off between efficiency and environmental impact is crucial during the operation of the gas turbine.

$$P = (\dot{m}_a + \dot{m}_f) C_{p,gas} (T_{inlet} - T_{outlet}) \tag{2.1}$$

$$\eta_{th} = \frac{P}{\dot{m}_f \times LHV} \tag{2.2}$$

2.2. Types of Combustion in Gas Turbines

Gas turbines are usually anchored by swirl stabilized flames. The aerodynamics of the flame is a combination of rotation and translation of the incoming flow due to a swirler. Therefore, the fluid flow entering the combustion chamber possesses both tangential and axial velocity components to enhance mixing and turbulence. This in turn induces localized axial and radial pressure gradients leading to a central recirculation zone [21].

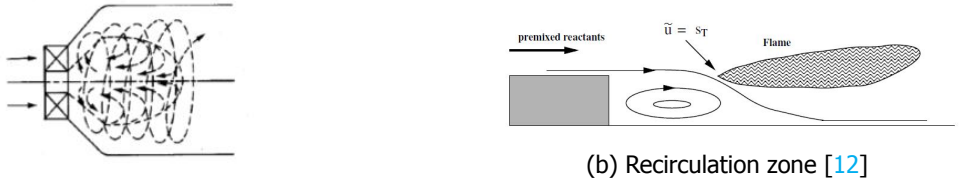

(a) Swirling Flame [22]

(b) Recirculation zone [12]

Figure 2.2: Flow physics of a swirling flame

The mechanism of swirl stabilization involves the recirculation of hot products into the main flame. The recirculated hot products play a role in heating up the incoming reactant mixture, thereby accelerating the process of achieving flame stability. Keeping the overall flow field fixed, gas turbine combustion can be broadly classified into premixed, partially premixed and non-premixed combustion.

As seen in figure 2.3, the fundamental difference between these modes of combustion depend on the way the fuel and oxidizer interact or react with each other.

- In case of non-premixed combustion, fuel and air enter the combustor zone independently and the mixing takes place inside. Fuel is injected into the chamber directly whereas only the oxidizer is imparted with a swirling flow to enhance mixing.
- In premixed combustion, the mixing of fuel and air takes place in a mixing tube or plenum before entering the combustor and the fuel-oxidizer mixture is imparted with a swirl.
- Lastly, a partially premixed flame consists of a pilot flame (rich flame), that anchors the main flame (premixed flame) to augment the flame stability. Thus, the behavior of this flame is a combination of diffusion and premixed flames [23].

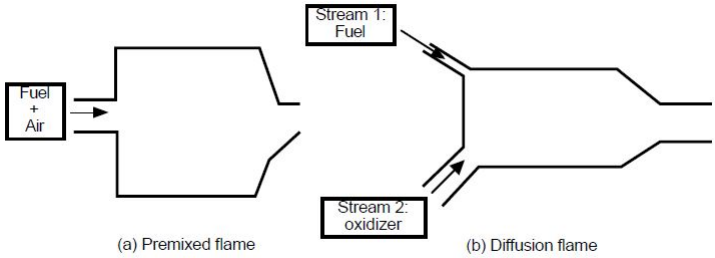

Figure 2.3: General representation of premixed and diffusion flames [12]

Typical power plants running on natural gas in the 1990s were setup with diffusion flames because of the ease of installation, compactness and good flame stability. This choice was indeed not ideal because of the burning of near-stoichiometric flame interfaces in the flame (shown in figure 2.4a), leading to high peak temperatures close to 2500 K. As a consequence of higher temperature, NO_x emissions also escalate [24]. A method to handle this upsurge of NO_x is achieved through direct steam injection into the combustion chamber. The high heat capacity of steam reduces the peak temperature and hence reduces NO_x emissions. This also enhances power output due to increase in turbine mass flow rate.

Despite having a poor emission performance, a wide range of applications such as aircraft engines, still utilize diffusion flames. However, lot of research has been performed on lean premixed combustion aiding to its advantages over non-premixed flames. Røkke and Hustad [7] conducted a study on a combustor test rig that was capable of operating in both diffusion (non-premixed) and premixed modes. For the same range of equivalence ratios, it was concluded that premixed mode produces lesser NO_x emissions when compared to diffusion mode. With the aim of lower emissions, premixed mode seems to be a promising choice because it exhibits lower flame temperatures when compared to diffusion flames. Premixing leads to a more homogeneous temperature and concentration distribution and avoids the formation of local stoichiometric flame fronts like in diffusion flames.

(a) Stoichiometric interface in diffusion flame [25] (b) Freely propagating premixed flame [26]

Figure 2.4: Flame schematic of premixed and diffusion flames

In general, perfect premixing is difficult to achieve, leading to spatial and temporal fuel-oxidizer unmixedness inside the combustor [27, 28]. Consequently, unmixedness produces more NO_x emissions than expected. In premixed combustion, when the flame speed exceeds the flow speed of the reactants, flashback of the flame happens in the upstream direction of the combustor [29]. Flashback susceptibility of a premixed system is enhanced when high reactive fuels such as hydrogen is combusted. This is fundamentally governed by the vortex breakdown of the above mentioned central recirculation zone [13, 21]. On the whole, each mode of combustion possesses its own set of pros and cons, leading to a confusion in making a choice. Keeping overall reduction in emissions and stringent regulations in mind, most modern gas turbines are equipped with remixed combustion systems. Hence, premixed combustion has been chosen as the mode of study in this thesis.

Combustion Type	Pros	Cons
Non-Premixed	Higher Flame Stability	Higher NO_x formation due to stoichiometric interface
	Less sensitive to GT load variations	Higher thermal loads
Premixed	Homogeneous temperature profile	Improper mixing maximizes pollutants
	Proper mixing can help achieve leaner mixtures	Flashback and autoignition problems come up

Table 2.1: Differences between premixed and diffusion flames

2.3. Gas Turbine Emissions

The types of pollutants and its formation mechanisms are explained in this section. In addition, relevant terminology regarding emission quantification has been dealt with in the succeeding paragraphs. The most common pollutants formed in gas turbine combustors are Carbon Monoxide (CO), Unburnt Hydrocarbons (UHC), Oxides of Nitrogen (NO_x), Soot, smoke and oxides of sulphur [6]. The environmental impact of each of these pollutants has been tabulated below.

Pollutant	Impact on environment and health
Carbon Monoxide (CO)	Toxic gas
	Reduced capacity of O_2 absorption by blood
Unburnt Hydrocarbons (UHC)	Toxic in nature
	Combines with NO_x to form photochemical smog
Nitrogen Oxides (NO_x)	Forms HNO_3 causing acid rain
	Photochemical smog, Greenhouse gas causing climate change
Sulphur Oxides (SO_x)	Toxic and Corrosive gas
	Acid rain forming reactant
Soot/ Smoke	Poor Visibility
	Allergy , Asthmatic problems, Nausea

Table 2.2: Impact of pollutants on health and environment

Out of the aforementioned pollutants, only CO and NO_x are prominent in gas turbines firing gaseous fuels such as natural gas. Pollutants such as smoke and soot are predominant when using liquid fuels [6, 30].

2.3.1. Pollutant Formation Mechanisms

The complexity of the flow and the chemical reactions involved in makes pollutant formation difficult to understand. Simultaneous dependence on factors such as temperature, concentration, pressure and residence time needs deeper understanding.

Oxides of Nitrogen (NO_x)

Nitrogen oxides of prime importance include NO, NO_2 and N_2O. NO and NO_2 together is defined as NO_x. Formation of NO_x is broadly classified into 4 pathways namely,

- Thermal NO_x or Zel'dovich mechanism [31]
- Prompt NO_x or Fenimore Mechanism [32]
- N_2O or Nitrous Oxide Mechanism [33]
- NNH Mechanism [34]

The behavior behind NO_x formation is highly non-linear in nature, depending on many concurrent variables such as temperature, pressure and residence time. The general expression for the formation rate of NO_x is given by Correa [35] as,

$$\dot{\omega} = A[N_2][O]exp\left(\frac{-E_a}{RT}\right) \tag{2.3}$$

where $\dot{\omega}$ is the formation rate in mol/m^3s, E_a is the activation energy of the particular reaction and A is the pre-exponential factor. From equation 2.3, it is clear that NO_x formation is similar to an Arrehenius expression. It was also stated that $\dot{\omega}$ was very sensitive to temperature changes. Hence, any kind of non-adiabaticity inside the combustor volume can cause hot zones, leading to enhanced NO_x formation.

Thermal NO_x : Zel'dovich Mechanism Thermal NO_x derives its name due to its strong temperature dependence. The thermal pathway of NO_x involves the formation of nitrogen oxides at high flame temperatures (T > 1800 K) and was first devised by Zel'dovich [31] in 1947. This involves the oxidation of atmospheric N_2 molecule by various radical species. At flame temperatures exceeding 1800 K - 1850 K, the oxygen radical [O] reacts the N_2 molecule thereby breaking the strong triple bond in the N_2 molecule and forming NO [9]. This is described in equation 2.4a and serves as the initiation reaction of the Zel'dovich mechanism. The activation energy of this reaction is very high (E_a = 75 kcal/mol) giving rise to a slow chemical reaction rate. Thus, equation 2.4a becomes the rate determining step of the overall mechanism. The N radical formed in equation 2.4a reacts the O_2 molecule to further enhance NO formation, as shown in equation 2.4b.

$$N_2 + O \underset{k_{1b}}{\overset{k_{1f}}{\rightleftharpoons}} NO + N \tag{2.4a}$$

$$N + O_2 \underset{k_{2b}}{\overset{k_{2f}}{\rightleftharpoons}} NO + O \tag{2.4b}$$

$$N + OH \underset{k_{3b}}{\overset{k_{3f}}{\rightleftharpoons}} NO + H \tag{2.4c}$$

Thermal NO_x has exponential dependence on temperature beyond a threshold of 1800 K. The rate of all the reactions in equation 2.4 get accelerated at higher temperature. Besides temperature, other factors such as residence time, reactant initial temperature and pressure do play a pivotal role in thermal NO_x formation. As the residence time in the combustor increases, higher NO_x formation happens. When the reactant temperature increases, the flame temperature increases leading to higher thermal NO_x formation. An increase in combustion pressure leads to higher reaction rates and enhanced thermal NO_x formation. A summary of the important factors influencing thermal NO_x is presented in figure 2.5.

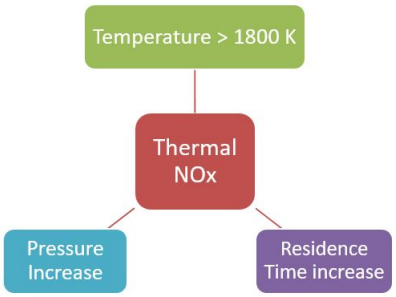

Figure 2.5: Important factors favouring the increase in thermal NO_x pathway

Nitrous Oxide Mechanism The presence of atmospheric N_2 molecule and O radical at lower flame temperatures (T< 1800 K) gives rise to another specie N_2O. The mechanism behind the formation of N_2O was first proposed by Malte and Pratt [33]. The genesis of N_2O is stated as a third body reaction with a 3 reaction pathway.

$$N_2 + O + M \rightleftharpoons N_2O(\cdot) + M \tag{2.5a}$$

$$N_2O(\cdot) + M \rightleftharpoons N_2O + M \tag{2.5b}$$

$$N_2O + M \rightleftharpoons N_2 + O + M \tag{2.5c}$$

where M is the third body, under the presence of which the reaction takes place. N_2 and O in the presence of the third body forms an unstable intermediate $N_2O(*)$ and immediately forms N_2O.

It was stated by Nicol et al. [36] that the overall reaction of this 3 step pathway is the initiating reaction. It is important to study the formation of N_2O because this specie acts as a base for enhanced formation of NO, after reacting with O radicals or H radicals or even CO [6]. This is shown in equation 2.6.

$$N_2O + O \rightleftharpoons NO + NO \quad (2.6a)$$
$$N_2O + H \rightleftharpoons NO + NH \quad (2.6b)$$
$$N_2O + CO \rightleftharpoons NO + NCO \quad (2.6c)$$

The reactants N_2O and O can lead to two different kinds of products. These reactants may either form NO or N_2 and O_2 as an alternate product set. The understanding of this conundrum is hard because the activation energy of reactions 2.7a and 2.7b are equal. Hence, a clear model cannot predict whether the two reactions are preferred over the other. On the whole, due to high dependence on oxygen concentration for the reaction to proceed, it was implied that N_2O mechanism is dominant in lean mixtures and lower flame temperatures [33]. The pressure dependence of this mechanism has been found to be high due to the presence of the third body. On increasing the pressure, the collisions between the three bodies enhance, leading to accelerated reactions.

$$N_2O + O \rightleftharpoons NO + NO \quad (2.7a)$$
$$N_2O + O \rightleftharpoons N_2 + O_2 \quad (2.7b)$$

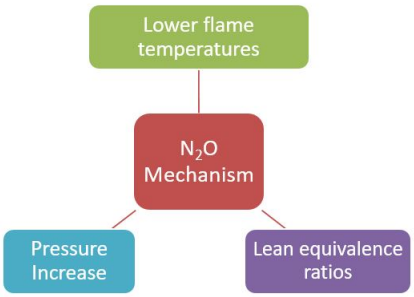

Figure 2.6: Important factors favouring the increase in NO_x by N_2O mechanism

Prompt NO_x First proposed by Fenimore [32], this mechanism relies on the attack of hydrocarbon radical on atmospheric nitrogen to produce a pathway for NO_x formation. The reactions involved in the prompt mechanism are as follows,

$$N_2 + CH \rightleftharpoons HCN + N \quad (2.8a)$$
$$HCN \longrightarrow CN \longrightarrow NCO \longrightarrow NO \quad (2.8b)$$

CH radical reacts with N_2 to form HCN, that further oxidizes in several stages to produce NO. In opposition to the notion that NO_x formation is kinetically controlled, Nicol et al. [36] stated that prompt NO_x is formed very early in the flame region. He proposed a theory that NO_x formation can be split into fast and slow NO_x based on their rates of formation, by performing experiments with ethylene-air flames between pressures of 1 and 3 atm [32]. It was found that the hydrocarbon radical attack was the main reason for fast chemistry and formation in early flame regions. Prompt NO_x is dominant at lower flame temperatures and lower pressures simply due to the fact that the thermal pathway dominates at higher flame temperatures and pressures.

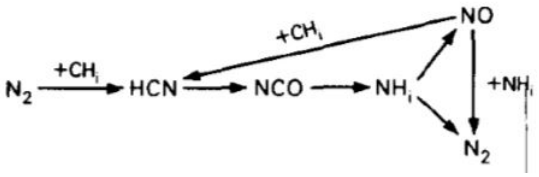

Figure 2.7: Chain of intermediate reactions involved in prompt pathway [37]

Heberling [38] extended the above work and tested the effect of prompt NO_x formation by testing premixed ethylene-air flames at different pressures (1-18 atm) and equivalence ratios (ϕ = 0.6-1.4). Figure 2.8 shows the NO levels as a function of the residence time, for different pressures. By extrapolating the linear plots to zero time (or fast formation of NO), the y-intercept represents the NO_x formed in the early flame region. Rest of the line corresponds to NO_x formed over a range of time or slow NO_x. The value of the intercept at lower pressures was found to be dominated by prompt NO. This is the reason why prompt NO_x is related with the early flame region. On moving to higher pressures, the value of y-intercept increases and the prompt NO formed is partly replaced by thermal NO. Increased reaction rates due to higher pressures accelerate the formation of thermal NO_x. This is the reason why prompt NO_x gets lowered largely at higher pressures.

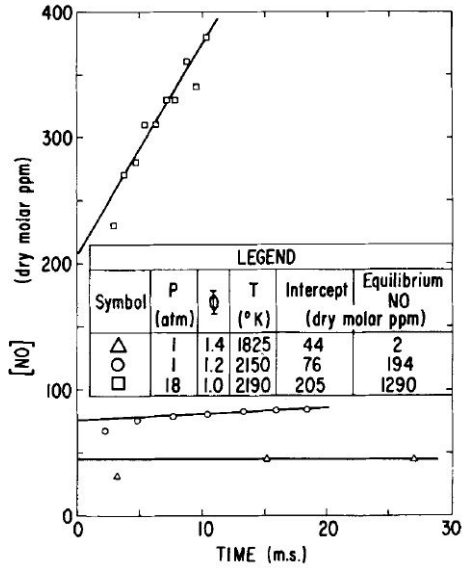

Figure 2.8: Formation of NO as a function of residence time : Y- intercepts represent NO formed in the early flame region [38]

Figure 2.9 shows the summary of the factors favouring the increase of NO_x by prompt pathway.

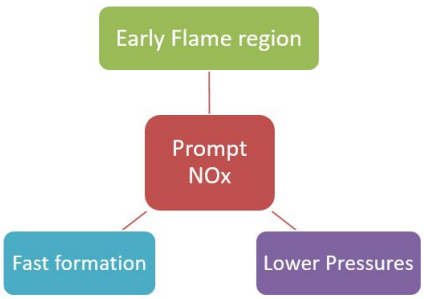

Figure 2.9: Important factors favouring the increase in NO_x by prompt mechanism

NNH Pathway

Bozzelli and Dean [34] proposed a new pathway on NO formation through an intermediate NNH. NNH is formed by the reaction of N_2 with H radical at lower flame temperatures. This reaction was found to be endothermic.

$$N_2 + H \rightleftharpoons NNH \quad (2.9a)$$
$$NNH + O \rightleftharpoons NO + NH \quad (2.9b)$$

NNH radical reacts with O radical to form NO and NH. The reaction of NNH and O can lead to 3 different kinds of exothermic products, NO + NH , N_2O + H or N_2 + OH.

$$NNH + O \rightleftharpoons NO + NH \quad (2.10a)$$
$$NNH + O \rightleftharpoons H + N_2O \quad (2.10b)$$
$$NNH + O \rightleftharpoons N_2 + OH \quad (2.10c)$$

It was found that this reaction has a larger energy state after formation when compared to other channels of reaction as shown in figure 2.10. All the reactions formed an intermediate HNNO. HNNO further dissociated to give different products with different activation energy values. A low value of pre-exponential factor for the NO+ NH reaction and HNNO dissociation, lead to quicker breaking of the N-N bond, even though the energy state is higher than the other two reactions. Entropic effects act as a driving force for the NO pathway to dominate in this set of reactions leading to a new NO_x mechanism.

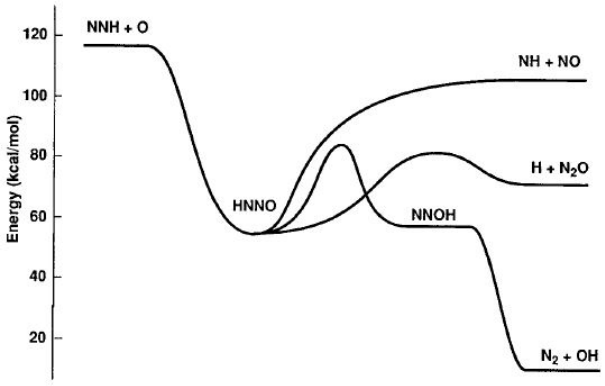

Figure 2.10: Potential Energy Diagram and Reaction channels of NNH + O [34]

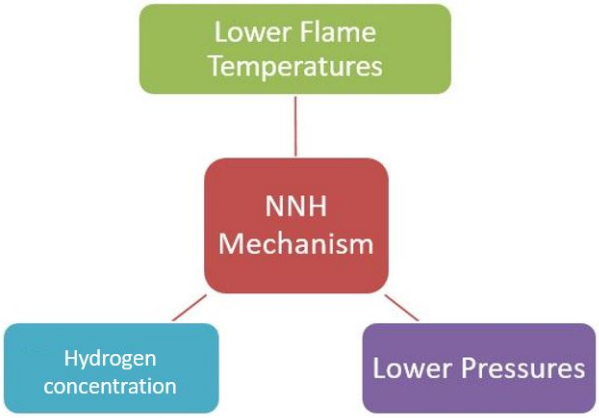

Figure 2.11: Important factor influencing the increase in NO_x by NNH pathway

Carbon Monoxide (CO)

Carbon Monoxide is another major pollutant formed in gas turbine combustors. The major reasons behind CO formation are the following as stated by Lefebvre and Ballal [6],

- **Improper Mixing :** If the fuel-oxidizer mixture is not homogeneous and contains spatial and temporal unmixedness inside the combustor, various rich and lean pockets exist inside the combustor volume. This favours CO formation.
- **Insufficient Residence Time or Incomplete combustion:** Due to low residence time in the combustor, the fuel does not burn completely. In order to reach the equilibrium values of CO, the flow must stay for an infinite residence time, which is unrealistic. Another reason can be due to lack of oxygen in the primary zone of the combustor and causing incomplete combustion.
- **Flame Quenching :** Local flame quenching can occur due to cooling air entrainment from the combustor liner leading to high amounts of CO.

In addition, CO is oxidation resistant and its conversion to CO_2 is considered to be the rate determining step. Another additional reason for CO formation can be through CO_2 dissociation at temperatures above 1000 K [39]. CO_2 can dissociate to give CO and O_2, thus augmenting CO formation, as shown in the equation below,

$$CO_2 \rightleftharpoons CO + 0.5\,O_2 \tag{2.11}$$

The overall oxidation of CO can be split into 4 steps [40]:

$$CO + O_2 \rightleftharpoons CO_2 + O \tag{2.12a}$$
$$O + H_2O \rightleftharpoons OH + OH \tag{2.12b}$$
$$CO + OH \rightleftharpoons CO_2 + H \tag{2.12c}$$
$$O_2 + H \rightleftharpoons OH + O \tag{2.12d}$$

As stated above, equation 2.12a is the rate determining step and acts as the initiation reaction. It can be seen that formation of OH, H and O radicals can accelerate the process of oxidation of CO to CO_2. In particular, equation 2.12c is a main reaction that removes CO and converts it to CO_2. Just like NO_x emissions, CO emissions too depend on various factors beyond the reasons mentioned above.

CO formation is highly dependent on the equivalence ratio. At very lean mixtures, the oxidation rates are too slow to completely oxidize CO. The chemical dissociation of CO_2 to CO can also be a reason for increased CO. An increase in pressure leads to large scale reduction of CO formation due to the suppression of chemical dissociation of CO_2 (equation 2.11) [6].

2.3.2. Technology towards Emission Reduction

Natural gas fired power plants run on gas turbines which are connected to electric generators to produce power. These power plants demand operation at highest thermal efficiency and lowest power consumption. This can be achieved at full load and higher turbine inlet temperatures, hence increasing emissions [41]. Figure 2.12 shows an overview of the existing emission reduction technologies. Explanation about EGR has already been explained in chapter 1.

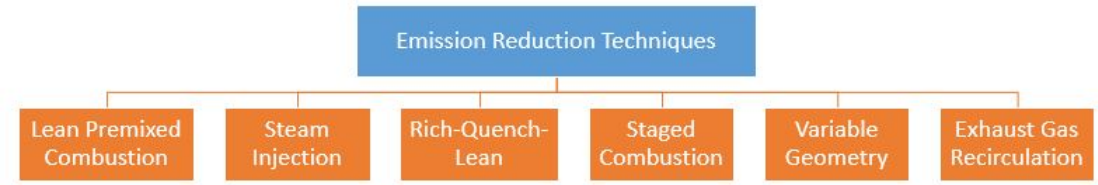

Figure 2.12: Emission reduction technologies employed in gas turbines [6, 30]

- **Lean Premixed Combustion:** When a premixed combustor runs at leaner conditions and corresponding lower combustion temperatures, then it is called lean premixed combustion. Due to lower flame temperatures, the corresponding NO_x levels are diminished. However, lean premixed combustion is prone to small disturbances resulting in combustion instabilities. Thus an inherent challenge is in designing these combustors with low noise levels.
- **Steam Injection:** Steam injection directly affects the NO_x emissions. Steam injection reduces the flame temperature, thereby diminishing thermal NO_x production. It is a feasible solution for power plants as a retrofit and helps in power boost. Due to the lower temperature achieved with steam injection, CO emissions are high due to the lower reaction rates.
- **Rich-Quench-Lean:** RQL combustion are separated as two zones- a fuel rich zone and a lean zone. The rich zone aims to consume all the oxygen in the air and the zone allows the burning of the remaining fuel. Slow NO_x reactions are prevented by sudden quenching between the two zones. The drawback lies in the inefficient transition between the rich and lean zones.
- **Staged Combustion:** The fuel flow distribution is changed between injectors such that the flame temperatures are maintained and the air flow is kept constant. This technique changes the equivalence ratios of local combustion zones, thereby reducing the overall emissions. Series and parallel combinations can be adopted in staged combustion.
- **Variable Geometry:** The distribution of the combustion air in the primary, secondary and dilution zone is varied using an adjustable unit. The equivalence ratios in each zone is thus change because of the air flow distribution. An optimum setting for airflow distribution can be set to get least emissions.

2.3.3. Quantifying Emissions

A background on the formation mechanism of pollutants has been covered so far. It is important to devise a method for representation of these emissions and for ease of comparison between different operating conditions on a common scale.

Emission Index

The emission Index (EI) is defined as the ratio of the mass of the pollutant in grams to the mass of the fuel in kg. The difference in units is to account for the order of magnitude difference between the two quantities. This quantity is the amount of pollutant formed per kg of fuel consumed, neglecting the dilution of air [42]. EI is a common method used in literature to quantify emissions.

$$Emission\ Index = \frac{Mass\ of\ pollutant\ (g)}{Mass\ of\ fuel\ (kg)} \tag{2.13}$$

Oxygen Correction

The order of magnitude difference between pollutant amount and actual mass of fuel is large. Another unit of representation is in parts per million by volume (ppmv). Usually when ppmv is used for representation, it is normalized to a reference oxygen level of 15%. The aim of this normalization is to eliminate the effect of variation in dilution of the oxidizer in different cases. This creates a common scale to compare different cases of oxidizer. Due to the presence of H_2O as part of the combustion process, it is important to convert the wet concentrations to dry concentrations. This is done as follows,

$$X_{dry} = \frac{X_{wet}}{(1 - X_{H_2O\ wet})} \tag{2.14}$$

The usual correction formula used for air oxidizer is represented below,

$$NO_{x\ 15\%O_2} = NO_{dry\ measured} \frac{(0.2095 - 0.15)}{(0.2095 - X_{O_2\ dry})} \tag{2.15}$$

The value of dry concentration X_{O_2} is obtained from equation 2.14. In equation 2.15, the value of 0.2095 represents the mole fraction of oxygen in air and 0.15 is the value at which the emissions are normalized. In case of introducing EGR, equation 2.15 can no longer be used because the derivation is based on the assumption of air as the oxidizer. The effect of vitiation of air with inerts such as CO_2 leads to the change in the emission behaviour and has to be addressed with a different approach [9].

$$C_xH_y + a(\alpha O_2 + \beta N_2 + \gamma CO_2) \rightleftharpoons (x + a\gamma)CO_2 + 0.5(yH_2O) + bO_2 + a\beta N_2 \tag{2.16}$$

Equation 2.16 represents the new equation with EGR oxidizer with mole fractions of O_2, N_2 and CO_2 represented as α, β and γ respectively. Elkady et al. [9] derived a new relation for NO_x correction based on this equation to represent the realistic normalization with 15% oxygen levels with EGR oxidizer as shown in equation 2.17 (specifically for fuel CH_4).

$$NO_{x\ 15\%O_2} = NO_{dry\ measured} \left(0.033231 \frac{(2 - \alpha)}{(\alpha - X_{O_2\ dry})} \right) \tag{2.17}$$

2.4. Premixed Flames

2.4.1. Governing equations of laminar premixed flames

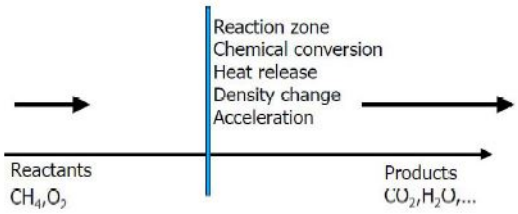

Figure 2.13: 1-D representation of a premixed flame [29]

1-D laminar premixed flames are defined as a propagation wave that turns from fresh gas into burnt gas without major transients. The detailed governing equations are explained in appendix D. The temporal derivatives in equations D.1, D.2 and D.3 are reduced to the following equations,

Mass Conservation

$$\rho u = constant \tag{2.18}$$

Momentum and species Conservation

$$\frac{\mathrm{d}(\rho(u + V_k)Y_k)}{\mathrm{d}x} = \dot{\omega}_k \tag{2.19}$$

Energy Conservation

$$\rho u C_p \frac{\mathrm{d}T}{\mathrm{d}x} = \dot{\omega}_t + \frac{\mathrm{d}(k\frac{\partial T}{\partial x})}{\mathrm{d}x} - \rho \frac{\partial T}{\partial x}(\sum_{1}^{N}(C_{p,k} Y_k V_k)) \tag{2.20}$$

where Y_k is the mass fraction of species k, u is the bulk flow velocity, V_k is the diffusion velocity and $\dot{\omega}_k$ is the chemical source term of species k which is determined from the reaction rate and Arrehenius law. The above equations can then be solved computationally through existing codes in Cantera [19] and CHEMKIN PREMIX module [20]. In addition to the numerical discretization, the chemistry of the process is incorporated by a relevant chemical mechanism such as GRI-Mech 3.0 [43]. In this way, an estimate of the mixture averaged laminar flame speed can be obtained. Figure 2.14 shows the importance of using detailed chemistry in the calculation of laminar flame speed. The difference can be explained by the Lewis number, which is the ratio of the thermal diffusivity and the species mass diffusivity. In case of simple chemistry assumption, Lewis number of all the species is assumed to be unity i.e, there is no preferential diffusion of species. This leads to large under-prediction of the laminar flame speed.

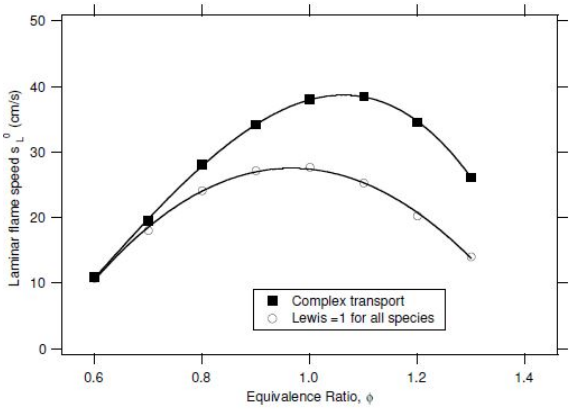

Figure 2.14: Effect of using complex and simple chemistry in laminar speed prediction [12]

2.4.2. Estimation of flame thickness

By applying scaling laws, an estimate of the laminar flame thickness can be found out. It can be written as the ratio of the thermal diffusivity α and the laminar flame speed s_L.

$$\delta = \frac{\alpha}{s_L} = \frac{k}{\rho C_p s_L} \tag{2.21}$$

where k is the thermal conductivity, ρ is the density and C_p is the heat capacity of the burnt gas.

2.5. Combustion regimes and Time scales

Due to intense turbulence inside the combustor, the size of the eddies are purely dependent on the Reynolds number, temperature and other thermodynamic properties of the flow. In case of a reacting flow like combustion, chemistry also comes into play. There is usually a difference in the time scales governing the flow and chemistry, considering the difference in reaction rates and flow rates.

2.5.1. Turbulence-Chemistry Interaction

Correa [35] broadly classified turbulence-chemistry interactions into flamelets and distributed reaction zones. Flamelets are defined as smaller strained flames whose ensemble makes up the whole flame. It was stated that reactions occur at a fixed strain rate, leading to faster reactions [44]. This means the chemical time scale much smaller than the mixing time scale. This region, shown in figure 2.15(a), behaves like a thin reaction zone or a flamesheet.

On the other hand, a counter effect of distributed reaction zones was first proposed by Bilger [45]. In this kind of regime in figure 2.15(b), the reactions are slow and occur at a greater volume. Hence, the reaction zone is spatially extended and smeared out in space. Table 2.3 shows the large disparity in the chemical times for various combustion reactions. This implies a clear difference between the chemical and the mixing time scales.

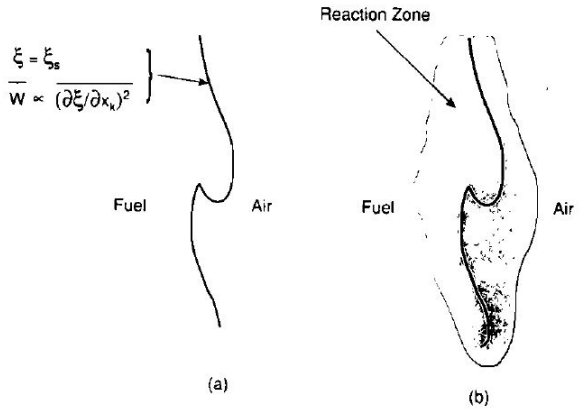

Figure 2.15: Turbulence-Chemistry interaction: (a) Flamelet and (b) Distributed reaction zone [35]

Reaction	Chemical Time Scale (ms)
$H + O_2 \leftrightarrow OH + O$	2×10^{-4}
$H + OH + M \leftrightarrow H_2O + M$	7×10^{-2}
$CH_4 + M \leftrightarrow CH_3 + H + M$	0.5
$CH_3 + OH \leftrightarrow CH_2 + H_2O$	2×10^{-3}
$CH + N_2 \leftrightarrow HCN + N$	3×10^{-3}
$O + H_2 \leftrightarrow OH + H$	2×10^{-2}
$N_2 + O \leftrightarrow NO + N$	40
$CH_4 + OH \leftrightarrow CH_3 + N_2O$	2×10^{-4}
$CO + OH \leftrightarrow CO_2 + H$	2×10^{-2}
$CH_2 + N_2 \leftrightarrow HCN + NH$	200

Table 2.3: Chemical Time scales from a 10 bar combustor [35]

One dimensionless quantity that represents the comparison between the flow time scale and the chemical time scale is the Damköhler number (Da).

$$Da = \frac{Flow\ time\ scale}{Chemical\ time\ scale} \tag{2.22}$$

In general, the flow time scale is defined as the ratio of the turbulent length scale l_t to the turbulence intensity u'. Chemical time scale is defined as the ratio of the flame thickness δ to the laminar flame speed s_L.

$$\tau_{flow} = \frac{l_t}{u'} \tag{2.23a}$$

$$\tau_{chemical} = \frac{\delta}{s_L} \tag{2.23b}$$

Another dimensionless quantity relating the chemical time scale and the Kolmogorov time scale is the Karlovitz number (Ka). Qualitatively, it is the reciprocal of Da with the only difference of using a different time scale for the flow.

$$Ka = \frac{Chemical\ time\ scale}{Kolmogorov\ time\ scale} \tag{2.24}$$

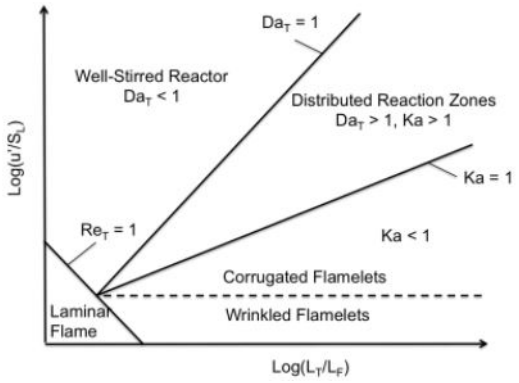

Figure 2.16: Borghi Diagram for premixed combustion [46]

A chart represented in figure 4.1 showing various turbulent combustion regimes was first put forward by Borghi [47], covering different Damköhler number, Karlovitz number and Reynolds number ranges with the corresponding flame shape characteristics. These numbers are plotted as a function of parameters of turbulence such as l_t and u'. This diagram is very useful in clear distinction between flame structures at various flow and chemistry conditions.

When u' < s_L, this zone refers to the wrinkled flame zone. The turbulent intensity is small enough to not affect the laminar flame speed, hence wrinkling the flame. When Da>1, the flow time scale is dominant over the chemical time scale. As a consequence, the reaction rates are determined by the turbulent mixing rates [12]. This corresponds to a thin reaction zone or flame sheet in which reactions take place. This covers the corrugated flamelet region in the Borghi diagram. In order to model the mixing rates, usually quantified through scalar dissipation rates, existing models such as Eddy-Break up model and Eddy-dissipation concept can be used.

On the other hand when Da<1, the process is governed by chemistry and will represent a more distributed reaction zone. This means the reaction rates are determined by chemistry. The hypothesis behind the concept of a Perfectly Stirred Reactor (PSR) is a direct application of Da regions less than one.

2.6. Chemical Mechanisms

The global combustion reaction of a hydrocarbon fuel in air is given as follows:

$$C_xH_y + (x + (y/4))(O_2 + 3.76\,N_2) \longrightarrow xCO_2 + y/2\,H_2O + 3.76\,(x + (y/4))\,N_2 \tag{2.25}$$

In case of combustion, there are a lot of complexities in chemistry, with the involvement of various radicals and intermediate species. The reaction is not elementary (with single collision between reactants) anymore and may involve multiple, preferential interactions along with diffusion. Hence, combustion is not a single step reaction and takes place as a sequence of elementary reactions. The collection of such elementary reactions leading to the final product is called a mechanism.

In the scope of natural gas combustion, various chemical mechanisms have been proposed with the involvement of different number of species and reactions. This section will explain the relevant chemical mechanisms that represent the combustion of natural gas at representative pressures and temperatures.

2.6.1. GRI-Mech 3.0

GRI-Mech 3.0 was first developed in 1999, by Smith et al. [43] of the Gas Research Institute and University of Berkeley. This mechanism was modelled to simulate natural gas combustion along with NO_x formation and reburn chemistry. It consists of 325 reactions and 53 species.

The advantage of this mechanism is that it includes C_2H_6 and C_3H_8 kinetics, which are important constituents of natural gas. It has been been optimized for the following conditions,

- Pressures between 10 torr and 10 atm
- Temperatures between 1000 and 2500 K
- For premixed systems, an equivalence ratio range of 0.1-5

However, in certain cases, older version of GRI Mech 2.11 has been reported to have given better results for NO_x chemistry. This was comprehended due to large differences between the reaction rates and pre-exponential factors of certain reactions in GRI Mech 2.11 and GRI Mech 3.0 [42]. GRI Mech 3.0, due to its robust nature with newer modifications on reaction rates has been chosen in this work.

2.6.2. Konnov Mechanism

This mechanism was developed to model C1-C3 hydrocarbon combustion and includes NO_x chemistry [48]. It contains 1200 reactions and 127 species. Various shock tube experiments and laminar flame speed measurements have been used to validate this mechanism. It was reported by Fackler [49] that the NO_x formation behaviour of this mechanism is limited in scope and does not predict the NO_x levels accurately.

2.6.3. C2 - NO_x Mechanism

Developed by Reaction Design, this mechanism was developed to model the combsution of H_2, CH_4 and C_2H_6 with NO_x chemistry included [50]. It contains detailed NO_x chemistry as in GRI Mech 3.0 with a broader operating range of pressures and temperatures [13]. This mechanism consists of 694 reactions and 100 species. On the downside, this mechanism does not include C_3H_8 kinetics.

2.6.4. C1-C3 Mechanism (Version 1412)

This mechanism was modeled by the CRECK Modeling group of Politecnico Di Milano by Ranzi et al.(hydrocarbon mechanism) [51], Faravelli et al. [52], Frassoldati et al. [53] and Cuoci et al. [54] (NO_x mechanisms). This mechanism simulates the partial oxidation, combustion and pyrolysis reaction of C1-C3 hydrocarbons with detailed NO_x chemistry. The high temperature mechanism with NO_x consists of 2141 reactions and 115 species.

2.7. Chemical Reactor Modelling

In chapter 1, a brief comparison has been made to weigh out the pros and cons of different methods of modelling emissions. Chemical Reactor Network (CRN) modeling was adopted to be the modelling approach in this work. This section will cover the types of reactors, its corresponding governing equations and existing work on CRN emission models. Within the scope of gas turbine combustion, where intense mixing with varying flow and temperature fields are present, two types of reactors can be used to model the physics.

- Perfectly Stirred Reactor (PSR) or Continuously Stirred Tank Reactor (CSTR)
- Plug Flow Reactor (PFR)

2.7.1. Perfectly Stirred Reactor

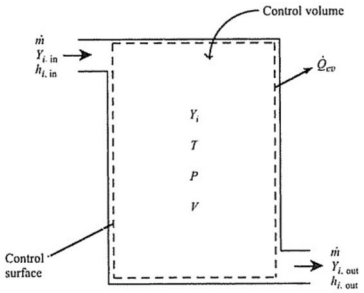

Figure 2.17: Perfectly Stirred Reactor [40]

A Perfectly Stirred Reactor is an ideal reactor in which perfect mixing takes place inside a specified control volume. Inside a PSR, mixing is uniform in space and assumed to be rapid and instantaneous, such that there are no temperature or species gradients. In addition, the temperature and concentration inside the combustor volume is equal to the outlet conditions [42].

The criterion to use PSR is when the Damköhler number is less than one (Da<1). The PSR hypothesis is valid in regions where turbulent eddy motion time scales are smaller compared to the chemical time scale. Since the mixing is so fast, chemistry becomes the rate determining factor [23]. The basic governing equations corresponding to a PSR are as follows [19].

Mass Conservation

Overall Mass conservation in a control volume is given by,

$$\frac{dm}{dt} = \sum \dot{m}_{in} - \sum \dot{m}_{out} + \dot{m}_{wall} \tag{2.26a}$$

Equation 2.26a is the equation used in Cantera [19] that includes mass flow through permeable walls. In this modelling case, $\dot{m}_{wall}$ is not relevant due to the absence of permeable walls and hence can be neglected.

Species Conservation

In addition to mass conservation, species also must be conserved. Since there is destruction as well as generation inside the control volume,

$$Input + Generation = Output + Accumulation \tag{2.27a}$$

$$\dot{m}_{in} + \dot{m}_{k,generated} = \dot{m}_{out} + \dot{m}_{accumulated} \tag{2.27b}$$

$$\dot{m}_{k,generated} = V\dot{\omega}MW + \dot{m}_{wall} \tag{2.27c}$$

$$\frac{d(mY_k)}{dt} = \sum \dot{m}_{in}Y_{k,in} - \sum \dot{m}_{out}Y_{k,out} + \dot{m}_{k,generated} \tag{2.27d}$$

where Y_k is the mass fraction of species k, V is the reactor volume in m^3, MW is the molar mass of the species k in $\frac{kg}{mol}$ and $\dot{\omega}$ is the chemical source term in $\frac{mol}{m^3 s}$

Energy Conservation

In case of a PSR (or called a ideal gas reactor in Cantera), energy must also be conserved. Since the volume of the PSR is fixed in our case, the internal energy U should be the state variable. The ideal

gas reactor model in Cantera takes the reactor temperature T as the state variable.

$$U = m\sum_k Y_k u_k(T) \tag{2.28a}$$

$$\frac{dU}{dt} = u\frac{dm}{dt} + mc_v\frac{dT}{dt} + m\sum_k \frac{dY_k}{dt} \tag{2.28b}$$

$$mc_v\frac{dT}{dt} = -p\frac{dV}{dt} - \dot{Q} + \sum_{in}\dot{m}_{in}\left(h_{in} - \sum_k u_k Y_{k,in}\right) - \frac{pV}{m}\sum_{out}\dot{m}_{out} - \sum_k \dot{m}_{k,gen}u_k \tag{2.29}$$

The total internal energy U is defined as the mass fraction weighted sum of all the component specific internal energies. This is represented in equation 2.28a. Here, m represents the mass (in kg) contained in the control volume. Equation 2.28b and 2.29 shows the unsteady internal energy equation to derive a state equation for temperature. The mean residence time in a PSR is given by the following expression,

$$\tau_{res} = \frac{\rho V}{\dot{m}} \tag{2.30}$$

2.7.2. Plug Flow Reactor (PFR)

A Plug Flow Reactor (PFR) is also called a tubular reactor, in which the flow moves as a ”plug” or accumulated mass in the axial direction. The concentration of reactants keep changing in the axial direction. The main assumption behind a PFR is radial mixing and no axial mixing. In other words, a fluid element upstream of the reactor does not mix with another which is axially spaced and mixing is only in the transverse direction [42]. Also, it is a steady state reactor with continuous flow and possesses uniform properties in the axial direction. Similar to a PSR, a PFR is also governed by mass, momentum, species and energy conservation, as shown in figure 2.18.

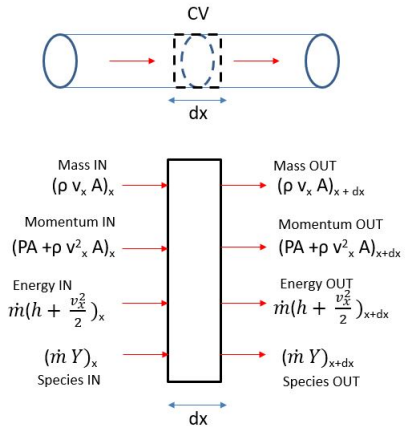

Figure 2.18: Control Volume Approach in PFR [40]

Since the flow is considered steady and one-dimensional, only the x direction equations are to be solved and other spatial derivatives along with the unsteady term are eliminated. The mass conservation is given by:

$$\frac{d(\rho u_x A)}{dx} = 0 \tag{2.31a}$$

Species conservation is given as [23]:

$$\frac{dY_i}{dx} = \frac{\dot{\omega} MW A}{\dot{m}} \tag{2.32a}$$

Energy conservation

$$\frac{\mathrm{d}(h + \frac{v_x^2}{2})}{\mathrm{d}x} + \frac{\dot{Q}'' P}{\dot{m}} = 0 \tag{2.33}$$

$$\frac{\mathrm{d}T}{\mathrm{d}x} = \frac{v_x^2}{\rho c_p}\frac{\mathrm{d}\rho}{\mathrm{d}x} + \frac{v_x^2}{c_p}\left(\frac{1}{A}\frac{\mathrm{d}\rho}{\mathrm{d}x}\right) - \frac{1}{v_x \rho c_p}\sum_{i=1}^{N} h_i \dot{\omega}_i MW_i \tag{2.34}$$

Equation 2.33 can be expanded and an expression for the temperature derivative is obtained in equation 2.34.

2.7.3. Existing CRN Models

Bragg [55] was the first to introduce the modeling concept of a combustor with a PSR-PFR configuration. He suggested that in the PSR the chemical time is assumed to be much slower than the mixing time and chemistry becomes the rate limiting step of combustion process. He stated that the whole combustion process inside the combustor volume can be split as two distinct zones, with the flame contained in the PSR and the dilution zone as the PFR.

Models built with air as oxidizer

Nicol et al. [36] built CRNs to simulate lean premixed combustion at atmospheric pressure, based on CFD results. They tested different configurations of CRNs to check which combination has good agreement wiht the experiments. Combinations such as single PSR (also called WSR - Well Stirred Reactor), PSR + PFR, parallel PSR and PFR combinations were built and compared with each other. This is shown in figure 2.19. The model results were compared with jet-stirred reactor experiments of nominal residence time of 1.7 ms. Out the tested reactor network configurations, the adiabatic PSR (arrangement A) and PSR + PFR with recirculation (arrangement C) had good agreement with the experimental NO_x levels. However, the CO levels were over predicted by a factor of 2 to 3.

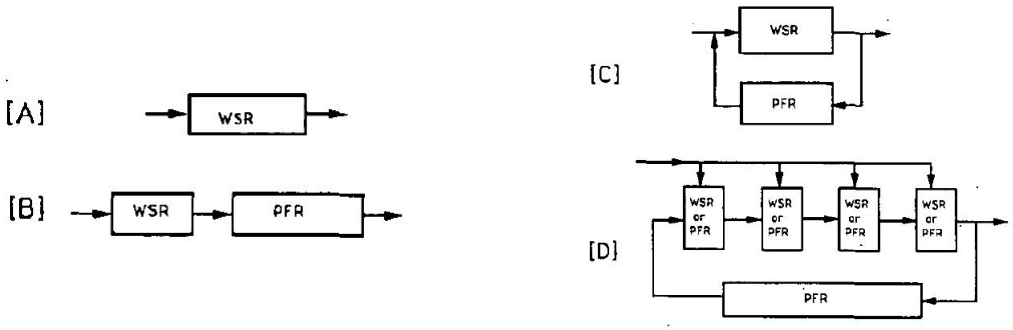

Figure 2.19: CRN Combinations used by Nicol et al.[36]

Iyer et al.[56] evaluated the emission performance for syngas combustion on diffusion, lean premixed and rich catalytic combustors, using a series of PSRs. The volumes representing different reaction zones were chosen based on existing correlations and typical reaction times. Their model consisted of 3 PSRs connected in series as shown in figure 2.20. The first one represented the main flame reactor, second the secondary burning reactor and the final volume was set to match the overall residence time of the combustor.

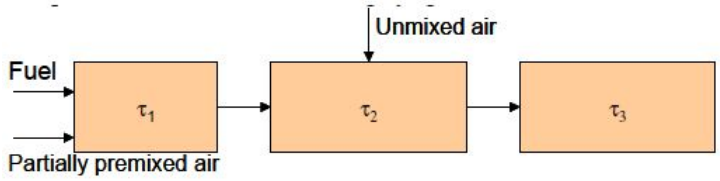

Figure 2.20: CRN used by Iyer et al. for lean premixed combustion [56]

They studied the sensitivity of emissions due to change in degree of premixing, pressure changes, reactant temperature changes and residence time effect. The model worked well in predicting the NO_x trends. The model results showed that when the degree of premixing was reduced by 20%, the NO_x and CO levels increased by a factor of 2.

Rutar et al. [57] conducted an experiment of lean-premixed combustion of methane/air flames on a jet-stirred reactor and validated the results using a 2 reactor model. A broad range of residence times (0.5-4.0 ms) and pressures (3-6.5 atm) were tested and validated using reactor modeling. GRI-Mech 3.0 [43] was used to model their CRN. In order to split the volume fraction between the 2 PSRs used in the CRN, the volume of the first reactor was increased till lean blow out of the flame occurred. Consequently, the volume of the second reactor was fixed to match the overall residence time of the JSR. This volume was cross validated by estimating the turbulent flame brush thickness δ_T based on the known values of turbulence intensity u' and turbulent diffusivity.

Figure 2.21 shows the variation of the volume fraction of the first reactor with respect to the total volume, as a function of residence time. It was observed that for lower residence times, the volume factor was close to 100% of the reactor volume, which means the whole JSR was modelled as a single PSR. On the other hand, for higher residence times, volume fractions close to 0% of the reactor volume matched with the experimental data. They concluded that smaller volume fractions implied smaller turbulent flames. It was concluded that NO_x can be predicted accurately by splitting the volume as a flame zone and a post flame zone at higher residence time. For lower residence times, the whole volume could be modelled as a single PSR.

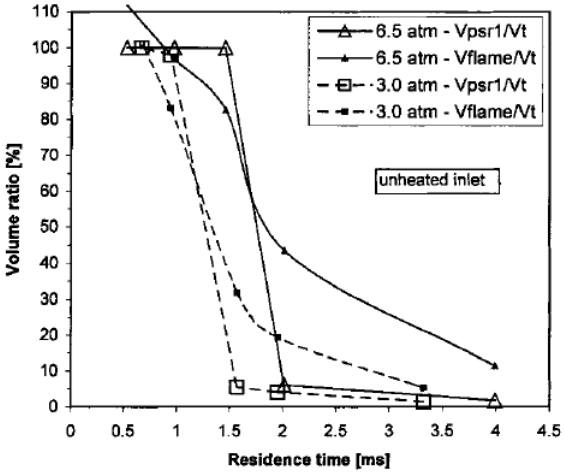

Figure 2.21: V_{PSR1}: Volume of the first PSR, V_{flame}: Volume of PSR from flame correlations, Variation of volume fraction of different network configurations with residence times [57]

Similar to the above approach, Fackler [49] modeled a CRN of lean premixed combustion for alternative fuel application. The experiments were conducted in a jet stirrred reactor at ambient pressure. An extension of this work was published by Fackler et al. [58] using GRI-Mech 3.0 based on CFD results as pre-requisite data. They used a 3-PSR modeling approach, of which PSR1 was the turbulent flame zone, PSR2 represented the recirculation reactor. PSR3 was called the shear reactor which represented the mixing of cold reactants and hot recirculated products, simulating a strained turbulent premixed flame. PSR1 representing the flame zone was also modelled using the volume at which blowout occurred. Their network is shown in figure 2.22. NO_x emissions were studied and contribution of various NO_x formation pathways were explained using their model. NO_x levels from the model had reasonable agreement with the experimental data.The model also predicted an increase in NO_x as the fuel changed from pure CH_4 to pure hydrogen due to both the Zel'dovich and N_2O pathways. Similar behaviour was observed from the model for syngas combustion.

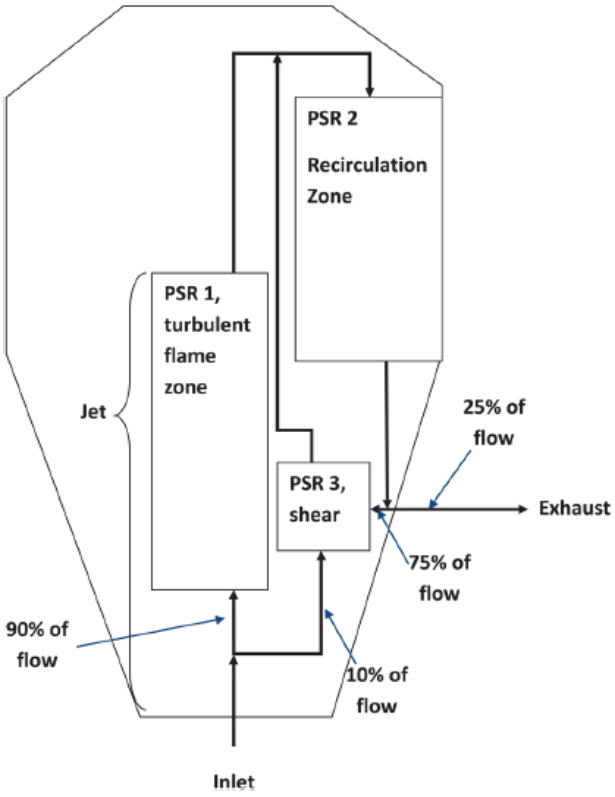

Figure 2.22: CRN of Fackler et al.[58]

Rosati [13] modelled lean premixed combustors operating on hydrogen fuel and built CRN models with similar methodologies. As shown in figure 2.23, the network composed of a PSR-PFR configuration. The PSR zone was further subdivided into a 3-reactor pattern, which was the default configuration of CHEMKIN [20]. This consisted of a mixer, flame reactor and recirculation reactor. The mixer reactor represented the flow region between the inlet nozzle and the start of the flame front. The length of the flame reactor was fixed based on mean flame front probability as defined in literature. In addition, heat loss to the surroundings was implemented through a heat loss function, which was defined based on the flame temperature and the experimental combustor exit temperature. The emission trends were reproduced through this modeling approach. The simulation results were obtained within 2 minutes. Parameters such as mass flow rate was a direct indicator to control the residence time and had an influence on the NO_x levels.

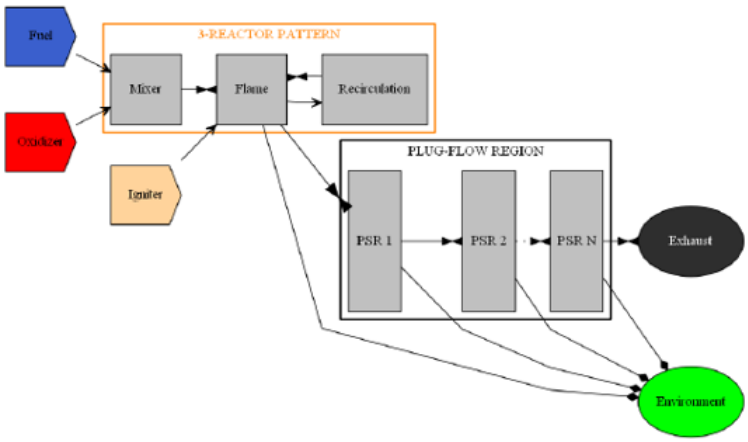

Figure 2.23: CRN architecture of Rosati[13]

A similar approach has been employed by Talboom [42] to model hydrogen premixed combustion. The variation in CRN architecture is an extra post-flame reactor between the PSR and PFR zone, which accounts for the unmixedness in the combustor flow field, as shown in figure 2.24. A part of the oxidizer directly flows into this post flame reactor in order to simulate unmixedness. The modelling of the experimental setup produced similar results of the previous CRN model by Rosati. NO_x levels were predicted with reasonable agreement.

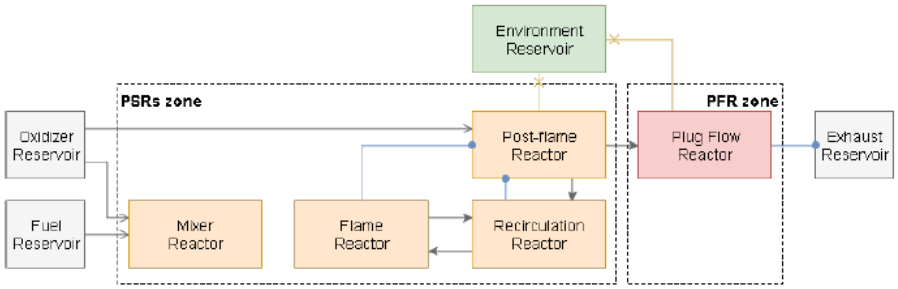

Figure 2.24: CRN architecture of Talboom [42]

Both of the above works were modelled using Cantera [19]. Instead of imposing the residence times on the reactors, the volume of each reactor was imposed based on flame front probability fields and flow fields.

Elkady et al. [59] studied perfectly premixed combustion using a combustor test rig along with a chemical kinetic model of natural gas-air combustion. They used a PSR-PFR network to model the flow physics of the test rig (As shown in figure 2.25). In this work, to split the volume between PSR and PFR, the chemical time scale has been utilized. The volume of the PSR is set in such a way that the residence time in it is equal to the chemical time scale.

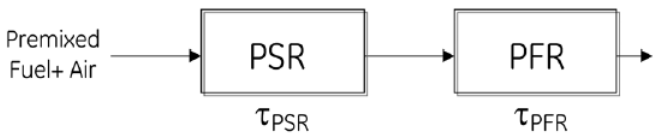

Figure 2.25: CRN of Elkady et al.[59]

The following correlation was used to estimate the chemical time scale,

$$\tau_{cts} = \frac{\alpha}{s_L^2} = \frac{\frac{k}{c_p}}{\rho_u s_L^2} \tag{2.35}$$

where k is the thermal conductivity of the gases in $\frac{W}{mK}$, C_p is the heat capacity of the gases $\frac{J}{kgK}$ and ρ_u is the density of the unburned reactants. They made a choice to extract values of k and C_p at an average temperature between the burned and unburned gases. ρ was chosen to be the density of the reactants. In a highly turbulent flame region in a leaner regime, the kinetics of the reactions slow down. Hence, the whole process is governed by chemistry and thus it becomes the dominating time scale [49].

Models based on EGR in gas turbine conditions

Li et al. [27] were one of the pioneers to make use of chemical kinetic validation of NO_x formation in gas turbines employing EGR. They based their qualitative approach based on the previous experiments of Elkady et al. [9, 60]. They presented CHEMKIN simulation results for natural gas combustion in EGR environment and at high operating pressures. A broad parametric study over a range of pressures, EGR ratios and quantitative results of the NO_x formation pathways in the new regime was presented in this work. They stated that EGR can lead to around 50% reduction in NO_x emissions at the same flame temperature in comparison to air. They also made use of a PSR PFR network, in which the overall residence time of around 26 ms was fixed. This value was based on the above mentioned experimental measurements. The PSR residence time was fixed at 1 ms and remaining 25 ms was imposed on the PFR, as shown in figure 2.26.

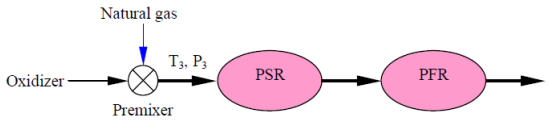

Figure 2.26: PSR-PFR Network used by Li et al.[27]

2.8. Exhaust Gas Recirculation

The general working principle of EGR has been explained in chapter 1. A schematic of EGR is shown in figure 2.28.

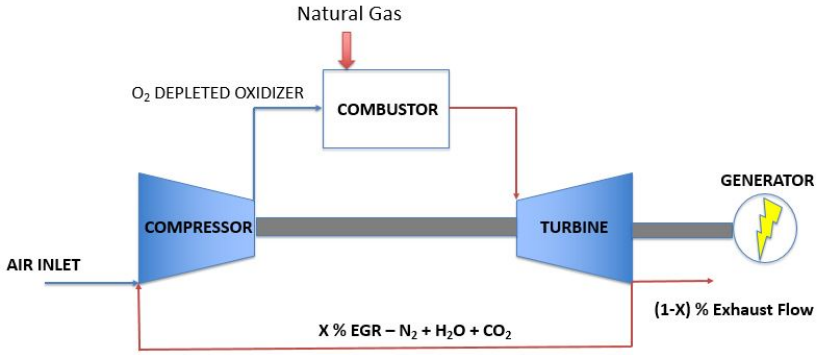

Figure 2.27: EGR layout : Fraction of exhaust gas is fed into the compressor inlet, preheating the oxidizer and depleting some fraction of O_2 in the oxidizer

In EGR applications, it is important to know the definition of EGR ratio. The ratio between the volume of flue gas recirculated to the GT inlet to the total volumetric flow at the exhaust is defined as the EGR ratio.

$$EGR\ Ratio = \frac{Volume\ of\ recirculated\ flue\ gas}{Total\ Volume\ of\ flue\ gas} \tag{2.36}$$

Experimental work and chemical modeling to analyze operability and emissions study with EGR was conducted on a combustor test rig [9, 60, 61]. Elkady et al. [9] have suggested that safe and stable operation up to 35% EGR can take place with a pilot flame. Further studies by Ali et al. [8] on micro gas turbines thermodynamic modeling showed that safe operations up to 55% EGR is possible. This corresponded to a increase in level of CO_2 from 1.6% to 3.7% by mol in the flue gas. This is ideal situation for efficient carbon capture (reduction of mass flow and increase of CO_2 content).

2.8.1. Chemical and physical effects of introducing EGR

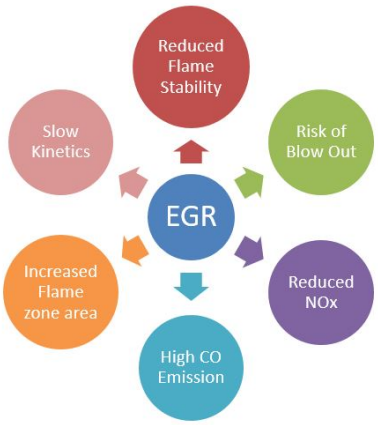

Figure 2.28: Effects of introducing EGR into the system

There are substantial changes in the flame physics and the chemical reaction rates due to this transition. Arai [62] explained the consequence of inert dilution in the oxidizer as slowdown of chemical kinetics. The presence of CO_2 slows down the reaction rates and the flame zone expands through space as an effect of this. Bolland and Mathieu [63] stated that the minimum oxygen concentration at the combustor inlet can go as low as 16-18 % by volume in standard gas turbines. Ditaranto et al. [64] and Evulet et al. [61] have proved that oxygen levels can decrease up to 14% at the inlet.

Although the advantage of using EGR leads to reduced NO_x emissions, there are certain limitations that need to be noted,

Reduction of Flame Stability : Flame stability is the outcome of complex aerodynamics and chemistry. When the equivalence ratio is reduced by increasing the air flow rate for a fixed fuel flow, the flame becomes unstable and blows off at a particular ϕ value. This phenomenon is called Lean Blow Out (LBO). When EGR is introduced in combination with lean premixed combustion, there are higher risks of blowout. This reduces the flame stability.

Laminar flame speed has been proven to be a good first order indicator of flame stability [64]. The flame has to be propagate at or above a certain speed in order to sustain the combustion reaction. Introducing inerts in the oxidizer reduces the laminar flame speed coupled with reaction rate deceleration and thus reduces the flame stability [65]. Therefore, higher EGR levels can reduce the flame speed drastically and can push the flame towards high risk of LBO.

Increase in CO Emissions : Elkady et al. [9] put forth few major reasons for increased CO emissions in the EGR regime. They are,

- Vitiation of the oxidizer leading to reduced O_2 for complete combustion
- Since CO_2 is a constituent of the oxidizer, it can dissociate at high flame temperatures to give CO.

$$CO + OH \rightleftharpoons CO_2 + H \tag{2.37a}$$
$$H + O_2 \rightleftharpoons O + OH \tag{2.37b}$$

At lower rates of mixing, CO_2 causes the reversal of reaction 2.37a to take place. This leads to increased CO formation due to CO_2 dissociation. It can thus be inferred that CO_2 is not just a diluent but a very active participant in species formation and kinetic slowdown. Liu et al. [66] found that at higher temperatures, H radicals are removed from reaction 2.37b leading to lesser OH. Due to the lack of OH, in reaction 2.37a CO formation is favoured to counteract this deficit.

Component Degradation : Since high temperature corrosive exhaust gases are introduced into the compressor, it may lead to thermal degradation of the compressor blades. However, this effect does not take place immediately in the system.

3

Model Development and Validation

In this chapter, the steps involved in developing the CRN model for emission prediction is discussed. Firstly, the flow field of swirl stabilized gas turbine flames is described. Based on chemical time scale approach and recirculation zone correlations, a CRN model is developed and described. The CRN model is validated against the flame cases of Elkady et al. [9, 60], Cheng et al. [67] and Sidwell et al. [68].

3.1. Flow Field of Swirl- Stabilized Flames

In the CRN approach, the type of reactor that best represents the physics is chosen based on the overall mean velocity flow field. This drives the necessity to understand the mean flow structure of swirl stabilized flames in gas turbines. Stopper et al. [69–71], Wehr et al. [72] and Weigand et al. [73] studied the flow field, temperature distribution and species distribution of swirl stabilized premixed and diffusion flames in gas turbine combustors using OH-PLIF and PIV techniques. Various pressures, temperatures and swirl numbers have been analyzed to comprehend the flow physics.

Figure 3.1a and 3.1b show the results of the mean flow field of diffusion and premixed flames respectively. The red streamlines in figure 3.1a represent the reversal of flow and the black ones represent the forward flow. A clear central recirculation zone is evident from the vector plot, indicating the swirl stabilizing mechanism. Similarly in figure 3.1b, the arrows in the lower velocity regions depict the recirculation zone. Large velocity variations are seen locally as an effect of pressure gradients. On the whole, the commonality between the two images is that the recirculation zone extends to approximately half the length of the combustor. Even though in figure 3.1b the whole length was not visualized, the end of the image indicates half the length of the test rig of Stopper et al. [69].

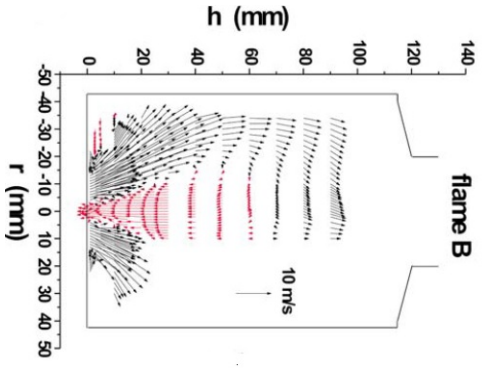

(a) Flow field inside the combustor rig of Weigand et al. (ϕ= 0.75) [73]

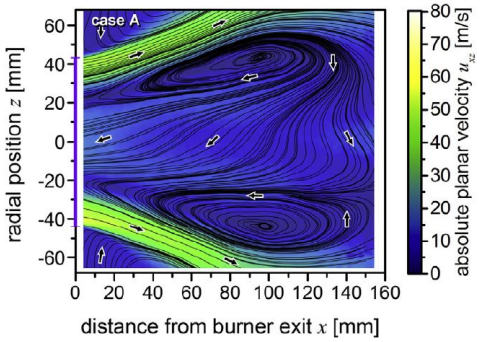

(b) Flow Field in a premixed flame [69]

Figure 3.1: Flow field of a swirling flame inside a gas turbine combustor

This characteristic of extension to approximately half the length implies that the major part of mixing and temperature changes occur up to the recirculation region. After this region, the streamlines seem to become parallel to each other and travel as ”lumps”, in which one lump does not interact with the axially displaced neighbouring lump (plug flow behaviour).

3.2. CRN Architecture

3.2.1. Recirculation Zone Length

In general, the length of the recirculation zone depends on an important parameter called the swirl number.

- **Swirl Number:** The geometric swirl number S is a non-dimensional quantity defined as the ratio of the axial flux of the angular momentum to the axial flux of the axial momentum. This is represented in equation 3.1.

$$S = \frac{\int_0^R u(2\pi w \rho r)dr}{\int_0^R u(2\pi u \rho r)dr} \tag{3.1}$$

where u is the axial velocity (m/s), w is the tangential velocity (m/s), r is the radius (m) and R is the maximum radius at the nozzle exit (m). The recirculation zone length is directly dependent on the swirl number S and the geometric design of the swirler. Since the objective of the research is to accurately model the emissions using CRNs, the effect of swirl on NO_x should also be considered. Claypole and Syred [74] investigated the effect of swirl aerodynamics on the NO_x emissions. They concluded that on changing the swirl number, NO_x formation remained unchanged despite the high temperature and residence time of corresponding recirculation zones. This is shown in figure 3.2. Majority of the NO_x is formed in the flame zone and the recirculation is a mechanism to stabilize the flame.

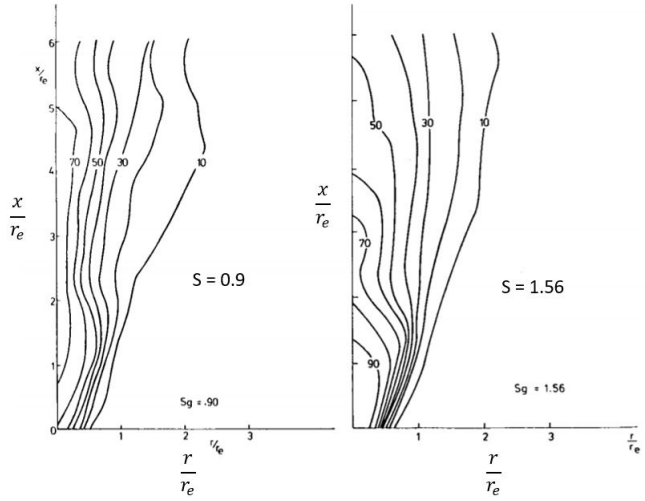

Figure 3.2: Contours of NO_x for different axial and radial positions (r_e : exit radius of nozzle, x: axial position , r: radial position [74]

Since the swirl number does not have an impact on the NO_x emissions, a simplified correlation with equivalence ratio for recirculation length can be considered.

Based on the vector plot of Weigand et al. [73] shown in figure 3.1a, a correlation can be found out between the equivalence ratio and the length of the recirculation zone. In order to generalize the trends, the axial and radial positions can be normalized with the length of the combustor L and diameter of the inlet nozzle D (25 mm) of experimental setup. This is shown in figure 3.3.

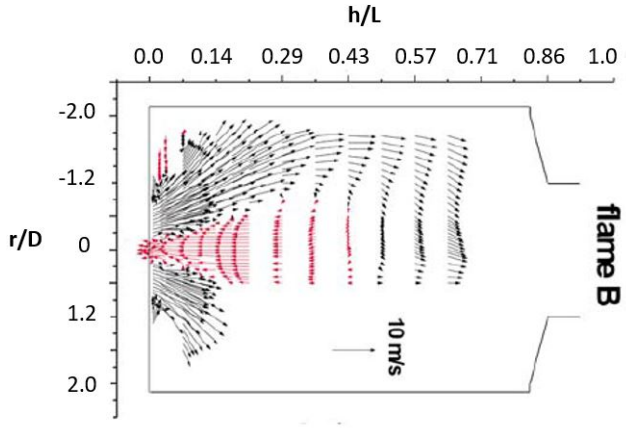

Figure 3.3: Axial position normalized with L and radial length normalized with D ; Modified from Weigand et al. (L : Combustor Length , D : Exit diameter of nozzle [73]

Figure 3.4 shows the comparison of two flames (B and C) at two different equivalence ratios ϕ =0.75 and ϕ =0.55. The marked red zone shows the recirculation zone in the combustor. For the model development, a linear interpolation was performed to establish a correlation between the normalized axial position and equivalence ratio. The same is done for the radial position as well. This is done in order to determine the volume up to which the recirculation zone extends.

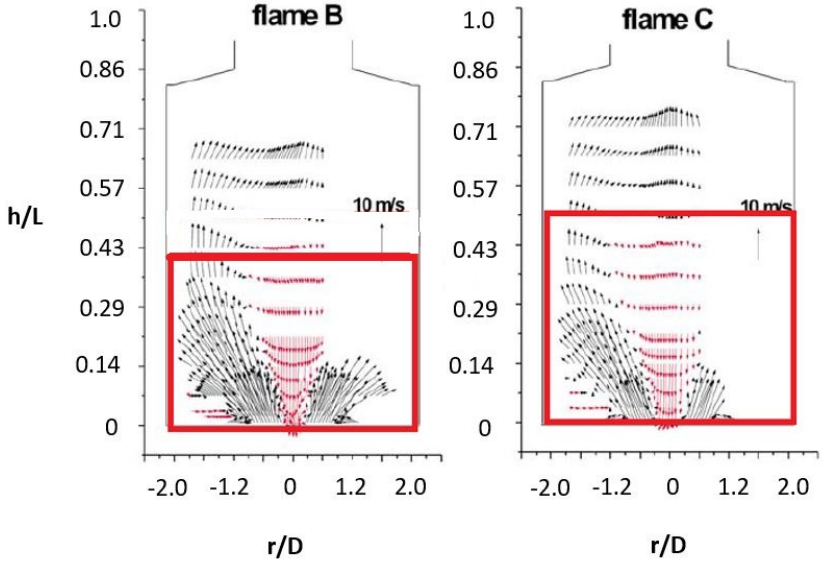

Figure 3.4: Flow Field at ϕ= 0.75 (Flame B) and ϕ = 0.55 (Flame C) [73]

The axial position correlation is found to be,

$$\left(\frac{x}{L}\right)_{recirc,zone} = 0.6925 - 0.35\phi \tag{3.2}$$

The radial position correlation is found to be,

$$\left(\frac{r}{D}\right)_{recirc,zone} = 2(1-\phi) \tag{3.3}$$

From the above correlations, an increase in equivalence ratio makes the recirculation zone smaller and narrower. When higher flame temperatures are reached the flame becomes narrower due to faster burnout.

3.2.2. Reactor Network Splitting

A clear difference in flow patterns before and after the recirculation zone is evident from figure 3.1a. The region after the recirculation is seen to be behaving in the form of parallel streamline plug flow, as explained in section 3.1. Hence, the whole combustor volume can be split into 2 zones, one with intense mixing and temperature rise and the other with close to parallel flow with radial diffusion and non-axial interaction. From the theoretical background covered in chapter 2, a perfectly stirred reactor (PSR) will best represent the recirculation zone and the downstream zone can be depicted through a plug-flow reactor.

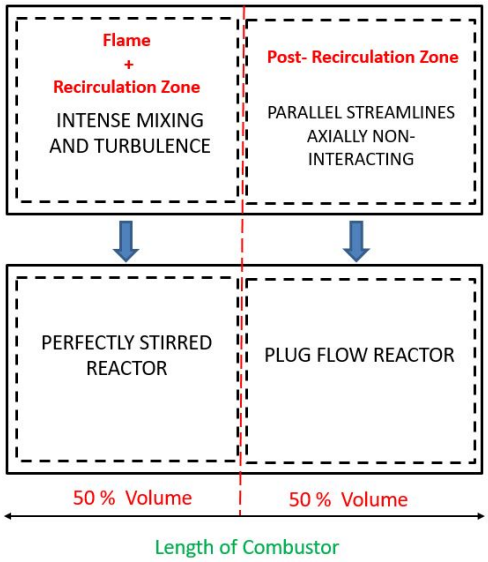

Figure 3.5: Combustor volume splitting based on flow behaviour

3.2.3. Splitting between Flame and Recirculation Reactor

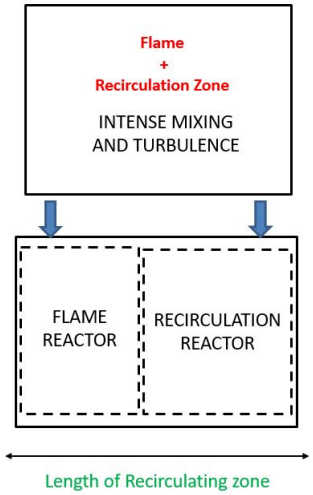

Figure 3.6: Volume splitting between flame zone and recirculation

The volume covering the recirculation zone encompasses the swirl stabilized flame. A major part of the reactions, pollutant formation and temperature rise takes place in the flame zone and its vicinity. The recirculation zone is basically the back flow of hot products into the flame zone, analogous to a feedback signal, that accelerates the ignition of the mixture. Thus, it is important to distinguish between the flame zone behaviour and the recirculation zone.

Therefore, the PSR zone is split into 2 regions namely - Flame reactor and Recirculation reactor, as shown in figure 3.6. The basis on which the volumes are split is explained in the following paragraphs.

3.2.4. Approach to determine flame reactor volume

The volume of the flame reactor influences the overall NO_x emission level of the model. Therefore, it is crucial to find the right methodology to determine its volume. Before determining the volume, the mechanism governing the process inside the flame zone has to be analyzed. The flame can be modelled using the flamelet hypothesis [44], where the ensemble of flamelets represents the whole flame. But this depicts higher Da regions (Da $\rightarrow \infty$), thus violating the PSR hypothesis [17]. The reasoning behind using a PSR is based on the Damköhler number hypothesis. A PSR is used in regions where Da $\rightarrow$ 0 , meaning the chemical time scale is dominant over the mixing time scale. In spite of intense turbulence, the volume of the flame zone is ultimately controlled by the kinetics of the reactions taking place. Additionally, lean premixed combustion combined with EGR leads to kinetic slowdown, consequently increasing the chemical time scale and decreasing Da. This implies that the chemical time scale is a valuable parameter for volume determination and corroborates the PSR hypothesis.

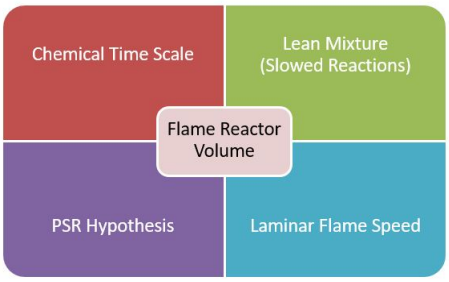

Figure 3.7: Factors governing the flame reactor volume

The methodology of using chemical time scale to determine the volume of the flame reactor was first proposed by Elkady et al. [59] to simulate natural gas-air combustion. It was also further utilized by Fackler [49] to model the JSR for emission modeling. This approach is more appropriate in this research work because the corresponding chemical time of EGR will be larger than the chemical time in air. This is a direct indication of kinetic slowdown of reactions. This approach has not been used in literature to model natural gas combustion in EGR regime and its robustness will be tested in this research work.

Chemical Time Scale Approach : The modeling approach uses the essential hypothesis that the flame reactor residence time is equal to the chemical time scale. In section 2.7.3, the chemical time scale is defined as,

$$\tau_{cts} = \frac{Flame\ Thickness}{Flame\ speed} = \frac{\delta}{s} = \frac{\frac{\alpha}{s}}{s} = \frac{\frac{k}{c_p}}{\rho s^2} \tag{3.4}$$

Here, s is the flame speed. The question now arises as to what description of the flame speed has to be used to define the time scale. There are two ways of defining the flame speed namely - Laminar Flame Speed and Turbulent Flame Speed. A simple relationship between these quantities was first proposed by Damköhler [75],

$$s_T = s_L + u' \tag{3.5}$$

where, s_T is the turbulent flame speed, s_L is the laminar flame speed and u' is the turbulence intensity of the flow. It is implied from equation 3.5 that the turbulent flame speed depends not only on the laminar speed but also on the intensity of turbulence in the flow.

A more generalized expression which is non-linear unlike equation 3.5 is given by,

$$\frac{s_T}{s_L} = 1 + a\left(\frac{u'}{s_L}\right)^b \tag{3.6}$$

where constants a and b varying for different turbulent speed models.

Correa [35] summarized on the influence of turbulence intensity on the NO_x formation chemistry. It was stated that in a lean regime, turbulence of the flow can be decoupled from the NO formation. Experiments were performed in a lean premixed combustor with 3 different kinds of flame holders namely- V-gutter with 70% blockage, perforated plate with 77% blockage and a single cup swirler. From figure 3.8, it can be observed that the NO formation does not differ significantly for all the types of flame holders. It was reported that each of the flame holders had fairly distinguishable recirculation zone shapes and hence different turbulence intensities. Thus, turbulence can be completely decoupled from NO_x chemistry in the lean premixed regime.

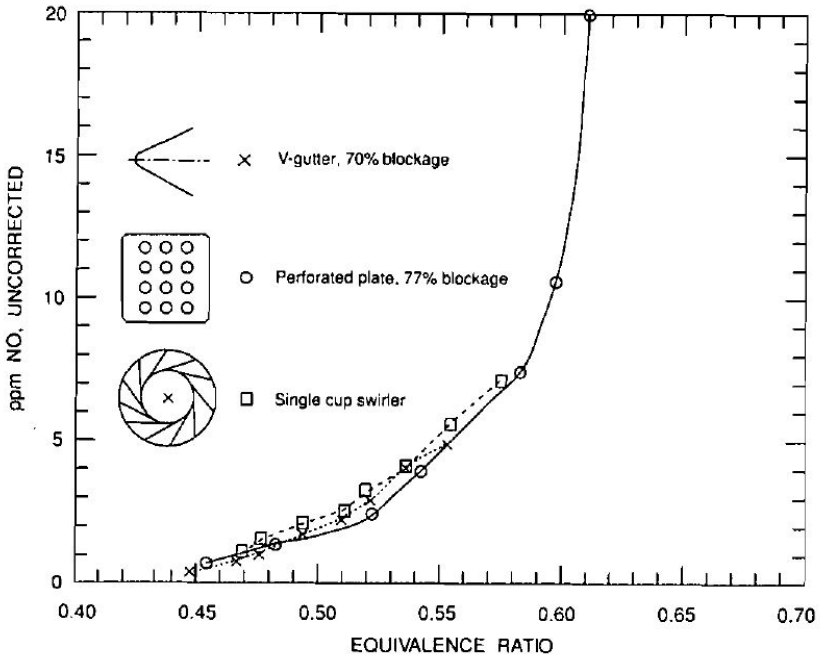

Figure 3.8: NO formation for different flame holders [35]

A turbulent flame can be seen as an ensemble of laminar flames, with an internal structure unaltered by turbulence. Even though the bulk speed of the flame travels with turbulent flame speed, local parts of the flame propagate relative to the unburnt mixture with the laminar flame speed (Figure 3.9). All the chemical reactions take place in these local regions propagating with the laminar speed. Hence, the laminar flame speed is used to define the chemical time scale.

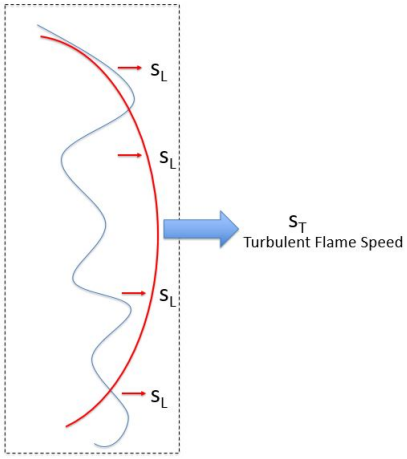

Figure 3.9: Description of turbulent flame speed as a collection of local laminar flame speeds

3.2.5. Model development methodology

The following procedure is followed for determining the volume of the flame reactor and the recirculation reactor,

- **Computing thermodynamic properties :** Thermal conductivity k and heat capacity C_p are calculated at the mean temperature. The mean temperature is computed as the average of the temperature of reactants (inlet temperature) and the temperature of products (adiabatic flame temperature). The density is computed to be the mean of the reactants and products. These properties are calculated using Cantera [19]

$$T_{mean} = \frac{T_{unburned} + T_{burned}}{2} \tag{3.7a}$$

$$k, C_p = (k, C_p)_{T_{mean}} \tag{3.7b}$$

$$\rho_{avg} = \frac{\rho_{unburned} + \rho_{burned}}{2} \tag{3.7c}$$

- **Determining Laminar flame speed s_L:** Using Cantera [19], a freely propagating premixed flame is coded to find the mixture averaged laminar flame speed. The initial conditions of pressure, temperature and composition is given from the experimental inputs mentioned in table A.1.

- **Estimating chemical time scale :** Using the values of k, C_p, ρ and s_L from the previous steps, the chemical time for a range of equivalence ratios is calculated according to equation,

$$\tau_{cts}(\phi) = \frac{\left(\frac{k}{C_p}\right)_{T_{mean}}}{\rho_{avg} S_L^2} \tag{3.8}$$

  Previous investigations using the above equation made use of the density of the unburnt products [58, 59]. However, as the density reduces by an order of 2 between the inlet and outlet, the average of the densities has been considered to compute the chemical time scale.

- **Calculating Volume of flame reactor and volume factor :** Using τ_{cts}, mass flow rate $\dot{m}$ (from experiment) and density of burned products ρ_{burned}, the volume of the flame reactor is computed. ρ_{burned} is used here because ignition and combustion takes place in the flame reactor.

This is also expressed as a function of equivalence ratios.

$$V_{flame}(\phi) = \frac{\tau_{cts}\dot{m}}{\rho_{burned}} \tag{3.9a}$$

$$FVF(\phi) = \frac{V_{flame}}{V_{combustor}} \tag{3.9b}$$

However, in the works of Rosati [13] and Talboom [42], the volumes were imposed in each reactor rather than the residence time. The residence time is imposed in each reactor to compute the volumes in this work. This is the fundamental difference in the modeling approach.

- **Calculating recirculation volume factor :** The recirculation zone is split into the flame reactor and the recirculation reactor. From equation 3.2, the length of the whole recirculation zone was estimated. When the volume of the flame reactor is divided by the cross sectional area of the combustor, a correlation for $\frac{x}{L}$ for the flame reactor can be obtained.

  Subtracting this value from equation 3.2 and multiplying the obtained value with the volume of the combustor gives the volume of the recirculation reactor. Recirculation Volume Factor (RVF) is also found out as the ratio of recirculation volume to the total volume of the combustor.

$$\left(\frac{x}{L}\right)_{flame} = \frac{V_{flame}}{A_{comb}} \tag{3.10}$$

$$\left(\frac{x}{L}\right)_{recirc} = \left(\frac{x}{L}\right)_{recirc,zone} - \left(\frac{x}{L}\right)_{flame} \tag{3.11}$$

$$V_{recirc}(\phi) = \left(\frac{x}{L}\right)_{recirc} \times A_{comb} \times L_{comb} \tag{3.12}$$

$$RVF(\phi) = \frac{V_{recirc}}{V_{comb}} \tag{3.13}$$

- **Establishing volume of plug-flow reactor :** The volume of the plug flow reactor can be calculated by subtracting the sum of FVF and RVF from the total volume of the combustor.

$$V_{plug,flow} = (1 - (FVF + RVF))V_{comb} \tag{3.14}$$

The final architecture of the CRN used in this work is visually summarized in figure 3.10.

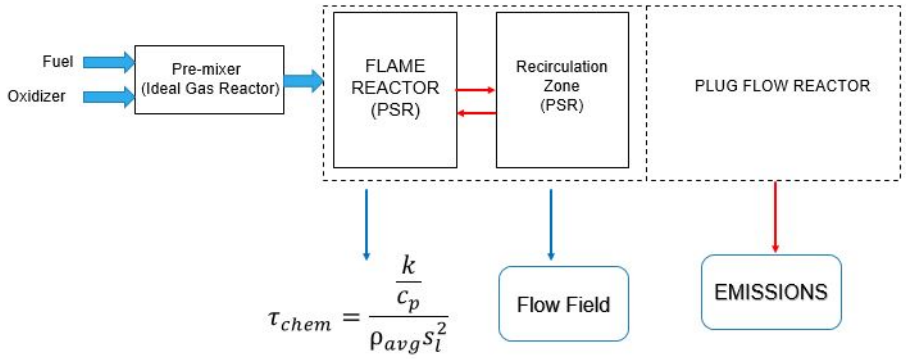

Figure 3.10: CRN Architecture used in this work

The overall structure and working of the code is summarized in figure 3.11. The computational time for each equivalence ratio is estimated to around 5-10 seconds. Depending on the range of flame temperatures, the total simulation time is in the order of few minutes.

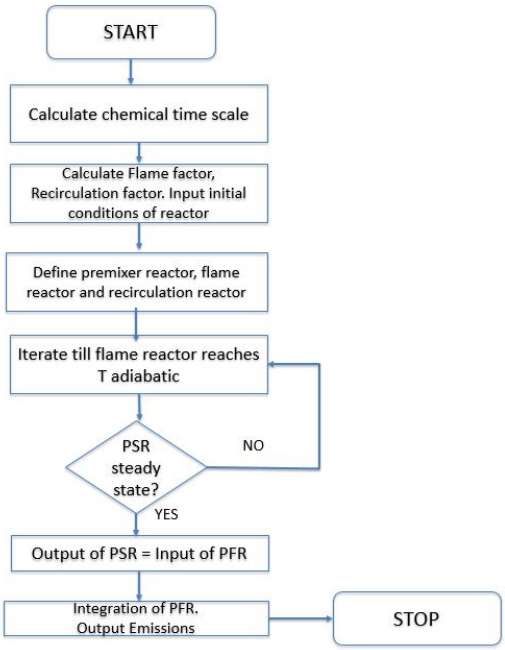

Figure 3.11: Flowchart of the code used in Cantera to simulate the model

3.2.6. Selection of common parameter for comparison

From figure 3.12, it can be seen that for a fixed equivalence ratio, there is a drop in the adiabatic flame temperature with increase in CO_2 content in the oxidizer stream. Hence, in order to attain the same flame temperature, extra fuel has to be injected. This will further increase the equivalence ratio.

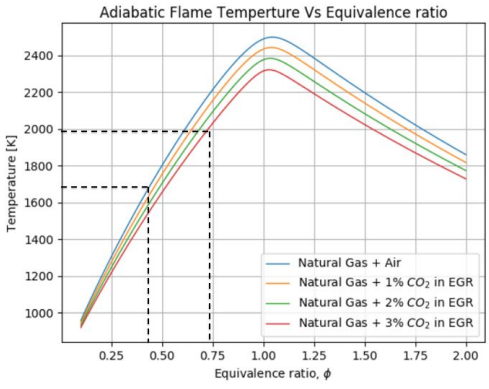

Figure 3.12: Equivalence ratio range for different oxidizer compositions between 1700 K and 2000 K

Addition of CO_2 in the oxidizer stream, increases the heat capacity of the working fluid when compared to air, as shown in figure 3.13.

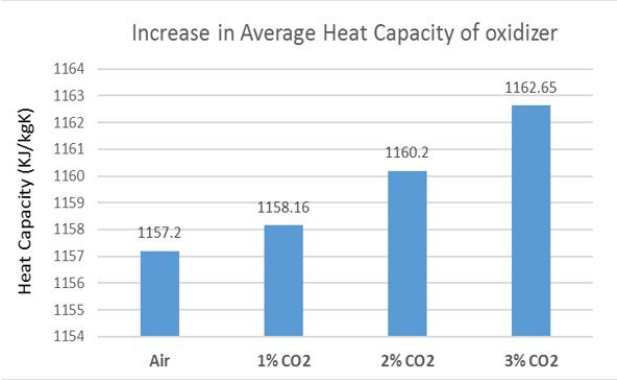

Figure 3.13: Heat capacity rise with increase in CO_2 (averaged over the range of equivalence ratios)

The increase in fuel flow can be attributed to this increase in heat capacity. This can be quantitatively proven from the energy balance in the combustor. For obtaining the same temperature difference ΔT and the LHV being the same, an increase in C_p implies an increase in the fuel flow rate. Hence, adiabatic flame temperature is used as the common parameter for comparison.

$$\dot{m}_f \times LHV = \dot{m} C_p \Delta T \tag{3.15a}$$

$$\dot{m}_f = \frac{\dot{m} C_p \Delta T}{LHV} \tag{3.15b}$$

3.2.7. Dependence on flame temperature

The overall trend of increasing laminar flame speed with increase in flame temperature is seen from figure 3.14. Another observation is the decrease in laminar flame speed with increasing CO_2 content in the oxidizer. This is an indicator of decrease in reactivity.

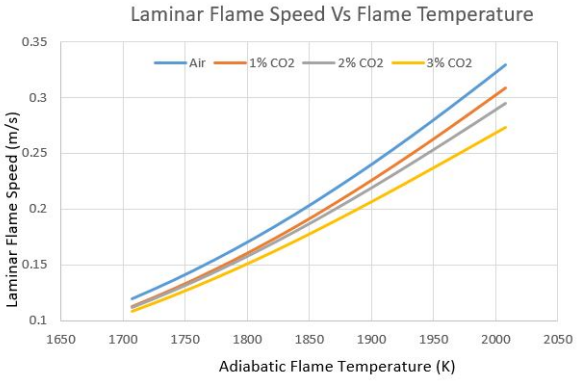

Figure 3.14: Laminar Flame Speed Vs Flame Temperature

Both the chemical time and FVF behave similarly with variation in flame temperature. It can be seen that the flame volume and chemcial time decreases with rise in flame temperature. In a physical sense, this means the flame burns in narrower volume when higher flame temperatures are achieved. When the CO_2 concentration increases, both these quantities increase. This is a sign of slow reaction rates induced by CO_2. A slow reaction rate implies a larger flame volume.

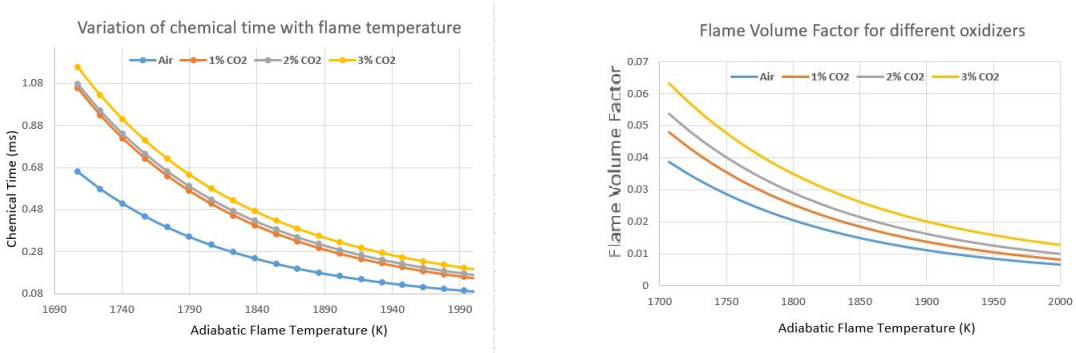

(a) Chemical time Vs Flame Temperature

(b) Flame Volume Factor Vs Flame Temperature

Figure 3.15: Variation with flame temperature

3.2.8. Model initial settings

After setting the volumes of the reactors, they are connected to each other by valves. This is done to maintain a constant combustor pressure. Table 3.1 presents the initial conditions set for the flame reactor. The igniter used to combust the fuel-oxidizer mixture is numerically modelled as a gaussian time varying mass flow of H radicals. It is modelled in such a way that this stream dies out after a certain period of time after which the combustion is self-sustained. The igniter mass flow does not the alter the outcome of emissions. It can rather be seen as a starter for the flame to sustain. This is modelled as the following using equation 3.16 and the variation is shown in figure 3.16,

$$\dot{m}_{igniter}(t) = Ae^{\left(\frac{4log(2)}{fwhm^2}\right)(t-t_0)^2} \tag{3.16}$$

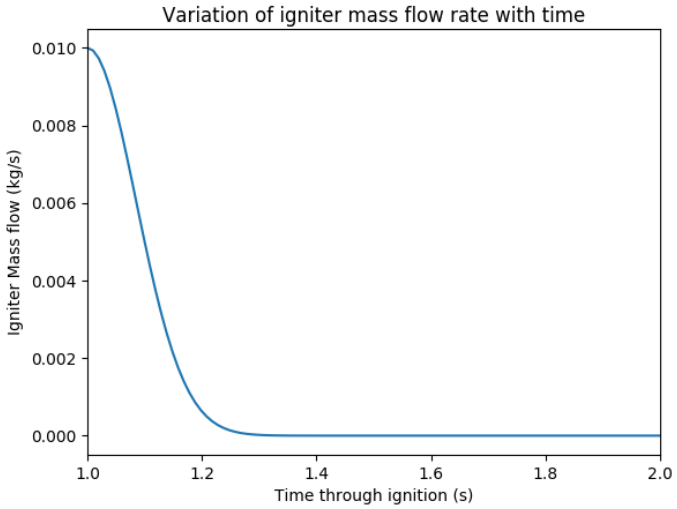

Figure 3.16: Gaussian time dependent mass flow of H radicals for ignition

Table 3.1 describes the convergence criteria and initial settings used in the Cantera code. The values of the valve coefficient and igniter amplitude are chosen based on the reduction of stiffness problems in the code.

Input	Unit	Value
Chemical Mechanism	-	GRI-Mech 3.0
Convergence Criteria	K	$T_{t+\Delta t} - T_t = 0.02$
Fuel	-	Natural Gas
Valve Coefficient	kg/s-Pa	1×10^{-5}
Igniter Amplitude	-	0.01

Table 3.1: Initial conditions and convergence criteria for model development

3.2.9. Model Assumptions

- The combustor is assumed to be adiabatic. Hence, heat loss to the surroundings or cooling by dilution air is not considered.
- All mixtures are assumed to be ideal gas mixtures. They are modelled as ideal gas reactors.
- Fast and instantaneous mixing is assumed in the flame zone.
- Local turbulence effects in the flow have not been considered. The overall flow field is simplified.
- The recirculation zone length is modelled by establishing a correlation with the equivalence ratio from previous experiments on swirl stabilized flames.
- When the products exit the flame reactor, it is modelled to have achieved the adiabatic flame temperature

3.3. Prediction accuracy of chemical mechanisms

Chapter 2 covered the relevant mechanisms pertaining to natural gas combustion, namely:

- Konnov Mechanism [48]
- C_2-NO_x Mechanism [50]
- GRI-Mech 3.0 [43]
- C1-C3 Mechanism (Ranzi Mechanism) [51–54]

There are fundamental differences in the number of species and reactions in these mechanisms, that make them distinct from each other. Hence, the prediction accuracy of emissions in the EGR regime of the combustor model is tested in this study.

Mechanism Name	Reactions	Species
GRI Mech 3.0	325	53
Konnov Mechanism	1200	127
C_2- NO_x Mechanism	694	100
C1-C3 Mechanism	2141	115

Table 3.2: Summary of available mechanisms for Natural gas combustion

In order to test the mechanisms, the experiments of Elkady et al. [9, 60] was used. Figure 3.17 clearly shows a difference in predictions of NO_x levels by each of the chemical mechanisms. Even though the overall trend of rising NO_x with flame temperature is followed, it can be seen that only GRI-Mech 3.0 and Ranzi Mechanism are closest to the experimental data points.

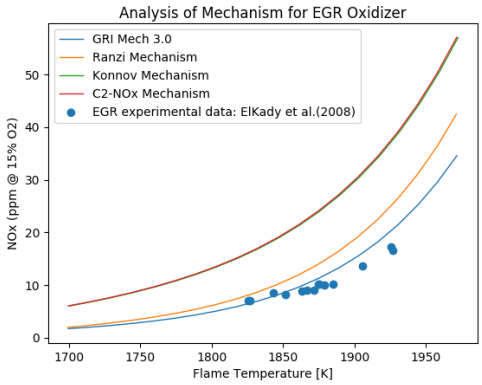

Figure 3.17: NO_x levels: Various Chemical Mechanisms (P = 10 bar)

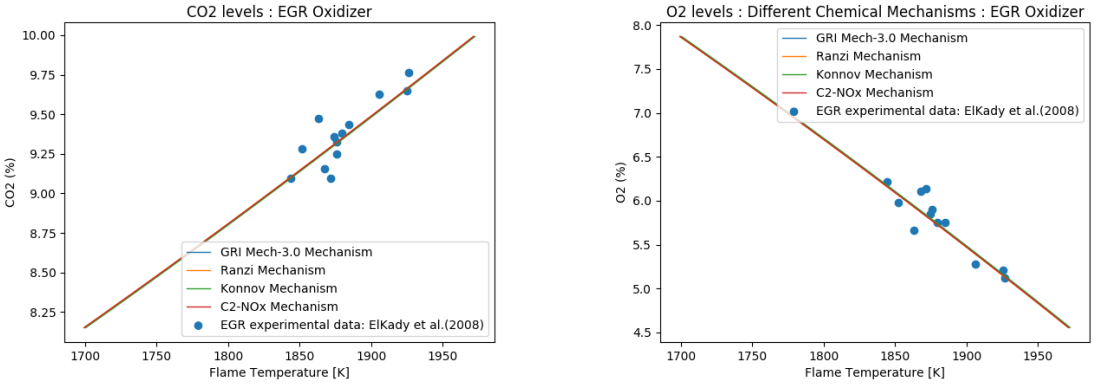

(a) CO_2 levels : Various Chemical Mechanisms

(b) O_2 levels : Various Chemical Mechanisms

Figure 3.18: CO_2 and O_2 levels (P = 10 bar)

Whereas, C2-NO_x and Konnov mechanisms over predict the NO_x levels in the model. At higher flame temperatures, they seem to over predict by a factor of 2, which is undesirable. From figures 3.18a and 3.18b, no significant differences in prediction are seen and the model is in good agreement with the experiments. It can be concluded that the inherent difference in NO_x prediction is because of the way NO_x chemistry is defined in each of the reaction mechanism. With the view of accurate NO_x predictions, GRI-Mech 3.0 has been chosen to be the base mechanism for simulations in this thesis work. In addition, the GRI-Mechanism has been reported to be very robust in various operating conditions [49].

3.4. Model Validation

In order to validate the modeling methodology, different flame cases have been utilized. All these cases possess similar flow fields and different initial conditions of the premixed mixture. Different ranges of flame temperatures have been considered to verify the validity of the model through a wide range of equivalence ratios.

3.4.1. Case 1: Natural Gas + Air / EGR : 10 bar (Elkady et al. (2008,2011))

Researchers from GE Global Research built a Dry Low NO_x (DLN) premixer combustor test rig at representative gas turbine pressure and temperature, to study the effect of EGR on the NO_x and CO emissions. In addition, tests on flame stability and combustion dynamics were studied to analyze the benefits and downfalls of introducing EGR [9, 60]. Further details about the experiment is given appendix A.

Table 3.3 and 3.4 show the composition of the fuel and oxidizer respectively as mentioned in the experiment. This is used as the input to the model. Table A.1 summarizes the experimental inlet conditions of the premixed mixture, which is used in the model. The NO_x and CO_2 trends of the model is verified with the corresponding experimental data. The reactor network is coded using Python 3.4 loaded with Cantera 2.3.0.

Constituent	Mole %
CH_4	94.22
C_2H_6	3.16
N_2	2.62

Table 3.3: Natural Gas used for the model (Taken from Li et al. [27])

Oxidizer	N2	O2	Ar	CO2
Air	78	21	1	-
EGR	78	18	1	3

Table 3.4: Oxidizer composition used in Elkady et al. [9]

Parameter	Value
Inlet Pressure	10 atm
Inlet Temperature	700 K
Total Mass flow of oxidizer	1.4 kg/s
Dimensions of Combustor (L ×B ×H)	12.2 ×2.4 ×2.4 $inch^3$

Table 3.5: Experimental Conditions of Elkady et al. [9, 60]

In figure 3.19, the NO_x and CO_2 levels are plotted as a function of the adiabatic flame temperature. The model is in good agreement with the experimental data for both these emissions. Figure 3.19a shows a clear decrease in NO_x levels for the same flame temperature, when EGR is introduced into the system. This is due to the presence of oxygen depleted oxidizer, that slows down the reaction kinetics as well as hinders the NO_x formation.

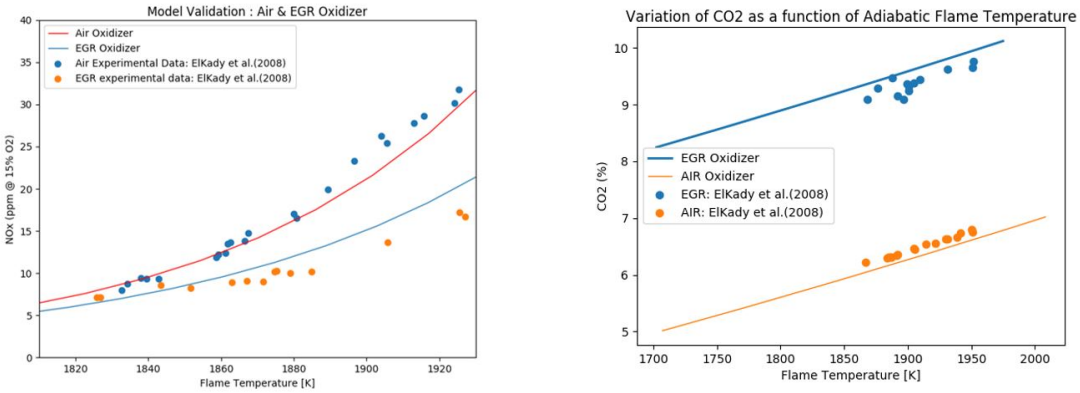

(a) NO_x levels : Experiment Vs Model

(b) CO_2 levels : Experiment Vs Model

Figure 3.19: Model Validation with the case of Elkady et al. [9]

Slight deviations start to occur at higher flame temperatures. This could possibly be due to the adiabaticity of the combustor model. In real time scenarios, the experimental setup is far from being adiabatic and has heat loss to the surroundings. Heat loss would alter the temperature levels inside the combustor and thus alter the NO_x levels. Figure 3.19b presents an increase in CO_2 levels for a given flame temperature, due to the presence of extra CO_2 in the oxidizer.

3.4.2. Case 2: Natural Gas & Natural Gas + H_2 in air (Cheng et al. (2009))

Laboratory experiments in gas turbine and atmospheric conditions were performed on the SimVal combustor facility of the National Energy Technology Laboratory by Cheng et al. [67].

Emissions from a Low-Swirl Injector stabilized lean premixed combustor have been reported in this work. More details on the experimental setup is mentioned in appendix A. The experimental conditions which were used for the model are summarized in table 3.6.

Parameter	Unit	Value
Inlet pressure	bar	10
Inlet temperature	K	600
Combustor Diameter	m	0.18
Combustor Length	m	0.31
Nozzle Diameter	m	0.0571
Fuel + Oxidizer	-	Natural Gas + Air
Equivalence Ratio	-	0.44-0.58
Inlet Velocity	m/s	60

Table 3.6: Experimental conditions of Cheng et al. [67]

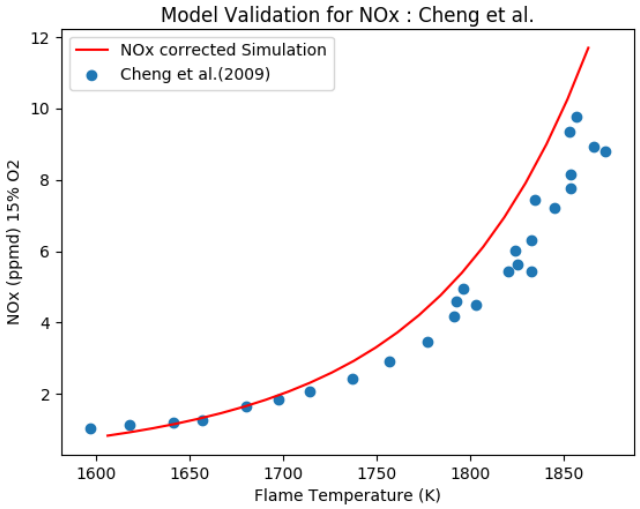

Figure 3.20: Model Validation with Experiments of Cheng et al. [67]

NO_x levels between 1600 K and 1850 K are computed with the experimental conditions as model inputs. Figure 3.20 indicates good agreement between the model prediction and the experimental data. The NO_x levels indicated here are majorly in sub 10 ppm levels because of low flame temperature and equivalence ratio. The good agreement with the experimental data demonstrates the validity of the modeling approach for a similar flow pattern of a swirling flame.

3.4.3. Case 3: Natural Gas & Natural Gas + H_2 in air - (Sidwell et al. (2006))

Sidwell et al. [68] performed tests on the effect of fuel composition on gas turbine emissions at elevated pressures and preheat temperatures on a lean premixed combustor. The combustor facility in this case is also the SimVal combustor as mentioned in the previous case. The effect of heat loss on the emissions is also investigated in this experimental work. Two cases have been used to validate the modeling approach. They are:

- 100% Natural Gas + Air combustion at 6.3 bar
- 80% Natural Gas + 20% H_2 + Air at 6.3 bar

Case 3a: Natural Gas + Air - 6.3 bar

One of the objectives in this work was on testing the NO_x levels in natural gas and air combustion at 6.3 bar. Table 3.7 summarizes the experimental data used as model inputs.

Parameter	Unit	Value
Inlet pressure	bar	6.3
Inlet temperature	K	550
Combustor Diameter	m	0.18
Combustor Length	m	0.31
Nozzle Diameter	m	0.0571
Fuel + Oxidizer	-	Natural Gas + Air
Air mass flow	kg/s	0.38

Table 3.7: Experimental conditions of Sidwell et al. [68]

From the Cantera simulation of the model, an accurate prediction of the experimental data is seen in figure 3.21. The NO_x levels are low in this case not only because of lower flame temperature but also due to lower combustor pressure. GRI Mech 3.0 [43] was used for the model. Prediction of emissions by the model at different pressures has been validated with experiments with similar flow fields. This proves the validity of the modeling approach for pure natural gas combustion.

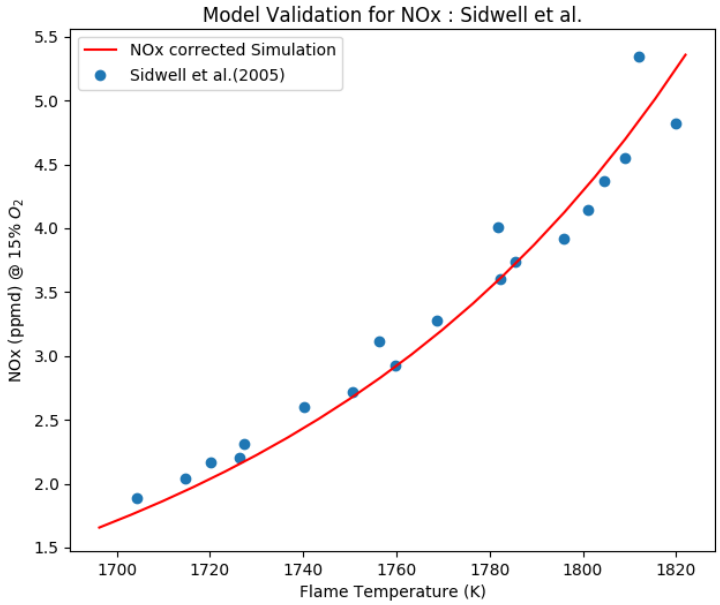

Figure 3.21: Model Validation with Experiments of Sidwell et al. [68]

Case 3b: NG-H_2 blend in Air - 6 bar (Sidwell et al. (2006))

In addition to pure natural gas combustion in air and EGR oxidizers, natural gas blends with H_2 is also validated with the experiments of Sidwell et al. [68]. Different blends of H_2 with natural gas were tested in this work. To validate the modeling approach, the 20% H_2 blend is used. The experimental conditions are the same as in case 3a, except for the fuel composition. From figure 3.22, it can be concluded that the model can closely predict the NO_x levels for natural gas and hydrogen blends. The effect of hydrogen injection has been validated with experiments in order to proceed with the parametric study on hydrogen injection.

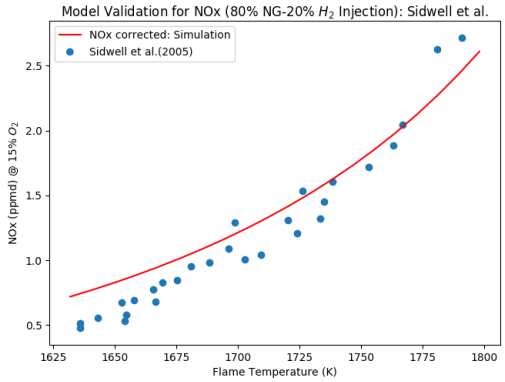

Figure 3.22: NG-H_2 blend: Validation with Experiments of Sidwell et al. [68]

3.5. Sensitivity of the PSR-PFR splitting ratio

As the recirculation zone length is modelled based on a simplified approach, the sensitivity of the PSR-PFR splitting ratio on the NO_x emissions is tested. The volume of the PSR is changed by changing the length of the recirculation reactor and keeping the flame reactor length fixed. As seen from figure 3.23, the 50-50 PSR-PFR volume split shows good agreement with the experimental data. When the splitting ratio is changed from 50-50, the model deviates from the desired values. The reason could possibly be because of the change in local residence time by virtue of the volume change in the recirculation reactor. When the volume of the PSR zone increases, the residence time increases, leading to greater NO_x formation. Since majority of the NO_x is formed in this zone, the optimum setting to match the experimental data is found to be the 50-50 split. However, this combination need not be universally applied to all cases and can be case dependent. For the scope of this study, this volume split is found to be in good agreement with the experimental trends.

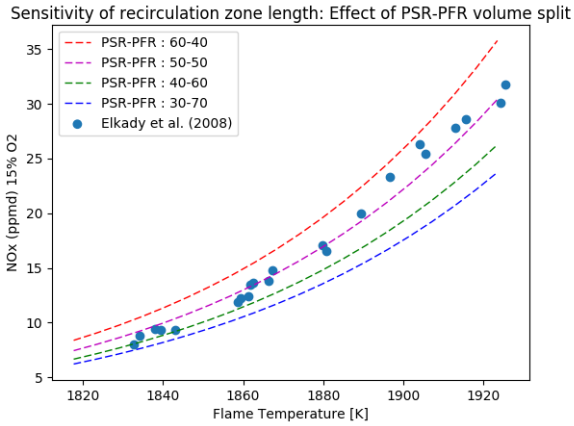

Figure 3.23: Effect of PSR-PFR volume split on the prediction ability of NO_x; Tested with the NO_x values of NG-Air mixture

4

Parametric study on the combustor model

The experimental conditions of Elkady et al. [9, 60] is considered as the base case for the parametric study on the model. In this chapter, the following parametric studies on the model are discussed:

- Influence of Air and EGR oxidizer on NO_x
- Effect of CO_2 content in the oxidizer
- Influence of combustor pressure
- Influence of Wet EGR : Comparison with dry EGR
- Influence of H_2 blending with Natural Gas
- Influence of premixing efficiency

4.1. Study 1: Influence of Air and EGR oxidizer on NO_x

When air is used as the oxidizer, the flame is strained and wrinkled due to turbulence, leading to quicker heat release. The flame zone is confined as a reaction sheet as a result of higher Damkohler numbers. When EGR is introduced, CO_2 is found to slow down the reaction kinetics and increase the chemical time scale, thereby shifting the combustion regime to Da < 1 or well-stirred reaction zone. In a physical sense, the flame zone is smeared out in space (as shown in figure 4.2), causing delayed heat release. According to the model, a higher chemical time implies a larger flame reactor volume with increased homogeneity. This effect is highlighted through the Borghi diagram in figure 4.1.

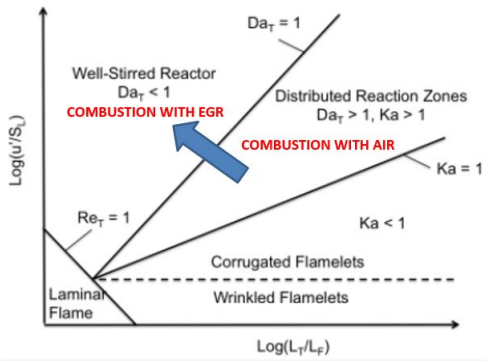

Figure 4.1: Flame zone shift from air to EGR (Modified from [46])

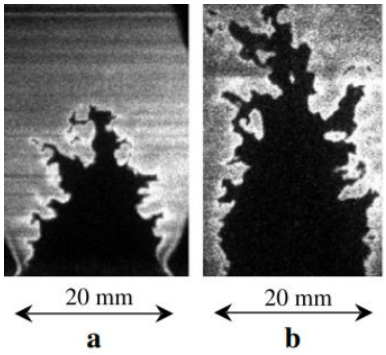

Figure 4.2: a) OH-PLIF image of CH_4 - Air flame ; b) OH-PLIF image of CH_4+ CO_2 diluted oxidizer; Flame volume increases with increase in CO_2 dilution [76]

In continuation of the model validation in section 3.4, it is important to analyze the reason behind the NO_x reduction on introducing EGR. To understand the NO_x suppression, the relative contribution by each NO_x formation mechanism is studied. Table 4.1 shows the reactions that were disabled in the model to obtain relative NO_x contributions. These reactions are the initiating reactions for NO_x formation and hence disabling them gives the relative contribution of the respective pathway.

Thermal disabled	**N_2O Disabled**	**Prompt disabled**	**NNH disabled**
$N_2 + O \leftrightarrow NO + N$	$N_2 + O + M \leftrightarrow N_2O$	$N_2 + CH \leftrightarrow HCN + N$	$NNH + M \leftrightarrow N_2 + H + M$
$N + O_2 \leftrightarrow N + O$	$N_2O + H \leftrightarrow NO + NH$		$NNH + O \leftrightarrow NO + NH$
$N + OH \leftrightarrow NO + H$	$N_2O + O \leftrightarrow 2NO$		

Table 4.1: Reactions disabled to obtain relative contribution

From figure 4.3, large contribution from thermal NO_x (yellow stacks) is seen for higher flame temperatures, indicating it to be the dominating mechanism in both air and EGR. In case of introducing EGR, the amount of thermal NO_x is reduced and is evident on comparing figures 4.3 and 4.4. This can be explained by the the rate limiting step of the thermal pathway,

$$N_2 + O \rightleftharpoons NO + N \tag{4.1}$$

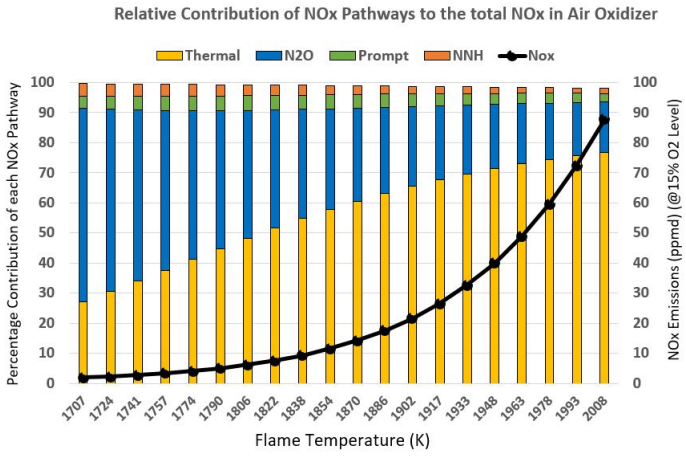

Figure 4.3: Relative contribution NO_x : Air (P = 10 bar)

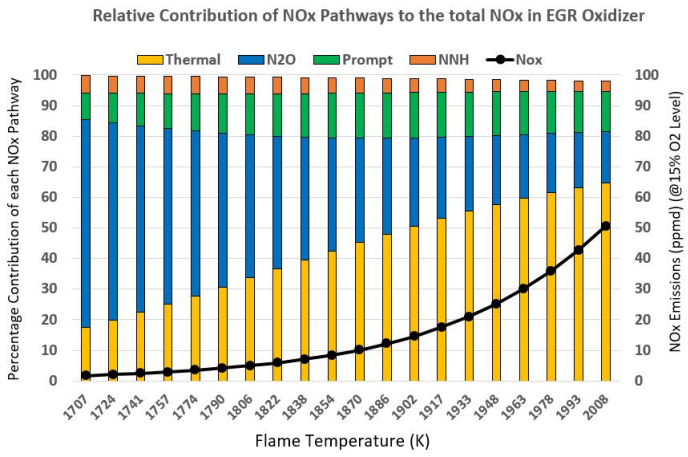

Figure 4.4: Relative contribution NO_x : EGR (P = 10 bar)

As a result of introducing EGR, the amount of O_2 in the oxidizer reduces and the [O] radical concentration drops. This inhibits the NO_x formation. From figures 4.5a and 4.5b, absolute contribution of NO_x pathways are represented. As explained, the major contributing factor of thermal NO_x in the air oxidizer is now curtailed due to oxygen depletion in EGR. It is highlighted in figure 4.6 that on introducing EGR, NO_x level reduction is enhanced with increasing flame temperature. The NO_x reduction due to the oxidizer change can go up to 40%.

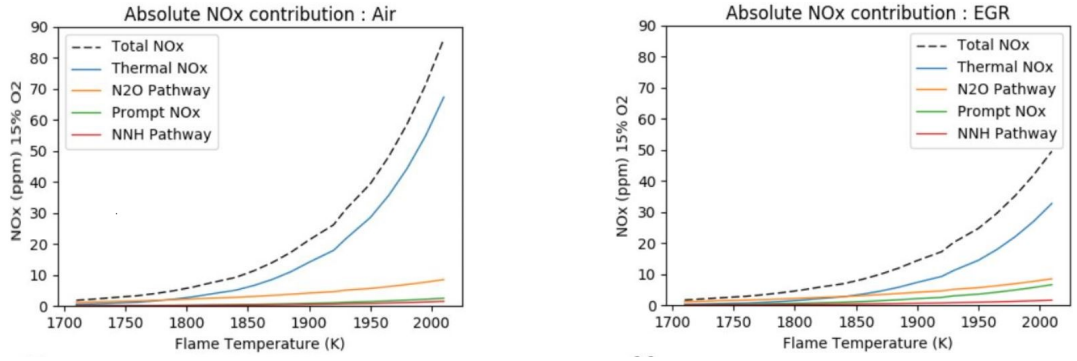

(a) Absolute NO_x contribution : Air

(b) Absolute NO_x contribution : EGR

Figure 4.5: Absolute NO_x contribution in Air and EGR (P=10 bar)

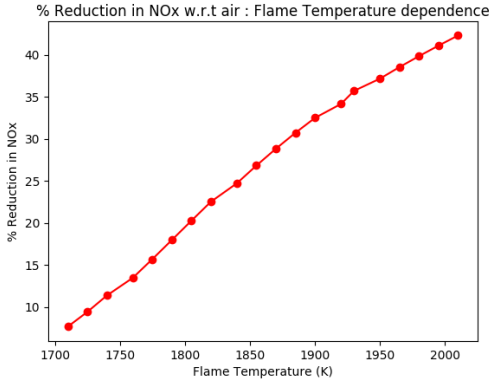

Figure 4.6: % Reduction in NO_x with respect to air (P = 10 bar)

4.2. Study 2: Effect of CO_2 content in the oxidizer

The effect of different compositions of CO_2 in the oxidizer is studied. This is a direct representation of introducing different EGR ratios into the combustor. Table 4.2 shows the oxidizer compositions used in this study.

Oxidizer	CO_2 (%)	O_2 (%)	N_2 (%)
Air	N/A	21	79
EGR1	1	20	79
EGR2	2	19	79
EGR3	3	18	79
EGR4	4	17	79

Table 4.2: Oxidizer Composition in mole % used in this study

4.2.1. NO_x Levels - CO_2 injection

At a fixed adiabatic flame temperature, NO_x emissions reduce with increase in CO_2 content in the oxidizer as shown in figure 4.7. Greater vitiation of the oxidizer with an inert species like CO_2 reduces the reaction kinetics extensively. NO_x formation is not only dependent on temperature but also on the amount of O_2 content in the oxidizer. The [O] species content reduces due to its replacement by CO_2, inhibiting the formation of NO (refer equation 4.1). Thus an increase in CO_2 increase the oxygen depletion as well. It can be concluded that introducing controlled amounts of CO_2 as part of the oxidizer enhances the NO_x reduction.

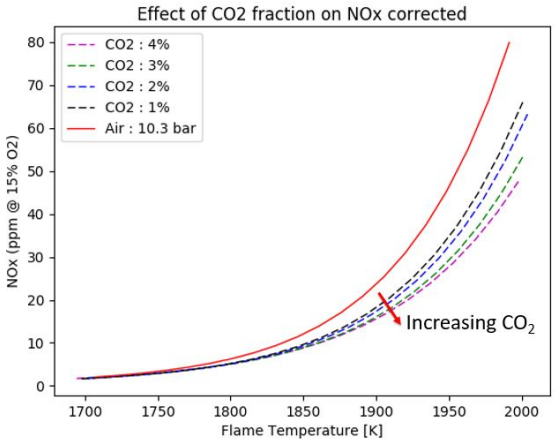

Figure 4.7: NO_x levels: Effect of CO_2 injection in the oxidizer (P = 10 bar)

4.2.2. CO Levels - CO_2 injection

CO levels increase with CO_2 concentration at a fixed flame temperature (figure 4.8). This can be because of the following reasons:

- EGR oxidizer contains lesser O_2 content than in air. As a consequence of increase in heat capacity of the fluid (explained in figure 3.13), extra fuel is injected to obtain the same flame temperature. Incomplete combustion can induce higher CO. Even though CO_2 injection leads to reduction of NO_x levels, a substantial increase in the CO levels is a direct indicator of the limitation of EGR. As already stated, the reasons can not only be the lack of oxygen, but can also be due to CO_2 dissociation.

$$CO + OH \rightleftharpoons CO_2 + H \tag{4.2}$$

- CO_2 in the oxidizer affects the equilibrium reaction between CO and CO_2 and favours CO formation.

- Due to inadequate residence time inside the combustor, the equilibrium concentration of CO is not reached. This leads to elevated levels of CO.

Due to increased CO_2 in the oxidizer, Le Chatelier's principle favours the direction that consumes CO_2. Thus, the reverse of equilibrium reaction in equation 4.2, which is the dissociation of CO_2 to CO, is favoured. This leads to higher CO levels by virtue of CO_2 concentration elevation.

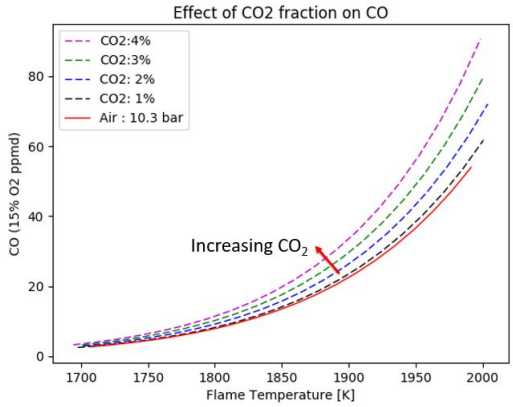

Figure 4.8: CO levels: Effect of CO_2 injection in the oxidizer (P = 10 bar)

Figure 4.9 indicates that the predicted CO levels in the model are higher by a factor of 2 when compared to the equilibrium CO levels. The equilibrium CO concentration correspondingly indicates the emissions at an infinite residence time. Since the residence time of the flow inside is the combustor is finite and limited, the time to reach the equilibrium concentration is insufficient. This can also be the reason for elevated CO levels in conjunction with oxygen depletion.

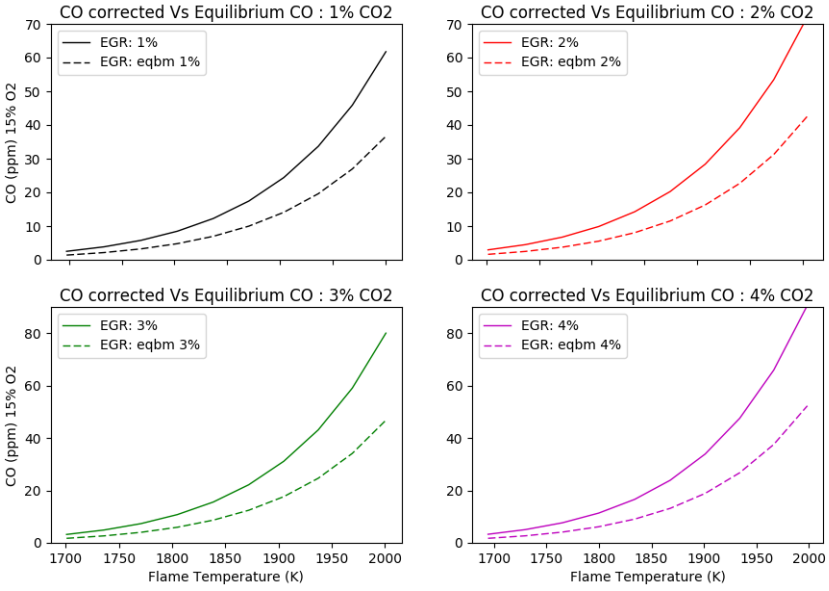

Figure 4.9: Comparison of CO levels vs Equilibrium CO levels : Change in CO_2 (P = 10 bar)

Hence, the overall conclusion of this study is that introducing CO_2 in the oxidizer, reduces NO_x substantially, with a simultaneous escalation in CO levels. This sets a upper limit on the amount of CO_2 content, keeping in view the CO levels. Figure 4.10 clearly represents the decrease in NO_x and increase in CO wiht CO_2 injection.

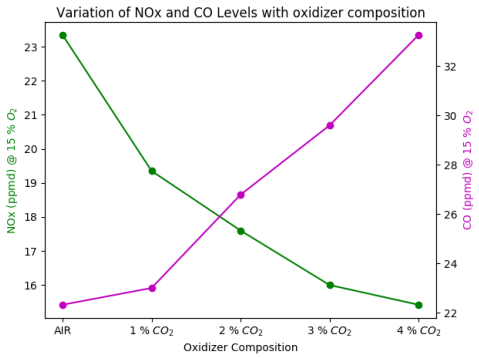

Figure 4.10: NO_x and CO levels at T_{flame}= 1900 K, P = 10 bar with change in oxidizer composition

4.3. Study 3: Influence of combustor pressure

The effect on NO_x and CO levels due to change in combustor pressure for a given EGR oxidizer composition is studied. Four pressures namely - 1 bar, 5 bar, 10 bar and 15 bar were chosen as the pressure values for testing.

Component	N_2	O_2	CO_2	Ar
EGR Mole %	78	18	3	1
AIR Mole %	78	21	N/A	1

Table 4.3: Composition of Air and EGR oxidizer used for this study

4.3.1. NO_x Levels

The dotted lines represent the EGR oxidizer and solid lines represent air oxidizer in figure 4.11. A clear increase in NO_x emissions with increase in flame temperature and combustor pressure is seen for both air and EGR oxidizers. For a given pressure and flame temperature, EGR seems to produce lesser NO_x than air.

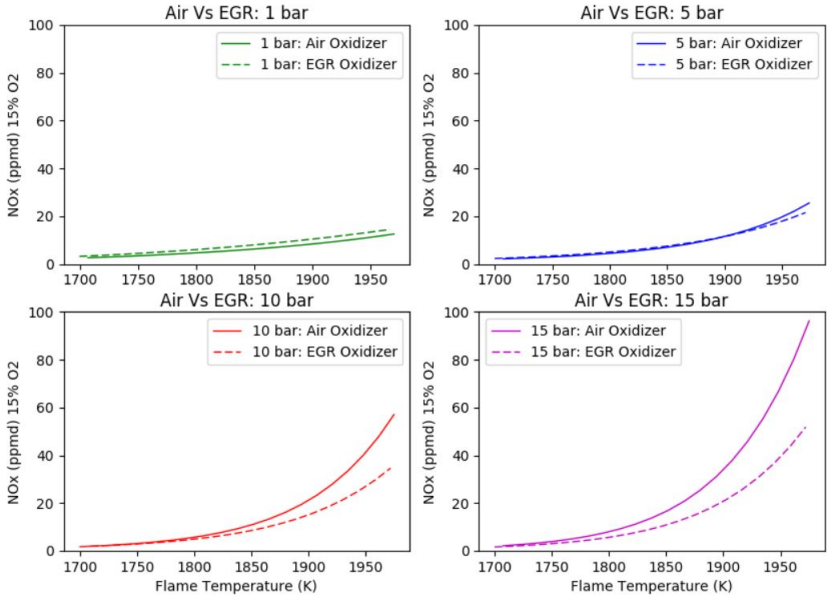

Figure 4.11: NO_x levels: Effect of Pressure - Air and EGR

At lower flame temperatures (< 1800 K), no significant difference in NO_x levels are seen irrespective of the pressure change. For lower pressure such as 1 bar, EGR produces more NO_x than air at the same pressure for the whole flame temperature range. Beyond 1800 K, rapid increase of NO_x is seen and substantial variations with pressure changes are observed. This implies that EGR is highly effective in NO_x reduction at higher pressures and flame temperatures. The percentage reduction in NO_x is enhances with increase in pressure, as shown in figure 4.12.

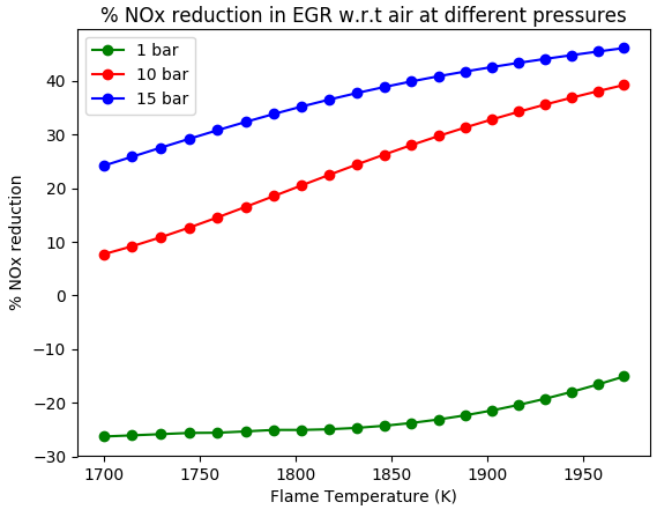

Figure 4.12: NO_x % reduction : 10 and 15 bar with respect to air

For 1 bar, the NO_x reduction is negative indicating an increase in NO_x in EGR with respect to air. In order to find the reason behind the obtained trend, the relative contribution of each NO_x formation pathway is studied. An increase in the contribution of thermal NO_x with increasing flame temperature is seen from figures 4.13 and 4.14. An evident rise in magnitude of thermal NO_x (yellow stacks) with increase in pressure can also be seen. At lower flame temperatures (ϕ = 0.56 or T_{flame} = 1700 K), majority of the contribution to the total NO_x comes from the N_2O mechanism.

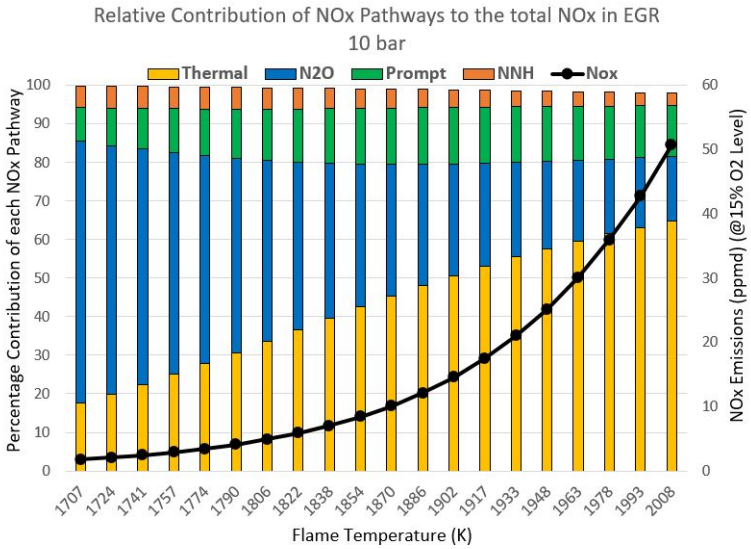

Figure 4.13: Relative NO_x contribution : EGR - 10 bar

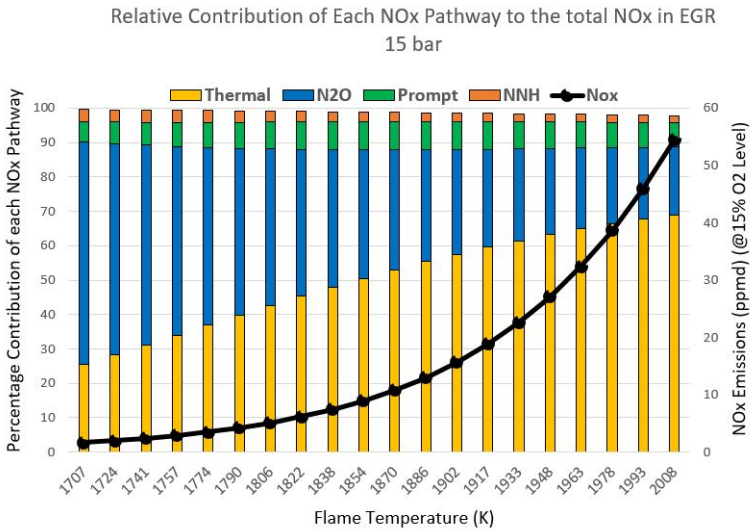

Figure 4.14: Relative NO_x contribution : EGR - 15 bar

The contribution of other mechanisms keep decreasing as a consequence of the domination of thermal NO_x. At T_{flame}= 2000 K (ϕ=0.75), its relative contribution increases from 62% at 10 bar to 70% at 15 bar. As already stated in chapter 2, the Zel'dovich mechanism activates at higher flame temperatures, typically beyond 1800 K. Hence, the domination of thermal pathway is further enhanced with increased pressure and explains the reason behind the significant rise in NO_x emissions. The absolute contribution of each NO_x pathway is shown in figure 4.15a and 4.15b. Thermal NO_x shows a strong dependence on temperature in both the pressures and dominates above 1800 K. The magnitude of each pathway is increased as a result of the pressure increase, especially the thermal pathway. The N_2O pathway contribution seems to contribute a little more with increase in pressure, as a result of third body collisions.

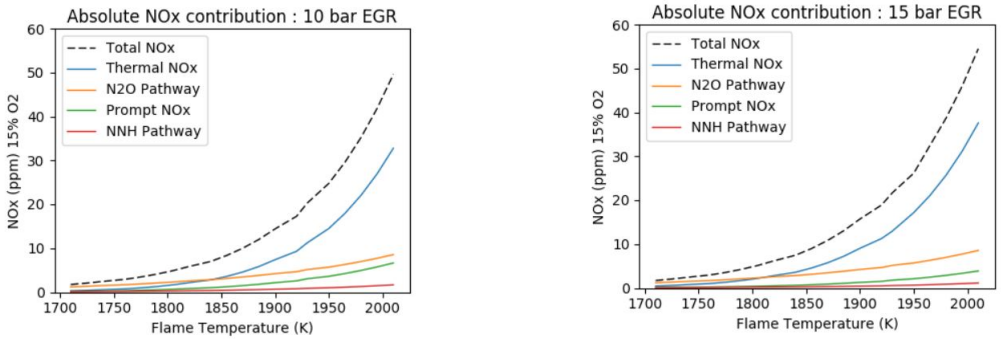

(a) NO_x contribution: 10 bar

(b) NO_x contribution: 15 bar

Figure 4.15: Absolute NO_x contribution : Between T_{flame}= 1700-2000 K

The role of NNH and prompt NO_x at 1 bar pressure is highlighted in figure 4.16. The contribution of thermal NO_x is minimal throughout the flame temperature range and the role of prompt NO_x becomes predominant. Due to this trend, EGR oxidizer forms more NO_x than air at lower pressures, which is a non-ideal situation. Prompt NO_x is lowered at higher pressures, simply because of the contribution of thermal NO_x.

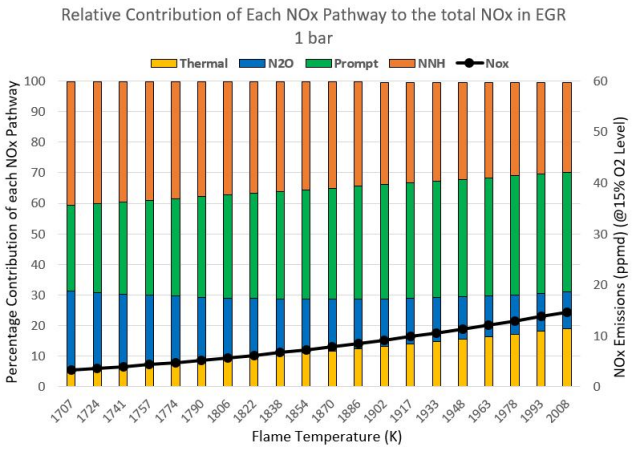

Figure 4.16: Relative NO_x contribution :EGR 1 bar

Figure 4.17b shows the absolute contribution of NO_x at 1 bar pressure. In contrast to higher pressures, thermal pathway does not contribute much to the total NO_x and is dominated by the other 3 pathways.

It can be concluded that when the pressure increases, the domination of thermal NO_x pathway leads to an increase in overall NO_x. Whereas at lower pressures, thermal NO_x decreases and prompt NO_x contributes larger to the overall NO_x.

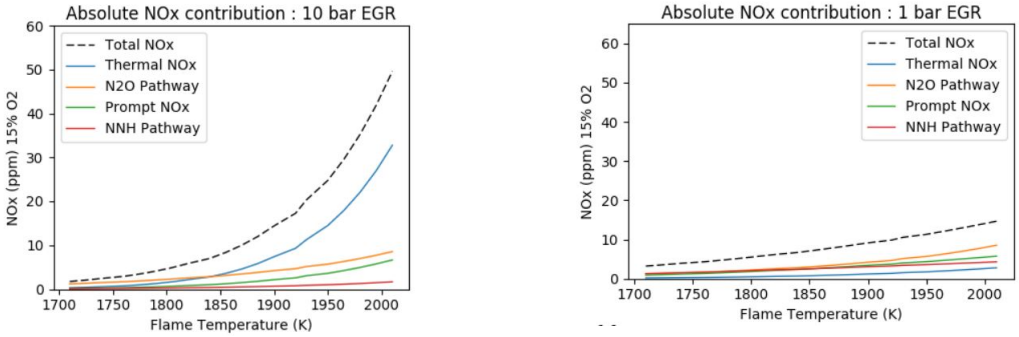

(a) NO_x contribution: 10 bar

(b) NO_x contribution: 1 bar

Figure 4.17: Absolute NO_x contribution : Between T_{flame}= 1700-2000 K

Reaction Path Diagram Cantera [19] can be used to generate reaction path diagrams, which provide a flowchart of how different NO_x pathways proceed based on the maximum molar formation rate. The effect of pressure in EGR at high and low flame temperature is generated for the model. Each diagram is scaled based on the maximum molar formation rate and the values indicated beside the arrows represent the fraction of the scale.

Reaction path diagrams were generated for 10 bar and 15 bar at T_{flame}= 1860 K and T_{flame} = 1730 K. Figure 4.18 shows the reaction path diagram of pressure change at 1860 K. It can be observed that when the pressure increases from 10 bar to 15 bar, the scale increases by an order of 10. This is logical because higher pressure induces accelerated reaction rates and enhanced third body collisions. The bold arrows represent the dominant NO_x pathway. The path where N_2 splits to form NO represents the thermal pathway. Thermal NO_x dominates at this flame temperature irrespective of the pressure change and only the magnitude of formation rates change between the two pressures. In addition, N_2O mechanism and NNH mechanism show up, but prompt NO_x is suppressed. For the same pressure change, when the reaction path diagram is generated for T_{flame} =1730 K, the prompt pathway shows

up (HCNO → HNCO → NCO). This is presented in figure 4.19. Also, the thermal NO_x pathway reduces in magnitude and the N_2O pathways appears to be the dominant mechanism at low flame temperature. Even in this case, the reaction rates amplify by a factor of 10 by the virtue of pressure change.

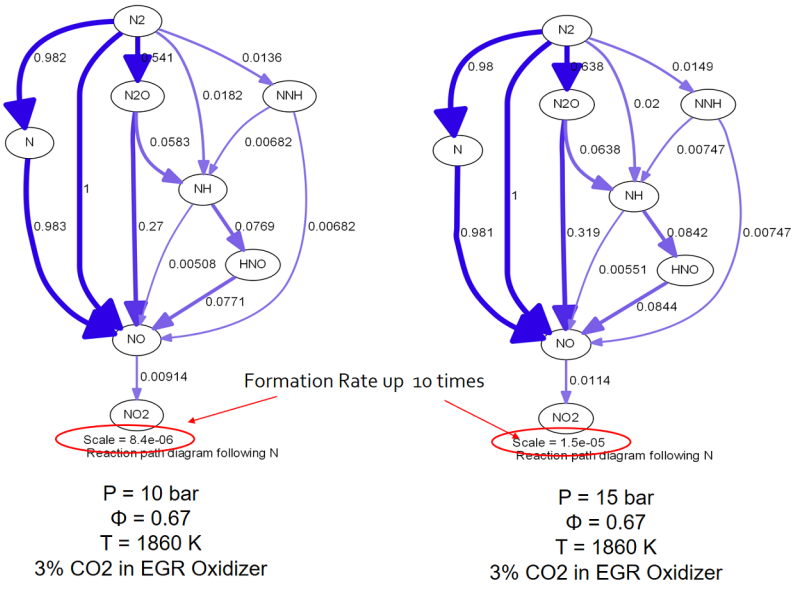

Figure 4.18: Reaction Path Diagram for T_{flame} = 1860 K : 10 bar and 15 bar

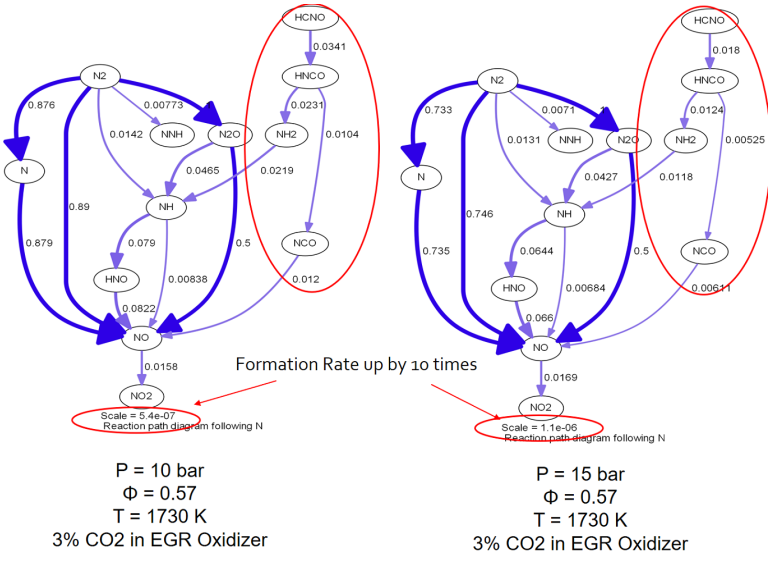

Figure 4.19: Reaction Path Diagram for T_{flame} = 1730 K : 10 bar and 15 bar

4.3.2. CO Levels

It can be seen from figure 4.20 that CO levels are suppressed to a great extent with increase in pressure. For the same adiabatic flame temperature, EGR produces more CO than air irrespective of the pressure change. CO levels increase with flame temperature for both air and EGR because of increasing consumption of oxygen at higher flame temperatures.

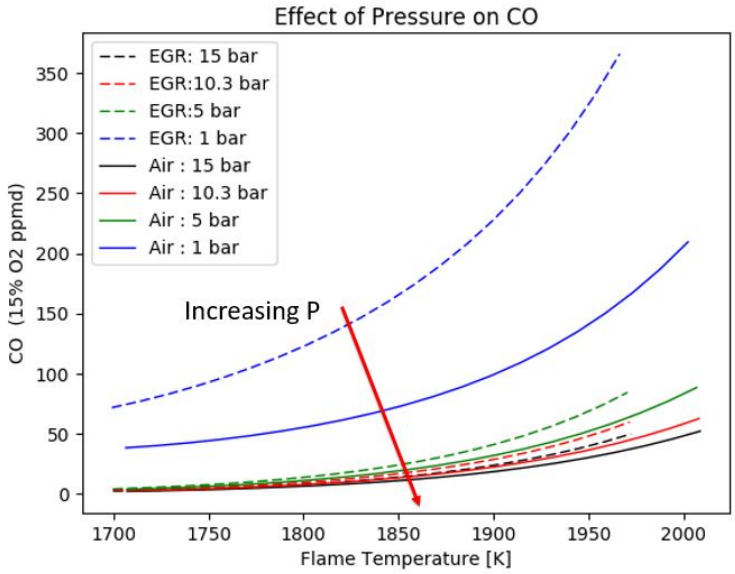

Figure 4.20: CO levels: Effect of Pressure - Air and EGR

$$CO + OH \rightleftharpoons CO_2 + H \tag{4.3a}$$

$$CO + 0.5\,O_2 \rightleftharpoons CO_2 \tag{4.3b}$$

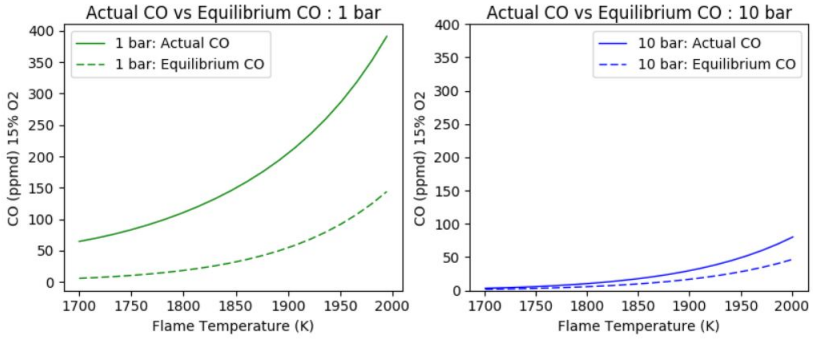

Figure 4.21: Impact of pressure on Actual CO and Equilibrium CO levels : EGR (P= 1 bar and 10 bar)

The reason for extensive reduction in CO levels is due to the inhibition of CO_2 dissociation at higher pressures. According to Le Chatelier's principle, an increase in pressure in a reaction, shifts the reaction towards the side with lesser number of moles of gas. Thus, equation 4.3b favours the formation of CO_2 at higher pressure. In the previous study, it was stated that the actual CO levels were higher than the equilibrium CO levels in EGR because of insufficient residence time. Figure 4.21 compares the impact of pressure on actual CO and equilibrium CO levels. At high pressures, the actual CO levels reach closer to the equilibrium CO levels when compared to low pressures, although it never attains equilibrium. The suppression of chemical dissociation of CO_2 at high pressures might be the reason for the decrease in magnitude of CO levels.

4.4. Study 4: Influence of Wet EGR : Comparison with Dry EGR and air

In parametric study 2, the effect of EGR by CO_2 injection is performed with dry EGR conditions. Dry EGR is in which the steam or moisture content formed at the exhaust is condensed out by means of a heat exchanger. Objectives to use EGR by directly introducing the wet exhaust gas without intermediate condensation. This is called wet EGR. The thermodynamic properties such as heat capacity and density of the working fluid changes due to the presence of H_2O and will have an impact on the emissions. The effect of H_2O dilution individually in flames has been studied in literature [77–79]. The effect of wet EGR on NO_x and CO is performed in this study. Table 4.4 summarizes the oxidizer compositions used.

Oxidizer	H_2O	CO_2	O_2	N_2
Air	N/A	N/A	21	79
Wet EGR1	2	1	20	77
Wet EGR2	3	2	19	76
Wet EGR3	4	3	18	75

Table 4.4: Wet EGR composition in mole% used in this study

4.4.1. NO_x levels

It is reported in literature that the dilution of H_2O enhances NO_x reduction by its combined thermal and chemical effect [79, 80]. The thermal effect is attributed to the high heat capacity of H_2O, which is almost twice the value of N_2, O_2 and CO_2. This is shown in table 4.5. The heat capacity is increased more than the dry EGR heat capacity as highlighted in figure 4.22. In figure 4.23, it can be seen that for a given flame temperature, wet EGR produces slightly lesser NO_x than dry EGR. In addition to the kinetic effect of CO_2, the kinetic effect of H_2O aids to the enhanced NO_x reduction. At 1 % CO_2, the NO_x reduction is 10% higher and becomes 5% at 3% CO_2.

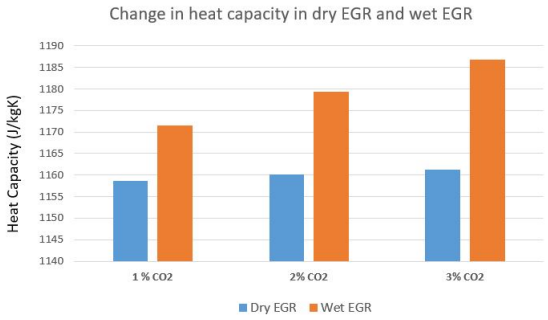

Figure 4.22: Heat capacity (J/kgK)change due to the presence of moisture in the oxidizer

Temperature (K)	H_2O	CO_2	N_2	O_2
1000	2.0267	1.232	1.167	0.910
2000	2.832	1.371	1.287	1.180

Table 4.5: Heat capacity (kJ/kgK) values of individual constituents of the oxidizer [7]

By virtue of the heat capacity rise, the flame temperature reduces and leads to reduced thermal NO_x. Since the comparison is made at the same flame temperature, the thermal effect is excluded. Thus, the reduction in NO_x can be attributed to the other NO_x pathways, due to increased H_2O content. From the conclusions of Li and Williams [79], H_2O dilution led to reduced CH concentration. Hence the reduction in prompt NO_x can be the reason for the total NO_x.

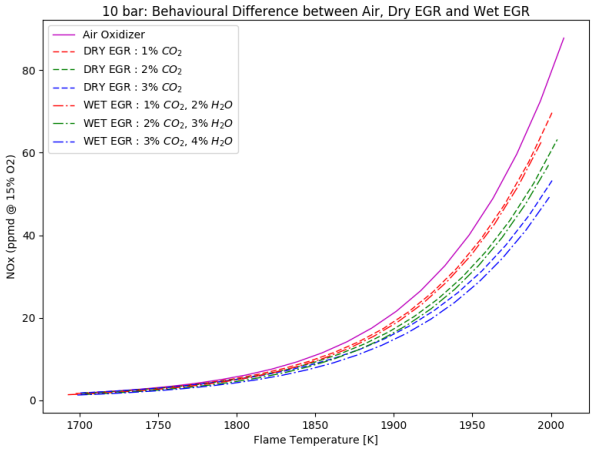

Figure 4.23: Effect of Wet and Dry EGR on NO_x levels ; P = 10 bar

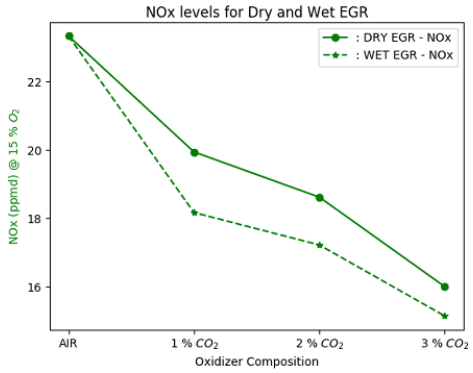

Figure 4.24: NO_x : Dry Vs Wet EGR, (P = 10 bar , T = 1900 K)

Equation 4.4 shows the main reactions consuming the CH radical, which is one of the primary radical in prompt NO_x formation. The concentration at steady state of CH radical as stated by Li and Williams [79] can be represented in terms of O, OH, CO_2 and H_2O concentrations (equation 4.5). The reaction rates k_1 to k_5 correspond to reactions 4.4a-4.4e respectively.

$$CH_2 + H \rightleftharpoons CH + H_2 \quad (4.4a)$$
$$CH_2 + OH \rightleftharpoons CH + H_2O \quad (4.4b)$$
$$CH + O_2 \rightleftharpoons CHO + O \quad (4.4c)$$
$$CH + H_2O \rightleftharpoons CH_2O + H \quad (4.4d)$$
$$CH + CO_2 \rightleftharpoons CHO + CO \quad (4.4e)$$

$$[CH] = \frac{(k_1[H] + k_2[OH])[CH_2]}{k_3[O_2] + k_4[H_2O] + k_5[CO_2]} \quad (4.5)$$

It is implied that when the concentration of H_2O increases, CH concentration drops. This corroborates the fact that the kinetic effect of H_2O in the oxidizer inhibits the formation of CH radical. Equation 4.6 refers to the rate-limiting step of the prompt pathway. A decrease in CH concentration due to the presence of H_2O leads to a decrease in HCN concentration. The HCN radical being the base for NO formation is curtailed from being formed, leading to reduced NO_x (figure 4.25).

From figures 4.26 and 4.27, no significant changes in the relative NO_x contributions are seen. As already explained, the inhibition of CH radical is the driving mechanism for overall NO_x reduction. This is by virtue of the kinetic effect of H_2O.

$$N_2 + CH \rightleftharpoons HCN + N \tag{4.6}$$

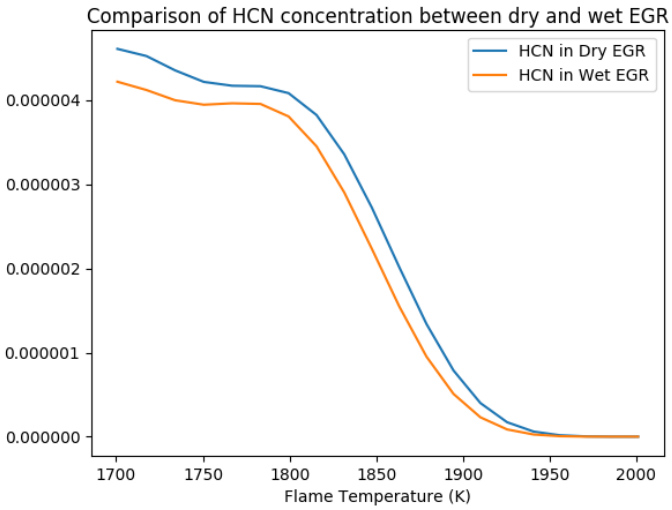

Figure 4.25: HCN concentration reduction in wet EGR (P = 10 bar)

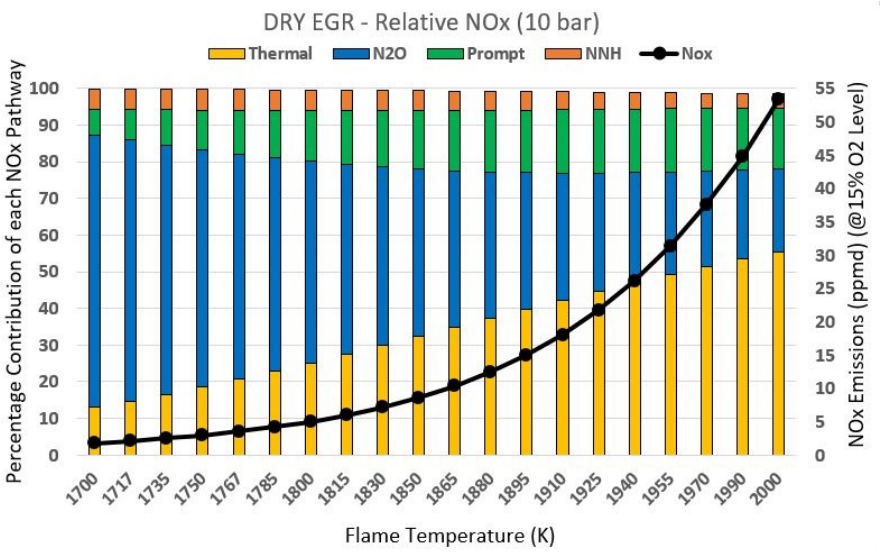

Figure 4.26: Relative NO_x contribution : Dry EGR (P=10 bar)

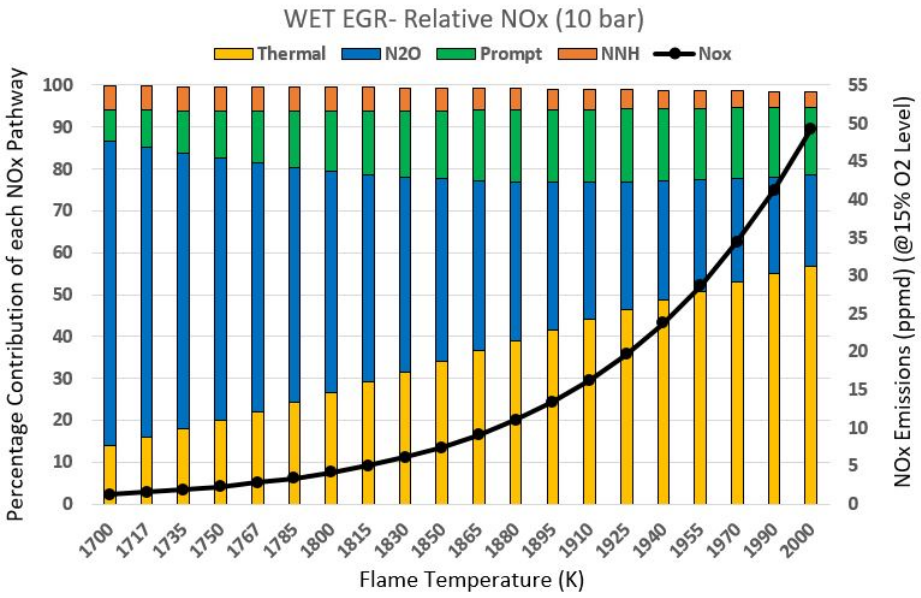

Figure 4.27: Relative NO_x contribution : Wet EGR (P=10 bar)

4.4.2. CO levels

For a given flame temperature, as shown in figure 4.28 wet EGR produces more CO than dry EGR. The presence of moisture in the oxidizer further reduces the laminar flame speed more than dry EGR (shown in figure 4.29a). Further reduction in flame speed and rise in CO levels are indicators of poor flame stability. Wet EGR produces 10-20% more CO than dry EGR, as shown in figure 4.29b.

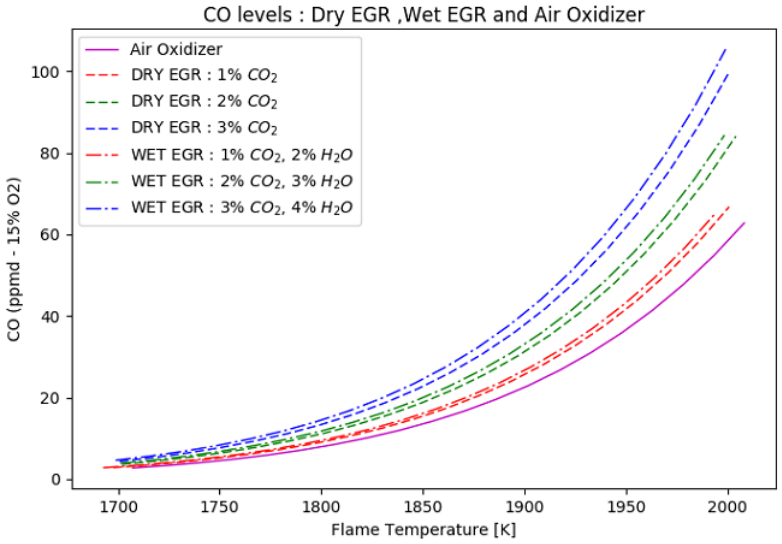

Figure 4.28: Effect of Wet and Dry EGR on CO Levels

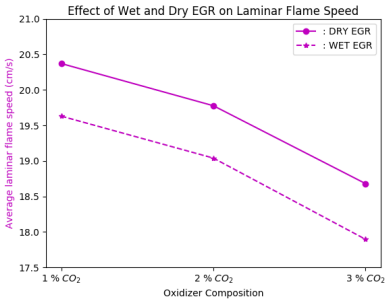

(a) Effect of Wet and Dry EGR on laminar flame speed

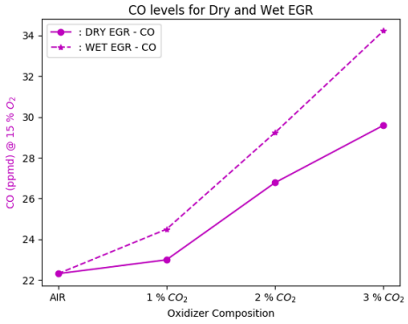

(b) CO : Dry Vs Wet EGR

Figure 4.29: Comparison of CO levels (T = 1900 K) and average laminar flame speed in dry and wet EGR (P=10 bar)

Even though insufficient residence time is a cause of high CO levels as in dry EGR, the slight rise in CO levels can also be attributed to the combined chemical effect of H_2O and CO_2.

$$O + H_2O \rightleftharpoons OH + OH \tag{4.7a}$$
$$OH + O \rightleftharpoons H + O_2 \tag{4.7b}$$
$$CO_2 + H \rightleftharpoons CO + OH \tag{4.7c}$$

The presence of H_2O leads to the production of OH radicals as shown in equation 4.7b. The OH radicals on reacting with O radicals form H atoms. The CO_2 in the oxidizer and increase in H concentration shifts the equilibrium of reaction 4.7c to the left, favouring higher CO levels.

4.5. Study 5: H_2 blending with Natural gas

The decrease in combustion reactivity and flame stability with the introduction of CO_2 was studied in section 4.2. This is indicated through the decrease in laminar flame speed and increase in CO levels. In order to alleviate the loss in reactivity, one method is to introduce H_2 into the combustor. Due to the inherent high reactivity of H_2, it enhances the reaction rates, widen the flammability limits and increase the flame speed [64, 81]. The study of emissions hydrogen-enriched flames has been studied in both atmospheric and gas turbine conditions.

Kinetics of NO_x formation is altered in the presence of H_2 [82–84]. Blending hydrogen with hydrocarbon fuels can reduce the high reactivity and also counter the kinetic slowdown due to EGR. Natural gas is enriched with hydrogen in different amounts and effect of this addition is performed in this study. The fuel compositions are chosen such that the laminar flame speed of pure natural gas-air mixture is maintained. The combinations are summarized in table 4.6.

Fuel Blend	CH_4	C_2H_6	N_2	H_2	Oxidizer	CO_2	O_2	N_2
Natural Gas	94.22	3.16	2.62	-	Air	-	21	79
20% H2 + 80 % NG	74.22	3.16	2.62	20	EGR1	2	19	79
25% H2 + 75% NG	69.22	3.16	2.62	25	EGR2	3	18	79

Table 4.6: Combination of Fuel and Oxidizer having similar laminar flame speeds

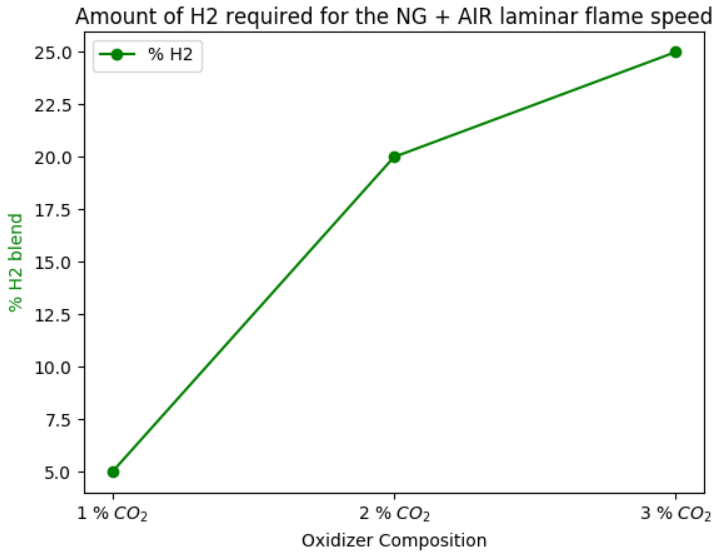

Figure 4.30: H_2 injection: Flame speed change (P=10 bar)

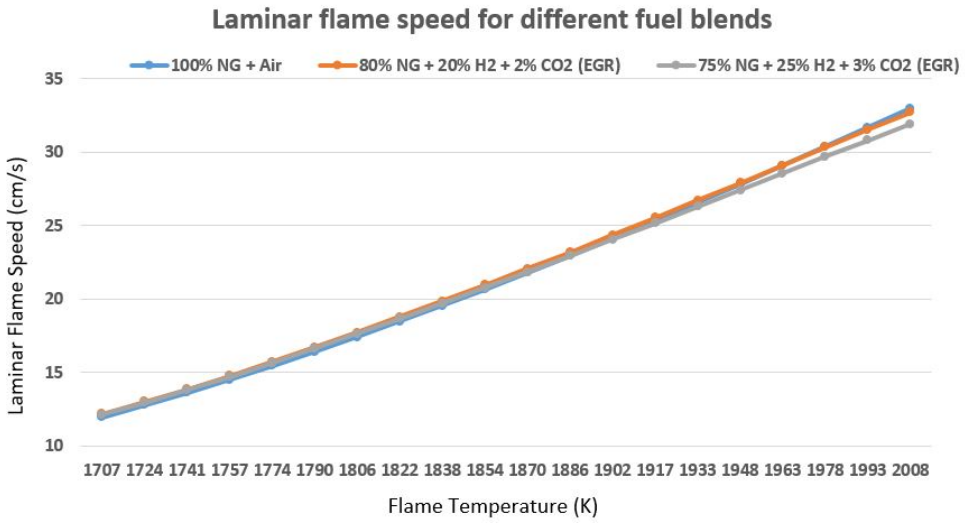

Figure 4.31: H_2 injection: Flame speed dependence on Flame Temperature (P=10 bar)

4.5.1. NO_x Levels

In figure 4.32, the influence of H_2 on the NO_x emissions is highlighted. All comparisons are made based on the NO_x level change of fuel blends with respect to the EGR oxidizer. For a given flame temperature, a slight increase in NO_x levels can be seen. Significant differences occur after a flame temperature of 1800 K and are not substantial at lower flame temperatures.

It can be seen that more than the composition of the fuel, the amount of CO_2 in the oxidizer determines the NO_x levels. The 75-25 blend produces lesser NO_x than the 80-20 blend solely due to the difference in CO_2 in the oxidizer. The kinetic effect of CO_2 in the oxidizer affects the NO_x more than the amount of H_2 in the fuel.

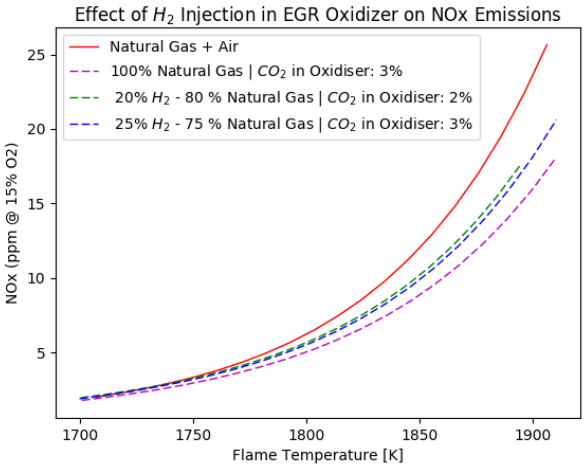

Figure 4.32: Effect of H_2 injection on NO_x levels (P=10 bar)

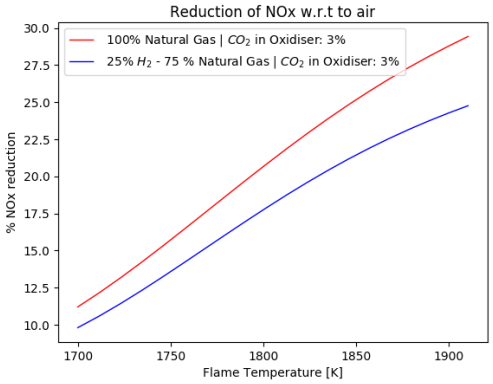

Figure 4.33: % NO_x reduction comparison with respect to air (P=10 bar)

For the same EGR composition, the 75-25 blend and pure natural gas cases have been presented. The reasoning behind the NO_x rise is analyzed. The relative NO_x contributions are represented in figures 4.34 and 4.35.

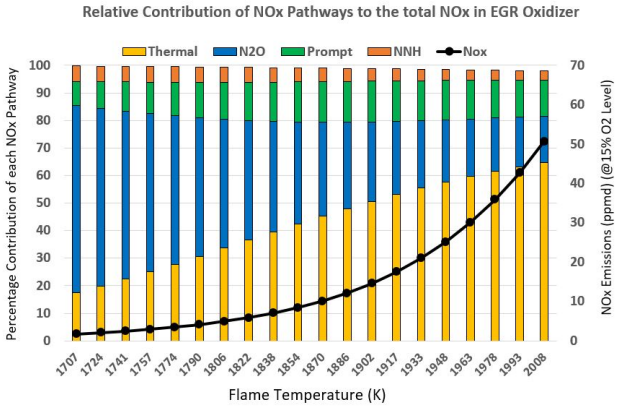

Figure 4.34: Relative NO_x contribution for pure Natural Gas + EGR (P=10 bar)

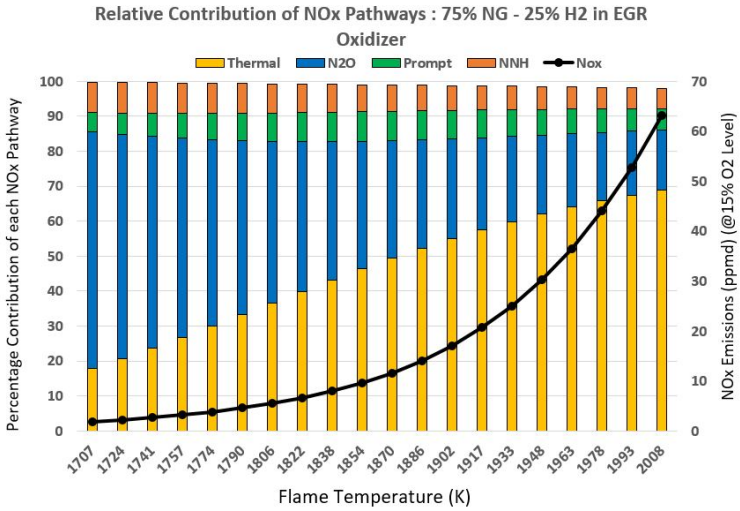

Figure 4.35: Relative NO_x contribution for 75% Natural Gas 25% H_2 + EGR (P=10 bar)

The presence of H_2 increases the reactivity and consequently accelerates the formation of thermal NO_x. In addition to the major contribution from the thermal pathway, a slight increase in the NNH pathway is seen for the 75-25 fuel blend. The additional contribution from the NNH pathway can be the reason behind the rise in NO_x levels with addition of H_2.

The increase in concentration of H in equation 4.8 favours the formation of NNH radical, which acts as a base for NO formation. The presence of excess H radicals can be attributed to the presence of H_2 in the fuel. An increase in the contribution of NNH pathway in addition to the thermal pathway is evident from figure 4.36.

$$N_2 + H \rightleftharpoons NNH \tag{4.8}$$

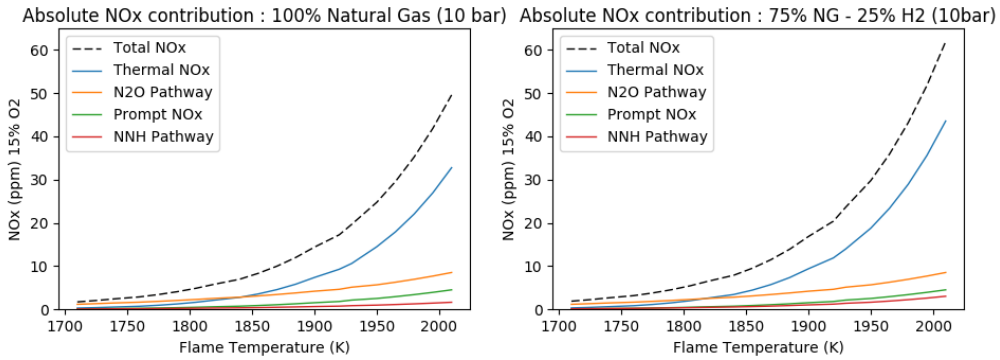

Figure 4.36: Absolute NO_x contribution for pure Natural Gas + EGR (P=10 bar)

The reaction path diagram at T = 1900 K is generated to visualize the species formation and its distribution. The reaction rate increases by a factor of 10, in the presence of H_2 in the fuel, indicating higher reactivity (figure 4.37). Another observation is the increase contribution of NNH pathway to the total NO_x, as already explained in the preceding paragraphs.

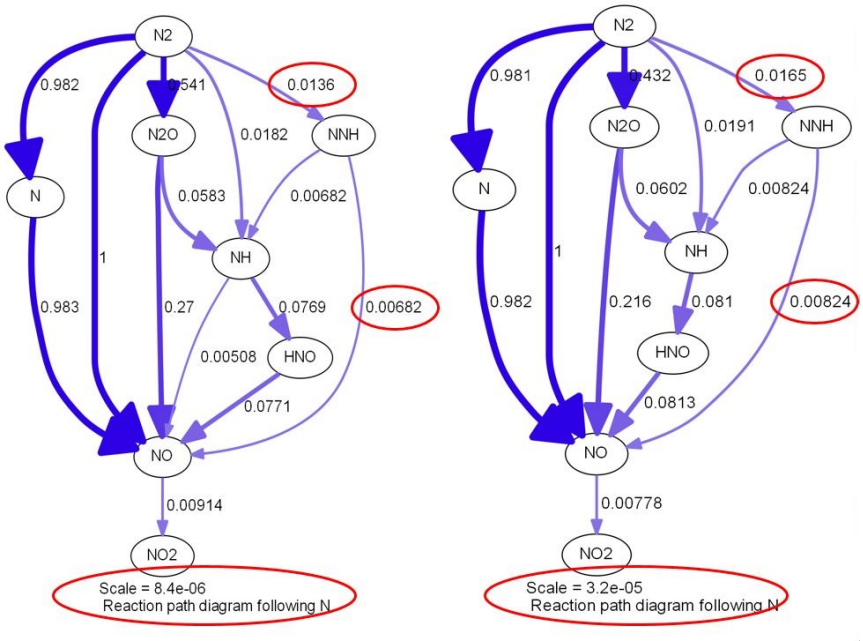

Figure 4.37: Reaction Path Diagram: Comparison between pure NG (LEFT) and 75% -25% blend (RIGHT) (P=10 bar, T= 1900K)

4.5.2. CO Levels

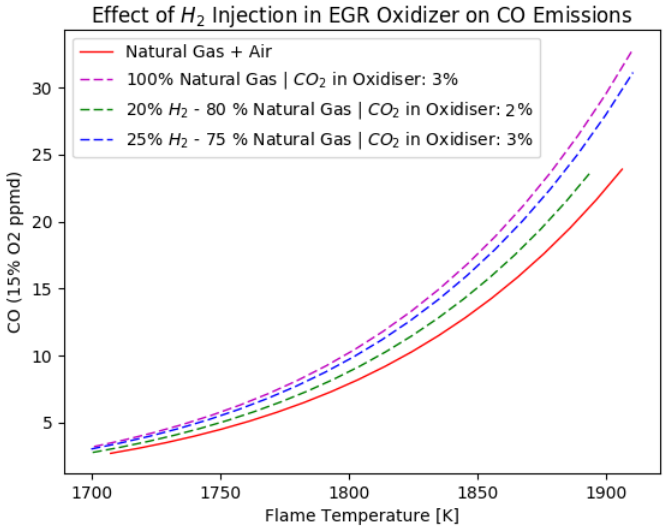

Figure 4.38: Effect of H_2 injection on CO levels (P=10 bar)

As shown in figure 4.38, the addition of H_2 leads to reduction of CO emissions, as compared to pure natural gas in the EGR oxidizer. The 80-20 blend shows the greater reduction in CO because of lesser CO_2 concentration and higher oxygen availability. The reduction in CO levels is an indicator of improved flame stability in the presence of H_2.

$$H + O_2 \rightleftharpoons OH + O \tag{4.9a}$$

$$CO + OH \rightleftharpoons CO_2 + H \tag{4.9b}$$

As a result of hydrogen enrichment, H radical favours the formation of OH and O radicals (reaction 4.9a). This is likely to promote CO oxidation to CO_2 as shown in reaction 4.9b, leading to decreased CO levels. Thus, the detrimental impact of increased CO is countered by hydrogen addition, with a compromise in slight increase in NO_x.

4.6. Study 6: Influence of premixer efficiency

So far, all the parametric studies have been performed under the assumption of perfectly premixed combustion. In other words, it is assumed that the fuel-oxidizer mixture is perfectly mixed at the inlet and there are no mixture strength variations inside the combustor volume. However in reality, there is always a degree of unmixedness, which could be both temporal and spatial [27, 28]. Unmixedness can thus lead to various rich and lean pockets inside the combustor, leading to varying temperature and concentration levels. Instead of a single global equivalence ratio, the value varies due to the non-ideal mixing in the premixer.

In order to model the unmixedness, the approach of Lyons [28] and Li et al. [27] is used in this study. The variation of equivalence ratio is assumed to follow a gaussian distribution with a specified standard deviation σ and the mean μ, which is the mean equivalence ratio. The mean otherwise would have been the global equivalence ratio in case of perfect mixing. The gaussian distribution is as follows,

$$f(\phi) = \frac{1}{\sqrt{2\pi}\sigma} e^{-\frac{(\phi-\mu)^2}{2\sigma^2}} \tag{4.10}$$

The gaussian distribution variation for different standard deviations is shown figure 4.39. It can be observed that with increase in σ, the curve spreads out, signifying more unmixedness inside the combustor. In case of ideal mixing, the curve would have been a vertical line starting from the mean value μ. Therefore, a definition of premixer efficiency can be established based on these parameters,

$$\eta_{premixer} = 1 - \frac{\sigma}{\mu} \tag{4.11}$$

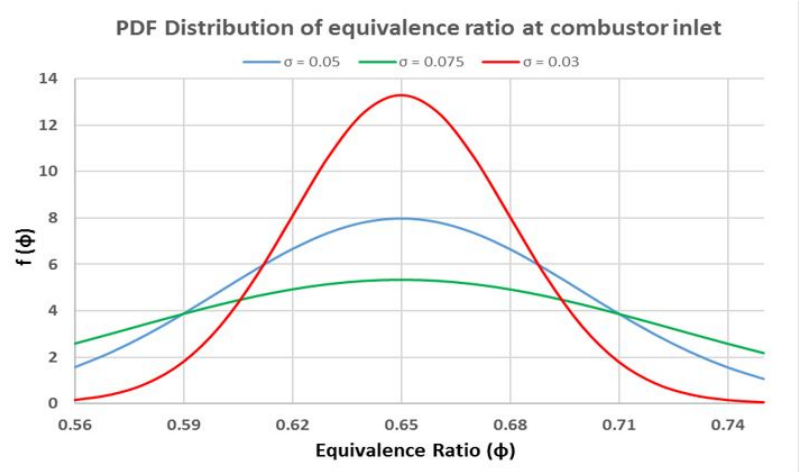

Figure 4.39: Gaussian distribution of equivalence ratio to simulate unmixedness

4.6.1. Modeling methodology : Parallel reactors

To implement unmixedness into the model, the combustor volume is split as parallel reactors, each possessing a different equivalence ratio. Each reactor represents the local conditions and produce different flame temperatures, NO_x and CO levels. Thus, a weighted average of the steady state values at the exhaust is computed, to get the predicted value under reduced premixing efficiency. In this

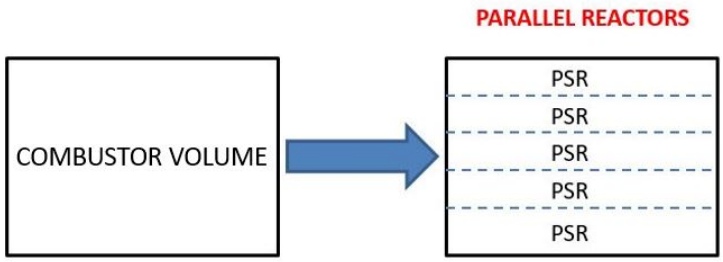

Figure 4.40: Splitting the reactor as parallel reactors

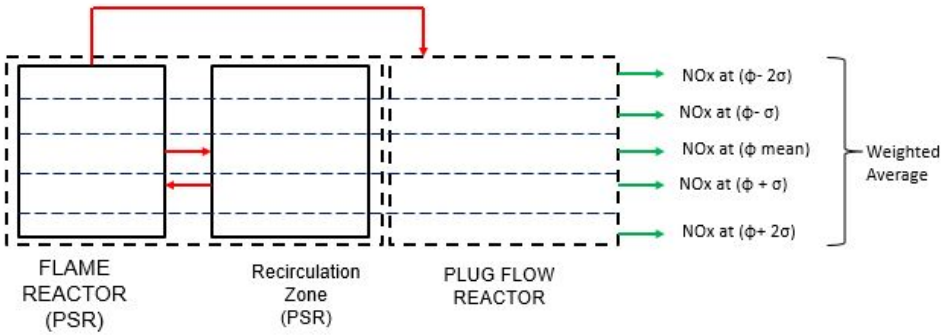

Figure 4.41: New CRN configuration with 5 parallel reactors

study, the volume is split as 5 reactors in the radial direction.

$$NO_{x_{unmixed}} = \frac{\sum f(\phi) NO_x(\phi)}{\sum f(\phi)} \tag{4.12a}$$

$$CO_{unmixed} = \frac{\sum f(\phi) CO(\phi)}{\sum f(\phi)} \tag{4.12b}$$

σ	$\eta_{premixer}$
0	100 %
0.03	95 %
0.05	92%

Table 4.7: Premixer efficiency values tested in this study

4.6.2. NO_x and CO levels

Even though it has been established that EGR (CO_2 injection) can reduce NO_x when compared to air due to slow kinetics and oxygen depletion, poor premixing can drastically counter the reduction. From figure 4.42a, it is seen that when the premixer efficiency drops, the NO_x emissions rise throughout the flame temperature range. For 5% drop in premixing quality, NO_x and CO levels rise by a factor of 1.3 on an average. For 8% drop in premixing quality, NO_x levels rise by a factor of 2 and CO levels by a factor of 2.3 on an average. Poor premixing has a counterproductive effect on NO_x reduction by EGR.

Similarly, unmixedness introduces equivalence ratio changes inside the combustor. This is highlighted in figure 4.42b. Inadequate mixing causes a rise in CO levels as well. Conclusively, poor premixing can cause escalation of both NO_x and CO emissions.

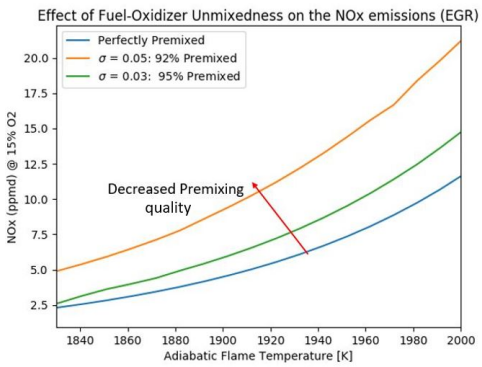

(a) NO_x : Effect of unmixedness (P=10 bar)

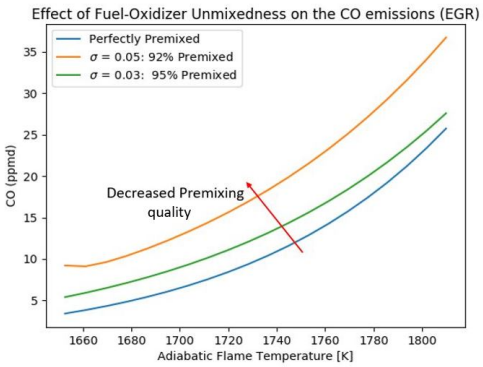

(b) CO : Effect of unmixedness (P=10 bar)

Figure 4.42: NO_x and CO variation with reduced premixer efficiency (P = 10 bar)

In conclusion, all the previous results consider the perfectly premixed condition, which is not always the case in a real combustor. The effect of premixing efficiency is an important factor to be considered in the model, in order to get a more realistic prediction of emissions. The rich and lean pockets of air-fuel mixture are heterogeneously distributed leading to different emission and temperature levels inside the combustor volume. Unfortunately, the spatial and temporal unmixedness inside the combustor is very hard to measure and certain assumptions regarding the unmixedness distribution have to made.

5

Conclusions

A systematic approach to analyze the emissions due to the effect of EGR on DLN gas turbine combustors has been developed in this study. A CRN model with a PSR-PFR configuration was used, splitting the whole combustor volume approximately in half before and after the recirculation zone. The first half was further partitioned into 2 PSRs namely, the flame reactor and the recirculation reactor.

The flame reactor volume was set based on the chemical time scale approach for both air and EGR regimes. This approach quantifies the flame zone volume based on the difference in reaction kinetics for different oxidizers. Instead of imposing the volumes of each reactor as performed in previous models, the residence time was imposed on each reactor in this model. The flame reactor is the part where majority of NO_x is formed and its volume is a critical parameter. CO_2 in the oxidizer leads to kinetic slowdown, thereby increasing the chemical time scale. Thus in a lean premixed regime coupled with EGR, the volume of the flame zone is kinetically controlled rather than the effect of mixing. Thus, the residence time is qunatified through the chemical time scale and is imposed instead of the volume.

Due to the independence of the swirl number and turbulence intensity on the NO_x levels, the recirculation zone length was modelled based on a simplified approach. To determine the volume of recirculation, a correlation of the axial and radial positions of the recirculation zone with the equivalence ratio was established from experimental mean flow fields and was used as a model input.

Out of the 4 chemical mechanisms tested, GRI-Mech 3.0 gave the closest prediction of NO_x experimental data. Due to distinct ways of defining the NO_x chemistry in each of the mechanisms, variation in NO_x prediction was observed. No significant difference in prediction was observed for the CO_2 and O_2 levels in all mechanisms. Considering inherent robustness and wide operating range, GRI-Mech 3.0 was chosen to be the base mechanism for further simulations. The model was also validated with the experimental emission levels for various flame cases with similar flow fields and was found to be in good agreement with the data.

The model has been built on a few assumptions and it is to be noted that all the conclusions drawn are based on the assumptions made. Since the non-adiabaticity of the combustor is not considered, it is expected that the values of emissions might be over-predicted. However, the experimental trends have been validated with various swirling flame cases. Through heat loss implementation, one can expect a shift in NO_x values because of lower flame temperatures (non-adiabatic flame temperature).

1. In addition to the model validation, the reason for NO_x reduction due to oxidizer change was analyzed and the flame zone volume change was assessed.
    - The characteristic of the flame zone was described using the Borghi diagram. CO_2 in the oxidizer slowed down the kinetics and the flame zone spread out in space due to increase in chemical time scale. From being a reaction sheet of high Damkohler number for air, combustion in EGR was found to shift towards the well-stirred reaction zone due to the reduction in Damkohler number.
    - The reason for the reduction in NO_x was done by comparing the relative and absolute contribution of different pathways to NO_x in air and EGR. It was evident that thermal pathway, the major contributor of NO_x in air, was curtailed in EGR due to low oxygen in the oxidizer. Thermal NO_x was reduced by as much as 40%, leading to less overall NO_x.
2. Introducing different amounts of CO_2 in the oxidizer was studied in order to analyze the effect of EGR ratio on the emissions. It was found that for a given adiabatic flame temperature, NO_x levels diminished by 25-40% due to lower oxygen concentration in the oxidizer. On the other hand, CO levels escalated to as high as 50% when compared to that of air. Insufficient residence time, low oxygen and change of equilibrium favouring CO_2 dissociation were identified as the key reasons for elevated CO levels.
3. The effect of change in combustor pressure was studied for both air and EGR oxidizers
    - An increase in pressure increased the NO_x levels for both air and EGR. For a fixed flame temperature and pressure, EGR produced less NO_x than air. EGR was found to be more effective in NO_x reduction at higher pressures.
    - Beyond 1800 K, thermal pathway dominated in the NO_x production and was augmented by pressure rise. At lower temperatures, the N_2O mechanism dominated the NO_x formation and its magnitude increased due to higher third body collisions with pressure rise.
    - On the other hand, CO levels reduced on increasing the combustor pressure. Higher pressure suppressed the dissociation of CO_2 to CO. This proved that high pressure was beneficial in reducing CO emissions.
4. The influence of wet EGR was also studied in addition to dry EGR. The fundamental difference lied in the introduction of moisture in the oxidizer. Wet EGR had a stronger effect on NO_x reduction due to the combined kinetic effect of CO_2 and H_2O. The enhanced reduction in NO_x was attributed to the reduction in the prompt pathway. The NO_x reduction enhanced by 5-10%. The kinetic effect of H_2O dilution was found to be the reason for the excess CO formation besides inadequate residence time.
5. To mitigate the drop in combustion reactivity due to EGR, use of H_2 enriched natural gas was tested. The fuel compositions are chosen such that the laminar flame speed of pure natural gas-air mixture is maintained. On the emissions front, hydrogen injection raised the NO_x levels by 5-10% and the CO levels dropped by a maximum of 12.5%. CO level suppression was a clear indication of the augmented flame stability and was found to be achieved with a slight compromise on NO_x levels.
6. The impact of fuel-oxidizer unmixedness inside the combustor volume is implemented in the model through parallel reactors. The model is tested for two premixer efficiencies 92% and 95%. It is found that both NO_x and CO levels increased with decreasing premixer efficiency. Due to the variation of equivalence ratio, difference in temperature and concentration levels caused emissions escalation. It can be concluded that if the system is installed with a good premixer, lower NO_x and CO levels through EGR can be easily achieved.

6

Recommendations for future work

In this chapter, recommendations for future research are discussed.

6.1. Recommendation 1 : Heat Loss Implementation

The CRN model in this work comprised of an adiabatic PSR-PFR network. Heat loss to the environment was not considered. In reality, to mimic the real conditions in a combustor, heat loss can be implemented into the model. The heat losses are expected to have an effect on the emissions. The flame temperature achieved in reality is less than the equilibrium flame temperature. Including heat loss in the model can vary the local temperature levels and hence the NO_x emissions. When the convective and radiative heat losses are taken into account, the emission data is expected to shift to a lower flame temperature region, as per literature. Fractional heat loss can be established as a function of the equivalence ratio. A relation can be established between the steady state exit temperature of the model without heat loss and the experimental exhaust temperature. This implementation can certainly give extra insights on the emission prediction.

6.2. Recommendation 2 : CRN integration with cycle simulations

The output emission and temperature data can be coupled with existing thermodynamic cycle simulation of the gas turbine system. This combination can help in understanding the correlation between the performance of the combined system and the combustor output. The inlet conditions to the combustor is given from the cycle compressor exit data. CRN can be used as a post-processing step for cycle calculations.

6.3. Recommendation 3 : Hybrid CFD-CRN model

The model developed in this thesis is a stand-alone model based on overall mean flow field characteristics from previous experiments. In other research works, CFD results are used as inputs to develop the CRN model. The flow field is simplified on the whole, without considering the local turbulence effects. The best way to account for both the flow and chemical intricacies is to couple CFD and CRN approaches. The output data of CFD can be fed as model inputs to develop the CRN architecture. Based on the grid size and velocities computed, local Damkohler numbers can be computed and local zones can be modelled as PSRs. However, the integrating algorithm could compromise on the computational cost and time. It is highly recommended to implement this integration for accuracy improvement. However, this is done at the expense of large computational cost.

An intermediate approach to account for both the chemistry and flow effects can be through Flamelet Generated Manifold (FGM) technique. This is basically a reduction technique taking into account the important aspects of chemistry and flame structure and formulating lookup tables. The similarity between the chemical time scale approach in this work and FGM is that both make use of the laminar flame inputs for computations. In FGM, the turbulent flame is treated as an ensemble of laminar flamelets which remain undisturbed by turbulence. Instead of a complete combustion study, the number of variables are reduced based on steady state assumptions and flamelet models.

6.4. Recommendation 4: Modeling diffusion flames

Lean Premixed Combustion has been successfully modelled using CRN architecture in this thesis. However, in many practical applications, diffusion flames are used. This flame always burns at a stoichiometric flame front with spatial unmixedness. The effects of EGR on diffusion flames is highly recommended to be researched through CRN models. The modeling possesses some inherent challenges because of the lack of clarity on the equivalence ratio variation in the vicinity of the reaction zone. There have been few attempts in literature to model these flames, considering only the stoichiometric flame front. More accurate modeling approaches need to be developed for better emission prediction.

Bibliography

[1] *National Research Council of the National Academies, Climate Stabilization Targets: Emissions, concentrations and impacts over decades to millennia,* National Academies Press (2011).

[2] *Directive 2010/75/EU of the European parliament and of the Council,* European Union (2010).

[3] A. S. Brouwer, M. van den Broek, A. Seebregts, and A. Faaij, *Operational flexibility and economics of power plants in future low-carbon power systems,* in *Applied Energy*, Vol. 156 (2015) pp. 107–128.

[4] M.Persico, *Deep part load operation of combined cycles and combined heat and power plants*, Master's thesis, Delft University of Technology, Delft (2017).

[5] M. Utamura, S. Hoizumi, Y. Takeda, T. Sasaki, H. Komatsu, S. Kirikami, T. Suzumura, T. Sasada, T. Ikeguchi, and S. Sugita, *Exhaust recirculation type combined plant,* (1998), US Patent 5,794,431.

[6] A. H. Lefebvre and D. R.Ballal, *Gas Turbine Combustion: Alternative Fuels and Emissions*, 3rd ed. (CRC Press, Florida, 2010).

[7] P. E. Røkke and J. E. Hustad, *Exhaust gas recirculation in gas turbines for reduction of CO_2 emissions; combustion testing with focus on stability and emissions,* in *International Journal of Thermodynamics*, Vol. 5805 (2005) pp. 167–173.

[8] U. Ali, T. Best, K. N. Finney, C. F. Palma, K. J. Hughes, D. B. Ingham, and M. Pourkashanian, *Process simulation and thermodynamic analysis of a micro turbine with post-combustion CO2 capture and exhaust gas recirculation,* in *Energy Procedia 63* (2014) pp. 986–996.

[9] A. M. ElKady, A. Evulet, A. Brand, T. P. Ursin, and A. Lynghjem, *Exhaust gas recirculation in DLN F-Class Gas Turbines for post-combustion CO_2 capture,* in *Proceedings of ASME Turbo Expo 2008: Power for Land, Sea and Air* (2008) GT2008-51152.

[10] T. Griffin, D. Buecker, and A. Pfeffer, *Technology options for gas turbine power generation with reduced CO_2 emission,* in *ASME Journal of Engineering for Gas Turbines and Power* (2008) 130-041801.

[11] F. Guethe, D. Stankovic, F. Genin, K. Syed, and D. Winkler, *Flue gas recirculation of the ALSTOM sequential gas turbine combustor tested at high pressure,* in *Proceedings of ASME Turbo Expo* (2011).

[12] T. Poinsot and D. Veynante, *Theoretical and Numerical Combustion*, 2nd ed. (Edwards, Philadelphia,USA, 2005).

[13] B.Rosati, *Prediction of emissions from combustion systems using 0D and 1D reacting flow models :Chemical Reactor Network modeling*, Master's thesis, Delft University of Technology, Delft (2015).

[14] A. Stagni, A. Cuoci, A. Frassoldati, T. Faravelli, and E. Ranzi, *A fully coupled, parallel approach for the post-processing of CFD data through reactor network analysis,* in *Computers and Chemical Engineering*, Vol. 60 (2014) pp. 197–212.

[15] A. Lebedev, A. Secundov, A. Starik, N. Titova, and A. Schepin, *Modeling study of gas-turbine combustor emission,* in *Proceedings of the Combustion Institute*, Vol. 32 (2009) pp. 2941–2947.

[16] R. F. D. Monaghan, R. Tahir, A. Cuoci, G. Bourque, M. Füri, R. L. Gordon, T. Faravelli, A. Frassoldati, and H. J. Curran, *Detailed multi-dimensional study of pollutant formation in a methane diffusion flame,* in *Energy Fuels*, Vol. 26 (2012) pp. 1598–1611.

[17] V. Fichet, M. Kanniche, P. Plion, and O. Gicquel, *A reactor network model for predicting NOx emissions in gas turbines,* in *Fuel*, Vol. 89 (2010) pp. 2202–2210.

[18] R. Park, T. H. Nguyen, D. Joung, K. Y. Huh, and M. C. Lee, *Prediction of NOx and CO emissions from an industrial lean-premixed gas turbine combustor using a chemical reactor network model,* in *Energy Fuels*, Vol. 27 (2013) pp. 1643–1651.

[19] D. G. Goodwin, H. K. Moffat, and R. L. Speth, *Cantera: An object-oriented software toolkit for chemical kinetics, thermodynamics, and transport processes,* http://www.cantera.org (2016), version 2.2.1.

[20] R. J. Kee, F. M. Rupley, E. Meeks, and J. A. Miller, *Chemkin-iii: A fortran chemical kinetics package for the analysis of gas phase chemical and plasma kinetics," sandia national laboratories report,* (1996).

[21] J. Beer and N. Chigier, *Combustion Aerodynamics* (Applied Science Publishers Ltd., London, 1974).

[22] S. Klein, *Gas turbine combustion lecture,* (2015), TU Delft.

[23] S. S. Marashi, *Network Modeling Application to Laminar Flame Speed and NOx prediction in Industrial Gas Turbines*, Master's thesis, Linkoping University Institute of Technology, Linkoping (2013).

[24] G. Leonard and S. Correa, *NOx formation in premixed high-pressure lean methane flames,* in *Fossil Fuel Combustion Symposium*, Vol. 30 (1990) pp. 69–74.

[25] S. Woolford, *Laminar non-premixed flames – introduction, non-reacting jets, simplified description of laminar non- premixed flames Yi versus experimental,* (2015).

[26] A. Williams, *Flames - A-to-Z guide to thermodynamics, heat & mass transfer and fluids engineering : Thermopedia,* (2015).

[27] H. Li, A. M. ElKady, and A. T. Evulet, *Effect of exhaust gas recirculation on NOx formation in premixed combustion system,* in *AIAA Aerospace Sciences Meeting Including The New Horizons Forum and Aerospace Exposition (Orlando,Florida)*, Vol. 226 (2009).

[28] V. J. Lyons, *Fuel air non-uniformity effect on nitric oxide emissions,* in *19th Aerospace Sciences Meeting, American Institute of Aeronautics and Astronautics* (1981).

[29] D. Roekaerts and M. Huijts, *Turbulent Reacting Flows- Oral Exam Notes*, Report (TU Delft, 2015).

[30] P. E. Røkke, *Environmental use of Natural Gas in a Gas Turbine*, Ph.D. thesis, The Norwegian University of Science and Technology (2006).

[31] Y. B. Zeldovich, D. Frank-Kamenetskii, and P. Sadovnikov, *Oxidation of nitrogen in combustion,* in *Academy of Sciences of the USSR* (1947).

[32] C.P.Fenimore, *Formation of nitric oxide in premixed hydrocarbon flames,* in *13th Symposium (International) on Combustion, The Combustion Institute* (1971) p. 373.

[33] P.C.Malte and D.T.Pratt, *The role of energy-releasing kinetics in NOx formation: Fuel lean, jet-stirred CO-air combustion,* in *Combustion Science and Technology* (1974) pp. 221–231.

[34] J. W. Bozzellli and A. M. Dean, *O + NNH : A possible new route for NOx formation in flames,* in *International Journal of Chemical Kinetics*, Vol. 27 (1995) pp. 1097–1109.

[35] S. Correa, *A review of NOx formation under gas-turbine combustion conditions,* in *Combustion Science and Technology*, Vol. 87 (1992) pp. 329–362.

[36] D. Nicol, P. C. Malte, and R. C. Steele, *Simplified models for NOx production rates in lean-premixed combustion,* in *International Gas Turbine and Aeroengine Congress and Expo* (1994).

[37] P. Glaborg, J. Miller, and R.J.Kee, *Kinetic modeling and sensitivity analysis of nitrogen oxide formation in well-stirred reactors,* in *Combustion and Flame*, Vol. 65 (1986) pp. 177–202.

[38] P.V.Heberling, *"Prompt NO" Measurements at high pressures,* in *16th Symposium (Int'l.) on Combustion, The Combustion Institute* (1976).

[39] A. T. Kirkpatrick, *Chemical equilibrium - thermodynamics : Introduction,* Colarado State University.

[40] S. R. Turns, *An Introduction to Combustion - Concepts and Application*, 3rd ed. (McGraw-Hill, 2000).

[41] L. E. Bakken and L. Skogly, *Parametric Modeling of Exhaust Gas Emission from Natural Gas Fired Gas Turbines,* in *Journal of Engineering for Gas Turbines and Power*, Vol. 118 (1996) pp. 553–560.

[42] M.G.Talboom, *Chemical Kinetics Study of the Hybrid Combustion System*, Master's thesis, Delft University of Technology, Delft (2016).

[43] G. P. Smith, D. M. Golden, M. Frenklach, N. W. Moriarty, B. Eiteneer, M. Goldenberg, C. T. Bowman, R. K. Hanson, S. Song, W. C. G. Jr., V. V. Lissianski, and Z. Qin, *Gri-mech 3.0,* (2008).

[44] N. Peters, *Laminar flamelet concepts in turbulent combustion,* in *21st Symposium (International) on Combustion, The Combustion Institute* (1986) pp. 1231–1250.

[45] R. Bilger, *The structure of turbulent nonpremixed flames,* in *22nd Symposium (International) on Combustion, The Combustion Institute* (1988) pp. 475–488.

[46] C. Cloney, *Introduction to turbulent flame structures,* (2016), Dalhousie University in Nova Scotia.

[47] R. Borghi, *On the structure and morphology of premixed flames,* in *Recent Advances in the Aerospace Sciences* (1985) pp. 117–138.

[48] A. A. Konnov, *Development and validation of a detailed reaction mechanism for the combustion of small hydrocarbons,* in *Symposium (Interantional) on Combustion*, Vol. 28 (2000).

[49] K. B. Fackler, *A Study on pollutant formation from the lean premixed combustion of gaseous fuel alternatives to natural gas*, Ph.D. thesis, University of Washington (2011).

[50] C. Naik, K. Puduppakkam, A. Modak, E. Meeks, Y. Wang, Q. Feng, and T. Tsotsis, *Detailed chemical kinetic mechanism for surrogates of alternative jet fuels,* in *Combustion and Flame*, Vol. 158 (2011) pp. 434–445.

[51] E. Ranzi, A. Frassoldati, R. Grana, A. Cuoci, T. Faravelli, A. Kelley, and C. Law, *Hierarchical and comparative kinetic modeling of laminar flame speeds of hydrocarbon and oxygenated fuels,* in *Progress in Energy and Combustion Science*, Vol. 38 (2012) pp. 468–501.

[52] T. Faravelli, A.Frassoldati, and E. Ranzi, *Kinetic modeling of the interactions between NO and hydrocarbons in the oxidation of hydrocarbons at low temperatures,* in *Combustion and Flame*, Vol. 132 (2003) pp. 188–207.

[53] A. Frassoldati, T. Faravelli, and E. Ranzi, *Kinetic modeling of the interactions between no and hydrocarbons at high temperature,* in *Combustion and Flame*, Vol. 135 (2003) pp. 97–112.

[54] A. Cuoci, A. Frassoldati, T. Faravelli, and E. Ranzi, *Formation of soot and nitrogen oxides in unsteady counterflow diffusion flames,* in *Combustion and Flame*, Vol. 156 (2009) pp. 2010–2022.

[55] S. Bragg, *Application of reaction rate theory to combustion chamber analysis,* in *Aeronautical Research Council Pub*, Vol. 131 (1953) pp. 1629–1633.

[56] V. Iyer, J. Haynes, P. May, and A. Anand, *Evaluation of emissions performance of existing combustion technologies for syngas combustion,* in *Proceedings of ASME Turbo Expo 2005: Power for Land, Sea and Air* (2005) gT2005-68513.

[57] T. Rutar, J. Malte, and J. Kramlich, *Investigation of NOx and CO formation in lean-premixed methane/air, high intensity, confined flames at elevated pressures,* in *Proceedings of the Combustion Institute*, Vol. 28 (2000) pp. 2435–2441.

[58] K. Fackler, M. Karalus, I. Novosselov, J. Kramlich, and P. Malte, *Experimental and numerical study of NOx formation from the lean premixed combustion of CH_4 mixed with CO2 and N2,* in *ASME Journal of Engineering for Gas Turbines and Power* (2011).

[59] A. ElKady, J.Herbon, D. Kalitan, G.Leonard, R. Akula, H. Karim, and M. Hadley, *Gas turbine emission characteristics in perfectly premixed combustion,* in *ASME Journal of Engineering for Gas Turbines and Power*, Vol. 134 (2012).

[60] A. ElKady, A.Brand, C.L.Vandervort, and A.Evulet, *Exhaust gas recirculation performance in dry low emissions combustors,* in *Proceedings of ASME Turbo Expo 2011* (2011) GT2011-46482.

[61] A. T. Evulet, A. M. ElKady, A. R. Brand, and D. Chinn, *On the performance and operability of GE's dry low NOx combustors utilizing exhaust gas recirculation for post-combustion carbon capture,* (2009) pp. 3809–3816.

[62] M. Arai, *Flue gas recirculation for low NOx combustion system,* in *Proceedings of 2000 International Joint Power Generation Conference* (2000).

[63] O. Bolland and P. Mathieu, *Comparison of two CO_2 removal options in combined cycle power plants,* in *Energy Conversion and Management*, Vol. 6 (1998) pp. 1653–1663.

[64] M. Ditaranto, H. Li, and T. Løvas, *Concept of hydrogen fired gas turbine cycle with exhaust gas recirculation: Assessment of combustion and emissions performance,* in *International Journal of Greenhouse Gas Control* (2015) pp. 377–383.

[65] Z. Zhao, J. Li, A. Kazakov, S. P. Zeppieri, and F. L. Dryer, *Burning velocities and a high temperature skeletal kinetic model for n-decane,* in *Combustion Science and Technology* (2004).

[66] F. Liu, H. Guo, G. Smallwood, and O. Guelder, *The chemical effect of carbon dioxide as an additive in an ethylene diffusion flame,* in *Combustion and Flame*, Vol. 125 (2001) pp. 778–787.

[67] R. Cheng, D. Littlejohn, P. Strakey, and T. Sidwell, *Laboratory investigations of a low-swirl injector with H_2 and CH_4 at gas turbine conditions,* in *Proceedings of the Combustion Institute*, Vol. 32 (2009) pp. 3001–3009.

[68] T. Sidwell, G. Richards, K. Casleton, D. Straub, D. Maloney, P. Strakey, D. Ferguson, S. Beer, and S. Woodruf, *Optically accessible pressurized research combustor for computational fluid dynamics model validation,* in *AIAA Journal*, Vol. 44 (2006).

[69] U. Stopper, W. Meier, R. Sadanandan, M. Stohr, M. Aigner, and G. Bulat, *Experimental study of industrial gas turbine flames including quantification of pressure influence on flow field, fuel/air premixing and flame shape,* in *Combustion and Flame*, Vol. 160 (2013) pp. 2103–2118.

[70] U. Stopper, M. Aigner, W. Meier, R. Sadanandan, M. Stohr, and I. S. Kim, *Flow field and combustion characterization of premixed gas turbine flames by planar laser techniques,* in *Journal of Engineering for Gas Turbines and Power*, Vol. 131 (2009).

[71] U. Stopper, M. Aigner, H. Ax, W. Meier, R. Sadanandan, M. Stohr, and A. Bonaldo, *PIV, 2D-LIF and 1D-Raman measurements of flow field, composition and temperature in premixed gas turbine flames,* in *Experimental Thermal and Fluid Science*, Vol. 34 (2010).

[72] L. Wehr, W. Meier, P. Kune, and C. Hassa, *Single-pulse 1d laser raman scattering applied in a gas turbine model combustor at elevated pressure,* in *Combustion and Flame*, Vol. 31 (2007) pp. 3099–3106.

[73] P. Weigand, W. Meier, X. R. Duan, W. Stricker, and M. Aigner, *Investigations of swirl flames in a gas turbine model combustor i. flow field, structures, temperature, and species distributions,* in *Combustion and Flame*, Vol. 144 (2006) pp. 205–224.

[74] L. E. Bakken and L. Skogly, *The effect of swirl burner aerodynamics on NOx formation,* in *Symposium (International) on Combustion*, Vol. 18 (1981).

[75] G. Damkohler, *The effects of turbulence on the flame velocity in gas mixtures,* in *NACA TM 1112* (1947).

[76] H. Kobayashi, H. Hagiwara, H. Kaneko, and Y. Ogami, *Effects of CO_2 dilution on turbulent premixed flames at high pressure and high temperature,* in *Proceedings of the Combustion Institute*, Vol. 31 (2007).

[77] L. Wang, Z. Liu, S. Chen, C. Zheng, and J. Li, *Physical and chemical effects of CO_2 and H_2O additives on counterflow diffusion flame burning methane,* in *Energy and Fuels*, Vol. 27 (2013) pp. 7602–7611.

[78] T. L. Cong and P. Dagaut, *Experimental and detailed modeling study of the effect of water vapor on the kinetics of combustion of hydrogen and natural gas, impact on NOx,* in *Energy and Fuels*, Vol. 23 (2009) pp. 725–734.

[79] S. C. Li and F. A. Williams, *NO_x formation in two-stage methane–air flames,* in *COMBUSTION AND FLAME*, Vol. 118 (1999) pp. 399–414.

[80] D. Giles, S. Som, and S. K. Aggarwal, *NOx emission characteristics of counterflow syngas diffusion flames with airstream dilution,* in *Fuel*, Vol. 85 (2006) p. 1729–1742.

[81] D. Winkler, P. Muller, S. Reimer, T. Griffin, A. Burdet, J. Mantzaras, and Y. Ghermay, *Improvement of gas turbine combustion reactivity under flue gas recirculation condition with in-situ hydrogen addition,* in *ASME Turbo Expo 2009: Power for Land, Sea and Air* (2009).

[82] H. Guo, G. J. Smallwood, F. Liu, Y. Ju, and O. L. Gulder, *The effect of hydrogen addition on flammability limit and NOx emission in ultra-lean counterflow CH4/air premixed flames,* in *Proceedings of the Combustion Institute*, Vol. 30 (2005) pp. 303–311.

[83] J. Ballester, R. Hernandez, A. Sanz, A. Smolarz, J. Barroso, and A. Pina, *Chemiluminescence monitoring in premixed flames of natural gas and its blends with hydrogen,* in *Proceedings of the Combustion Institute*, Vol. 32 (2009) pp. 2983–2991.

[84] R. W. Schefer, D. M. Wicksall, and A. K. Agrawal, *Combustion of hydrogen-enriched methane in a lean premixed swirl-stabilized burner,* in *Proceedings of the Combustion Institute*, Vol. 29 (2002) pp. 843–851.

[85] U. of Toronto Institute for Aerospace Studies, *Laminar premixed flames,* .

[86] L. E. Bakken and L. Skogly, *Investigation of Lean Premixed Swirl-stabilized Hydrogen Burner with Axial air injection using OH-PLIF imaging,* in *Journal of Engineering for Gas Turbines and Power*, Vol. 137 (2015).

A

Experimental Setup for model validation

A.1. Elkady et al. (2008,2009)

Researchers from GE Global Research built a Dry Low NO_x (DLN) premixer combustor test rig at representative gas turbine pressure and temperature, to study the effect of EGR on the NO_x and CO emissions. In addition, tests on flame stability and combustion dynamics were studied to analyze the benefits and downfalls of introducing EGR [9, 60].

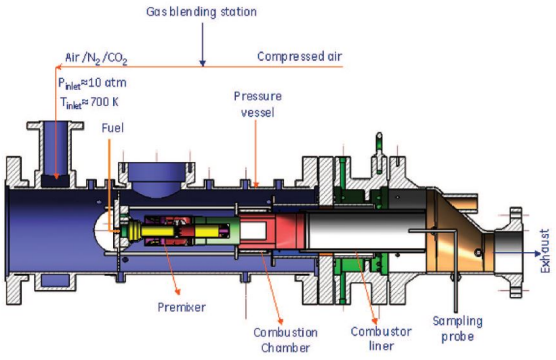

Figure A.1: DLN Combustor Test Rig of GE [9]

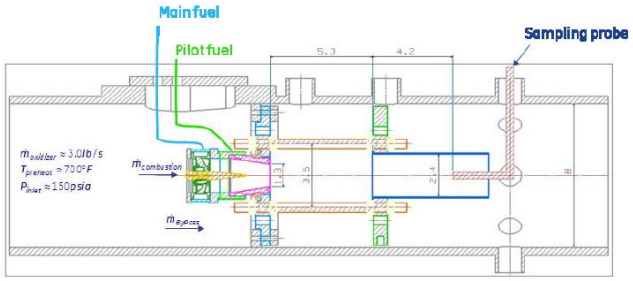

Figure A.2: Combustor Dimensions in British Units [60]

Figure A.1 shows the experimental test rig. The research nozzle is modified from a F-class gas turbine combustor. The setup has the ability to be operated in fully-premixed, partially premixed and diffusion modes of combustion. It contains a pressure vessel with a liner which represents the combustion chamber. The premixer is a plenum present upstream of the combustor, where premixing

of natural gas fuel and pre-heated oxidizer takes place. In order to mimic the EGR conditions, inerts such as CO_2 is blended with air in a gas blending station before entering the premixing chamber. The whole operation was tested for "Dry-EGR" where H_2O is condensed out of the exhaust before mixing with the inlet air. Additionally, the effect of minor species has not been studied in this experiment. The inlet air is preheated to a temperature of 700 K and pressurized at 10 atm.

Parameter	Value
Inlet Pressure	10 atm
Inlet Temperature	700 K
Total Mass flow of oxidizer	1.4 kg/s
Dimensions of Combustor (L ×B ×H)	12.2 ×2.4 ×2.4 $inch^3$

Table A.1: Experimental Conditions of Elkady et al. [9, 60]

From figure A.2, it is seen that the oxidizer flow is split into two streams, one of which goes into the combustor and other for bypass cooling. Since the authors have not mentioned the splitting ratio used, residence time data from Li et al. [27] was used to get an estimate of the mass flow getting into the combustor. An average overall residence time of 26 ms was used for their chemical simulations of the mentioned experimental setup. Hence, a reverse calculation using the following correlation, gave an estimate of the splitting ratio.

$$\dot{m}_{combustion} = \frac{\rho_{burned} V_{comb}}{\tau_{residence}} \tag{A.1}$$

Using Cantera [19], the equilibrium density of the burnt products at the adiabatic flame temperature was estimated at constant enthalpy and pressure, for different equivalence ratios. ρ_{burned} was in the order of 2 kg/m^3, volume is calculated to be 1.15 $\times 10^{-3} m^3$ and residence time was taken as 26 ms. Hence, a splitting ratio of around 10 % of the total oxidizer mass flow was the estimated value. However, this splitting ratio is different for various EGR ratios. This is done in order to account for the extra mass flow entering the combustor and maintaining the overall residence time. In these experiments, a small amount of pilot fuel flow was added to the premixed mixture to reduce the LBO limit.

The fuel-oxidizer mixture is imparted with a swirl through a double annular counter rotating swirler (DACRS). This enhances mixing and increases the premixer efficiency. In order to switch between the premixed and pilot modes, independent fuel supply systems are present. A sampling probe is present at the end of the combustor liner, which is used to analyze the exhaust emissions. To compare the NO_x emissions between air and EGR, comparison was made at the same flame temperature. This was done to eliminate the dependence of flame temperature on the EGR ratio. Hence, same flame temperatures were obtained by changing the mass flow of the fuel.

A.1.1. Fully Premixed Vs Partially Premixed

A partially premixed flame is an hybrid of premixed and non-premixed combustion, in which a rich pilot flame anchors the lean premixed regime. The purpose of using a pilot flame is to augment the flame stability and reduce the Lean Blowout (LBO) of the flame. It was observed and reported by Elkady et al. [60] that introducing a pilot flame in the experiment did not change the emissions, but only lead to spreading of the flame front. Citing the difficulties in modeling the pilot flame in Cantera and considering that there are no substantial differences in emissions on introducing pilot flames, the model in this work has been built without a pilot flame. Hence, the combustion process has been considered to be in fully premixed mode of operation.

A.2. Cheng et al. (2009) and Sidwell et al. (2005)

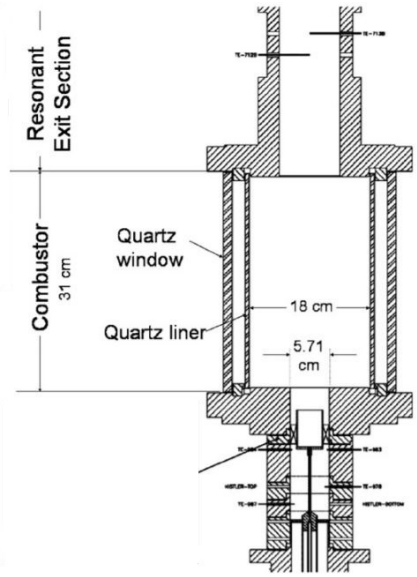

Figure A.3: Simval Combustor used in NETL [67, 68]

Sidwell et al. [68] and Cheng et al. [67] studied lean premixed methane-air flames and hydrogen enriched methane air flames using the combustor setup used at the National Energy Technology Laboratory. The test rig is shown in figure A.3. It is attached with a Low Swirl Injector (LSI) for the swirl stabilized flame. The combustor is 31.8 cm long and has an innder diameter of 18 cm. The injector diameter is 5.71 cm, which is a direct representation of can-type combustors. Optical access is provided to observe the behaviour of the flame. Cheng et al. [67] performed experiments between 4 to 10 atm and Sidwell et al. [68] at 4.3 and 6.3 bar. Preheat tempertaure range between 500-600 K was utilized for the experiments.

B

Investigation of LBO limits with CO_2 content

B.1. Study 4: Lean Blow Out (LBO) and Flame Stability

When compared to air, CO_2 in the oxidizer reduces NO_x and increases CO at the same adiabatic flame temperature. In addition, it can also reduce the reaction kinetics leading to slower rates of reaction. As a result, flame stability issues can arise, affecting the operation of the gas turbine. Two important parameters that are indicators of flame stability are LBO limit and laminar flame speed. LBO is defined as the equivalence ratio at which the flame does not ignite anymore.

The increase in CO with oxygen depletion by CO_2, for a given residence time is also an indicator of reduced combustion reactivity. In order to perform this analysis on the model, the mass flow of the fuel was fixed and the oxidizer mass flow was reduced in steps from equivalence ratio 1 to 0.1.

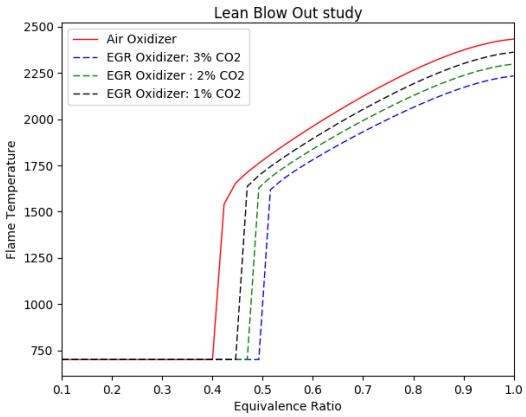

Figure B.1: Tracking ϕ_{LBO} for different oxidizer compositions

From figure B.1, it can be seen that in order to obtain the same flame temperature, more amount of fuel has to be injected with increasing CO_2 in the oxidizer. This can be explained by the combustor heat balance equation,

$$\dot{m}_f \times LHV = \dot{m} C_p \Delta T \tag{B.1}$$

Addition of CO_2 increases the heat capacity of the working fluid, leading to extra fuel to obtain the same flame temperature. Even though the oxidizer is O_2 depleted, extra O_2 is produced from the dissociation of CO_2 in the oxidizer. Around an equivalence ratio of 0.4 to 0.5, the mixture fails to ignite. This is indicated by the sudden drop in temperature and the corresponding equivalence ratio is the LBO limit of the mixture.

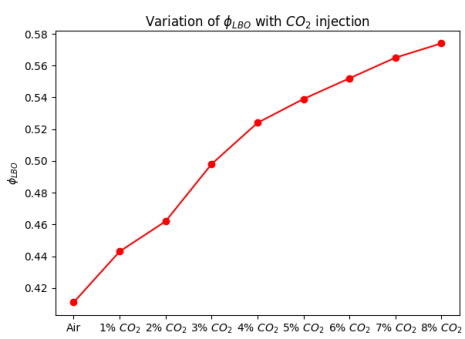

(a) ϕ_{LBO} with CO_2 injection in the oxidizer

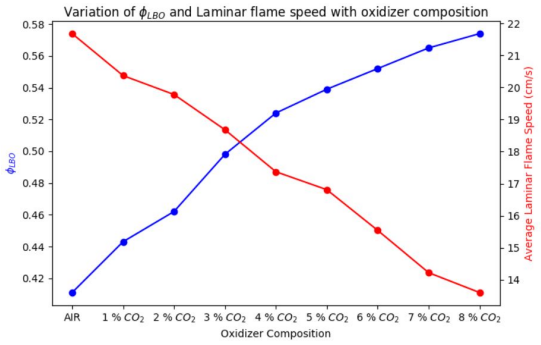

(b) Flame stability with CO_2 injection

Figure B.2: NO_x and CO levels at T_{flame}= 1900 K with change in oxidizer composition

Figure B.2a shows a clear increase in ϕ_{LBO} with increasing CO_2 concentration in the oxidizer. Higher value of LBO indicates narrow flammability limits. This means the flame operating in EGR environment is bound to extinguish earlier than in air. The rise in LBO limits can be explained by the reduction of laminar flame speed. A flame must possess a threshold speed value to sustain the reactions. If the flame speed reduces beyond a certain point, the flame is not stable anymore. Simultaneous reduction in flame speed with increase in LBO is presented in figure B.2b.

Flame stability is sometimes used interchangeably with the term called combustion reactivity [11]. The laminar speed is indeed the first order indicator of the combustion reactivity. Reduced laminar flame speed implies, reduced combustion reactivity or flame stability.

B.2. LBO reduction in Hydrogen enriched flames

A clear increase in laminar flame speed with addition of H_2 for a given oxidizer composition is seen in figure 4.31. This is due to increased reactivity by virtue of H_2 injection. However, the effect of oxidizer composition seems to have a stronger influence than the fuel blending change. For a fixed fuel composition, addition of CO_2 reduces the flame speed, corroborating the influence of CO_2 over H_2.

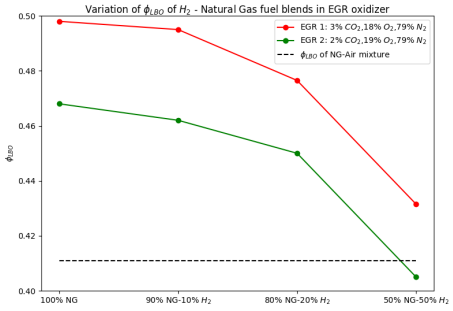

Figure B.3: H_2 injection: Change of LBO

Figure B.3 displays the reduction of LBO with increase in H_2 concentration in the fuel, for different EGR oxidizers. The increase in blending ratio shifts the LBO closer to that of air. This provides evidence that H_2 addition can widen the flame stability due to augmented reaction rates.

C

PFR Model in Cantera

The Plug Flow Reactor can basically be modelled by two ways namely,

- **Flowreactor( ) module:** Cantera has a built in module to simulate a steady state plug flow reactor with a fixed cross sectional area. Time integration is done along the length of the reactor, which is part of this module. However, Reservoirs, valves and flow controllers cannot be used in this module. This cannot ensure the prevention of pressure loss and would violate the assumption of 100% combustion efficiency.
- **Series of PSRs:** In a PFR, it is assumed that there is only radial diffusion and no axial diffusion. Based on this assumption, the PFR volume can be discretized spatially as a series of PSRs and integrated individually. It takes into account the non-interaction between the axially displaced fluid elements. The output of one PSR is fed as the input of the next one, until the end of the PFR length. This has been proven to be quicker in producing results and hence been used in this thesis.

C.1. Number of PSR in series

To spatially discretize the PFR, it is split as a series of PSRs as shown in figC.1. The number of PSRs to be used for this purpose is a parameter by itself. A total of 1000 PSRs were used for discretization and integration. In the thesis of Rosati [13], the CRN model was calibrated for 1000 reactors and produced good results.

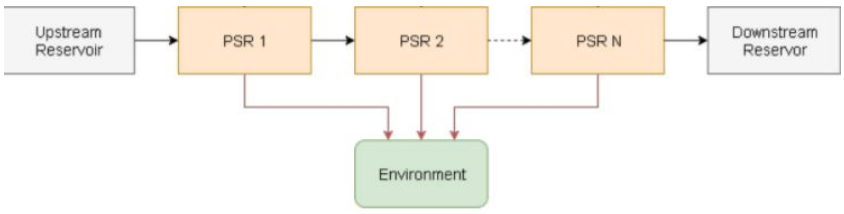

Figure C.1: PFR as a series of PSRs [42]

D

Premixed Flames

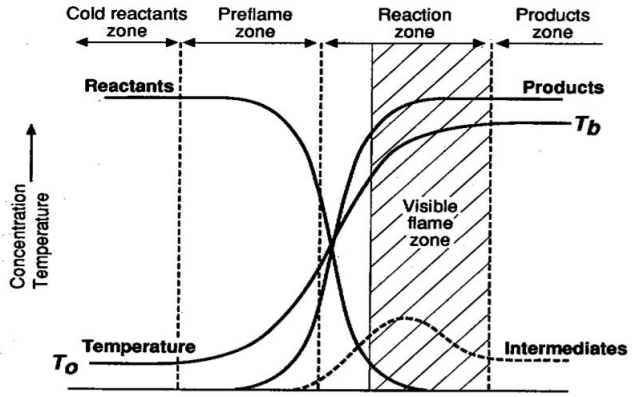

Figure D.1: Zones in a laminar premixed flame [85]

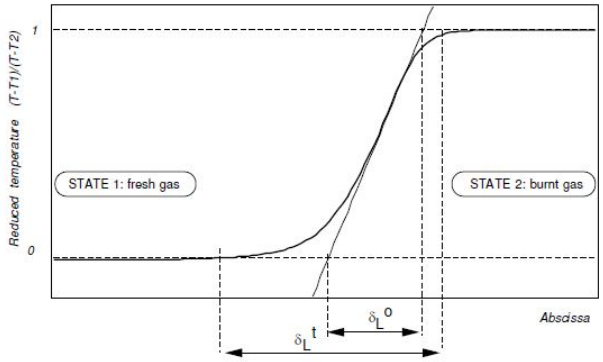

Figure D.2: Laminar premixed flame thickness [12]

As already explained, when fuel-oxidizer mixing takes place upstream of the combustor, then the flame is called a premixed flame. Depending on the flow velocities, the flames can either be laminar premixed or turbulent premixed flames. Figure D.1 shows the different zones in a laminar premixed flame. The reactants entering the combustor gets preheated by the burnt products through conduction and counter diffusion. After the preheat zone, there is a thin reaction zone in which the reactants turn into the burnt gases rapidly. Then comes the products zone, responsible for the temperature gradient between the upstream and downstream direction leading to conductive heat transfer. Figure E.1 shows a schematic representation of the temperature rise during the transition of reactants to

products in a laminar premixed flame.

The thickness of the reaction zone is basically assumed to be the laminar flame thickness δ_L. The speed at which the flame self-propagates through its own thickness is called the laminar flame speed s_L. This quantity is of high importance in combustion science, as it represents the rate of chemical reactions happening in the flame zone along with the mixing domain. Laminar flame speed decreases with the changes in the following quantities,

- Pressure increase
- Reactant temperature decrease

The dependence of s_L on equivalence ratio is similar to that of adiabatic flame temperature. It increases up to $\phi = 1$ and then starts decreasing.

The transport equations involved for these premixed flames are as follows,

Mass Conservation

$$\frac{\partial \rho}{\partial t} + \frac{\partial \rho u}{\partial x} = 0 \tag{D.1}$$

Momentum and species Conservation

$$\frac{\partial (\rho Y_k)}{\partial t} + \frac{\partial (\rho (u + V_k) Y_k)}{\partial x} = \dot{\omega}_k \tag{D.2}$$

Energy Conservation

$$\underbrace{\rho C_p \frac{\mathrm{D}T}{\mathrm{D}t}}_{Convection\ Term} = \underbrace{\dot{\omega}_t}_{Source\ Term} + \overbrace{\frac{\partial (k \frac{\partial T}{\partial x})}{\partial x}}^{Conduction\ Term} \underbrace{- \rho \frac{\partial T}{\partial x} (\sum_{1}^{N} (C_{p,k} Y_k V_k))}_{Species\ Diffusion} \tag{D.3}$$

where Y_k is the mass fraction of species k, u is the bulk flow velocity, V_k is the diffusion velocity and $\dot{\omega}_k$ is the chemical source term of species k which is determined from the reaction rate and Arrehenius law. The above set of equations are closed by estimating V_k (diffusion velocity) using Fick's law of diffusion. With the aforementioned equations and relevant boundary conditions (u(x=0) = u1 and T(x=0) = T1), the problem is well posed and can be defined as a non-linear boundary value problem [12].

Newton's method with minor modifications are used to solve the equations. In Cantera, the convective terms are discretized by upwind differencing and the diffusive terms are discretized by central differencing. Also an adaptive grid size is taken at each iteration, depending on the gradient between the previous and the current time step.

E

Premixer Modeling

Since the thesis deals with lean premixed combustion, the fuel-oxidizer mixture is modelled in two different ways, namely :

- **set.equivalence.ratio() method :** Cantera has the set.equivalence.ratio() module in which the fuel composition, oxidizer composition and the equivalence ratio are given as inputs. The module outputs the mixture properties such as density, heat capacity along with the composition data.
- **Ideal gas reactor :** The premixer can also be modelled as an ideal gas reactor. The oxidizer mass flow is chosen from the experiments and the fuel flow is calculated from correlations, explained in the succeeding paragraphs. This method is more versatile than the previous method and can be used for a range of mass flow rates.

E.1. Premixer reactor modeling

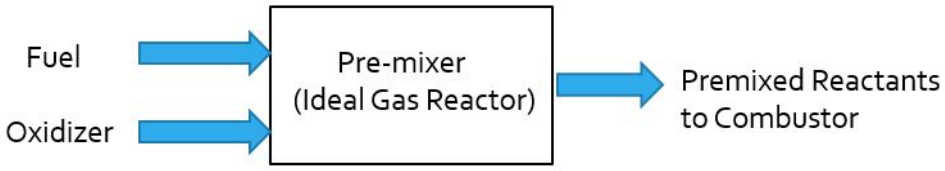

Figure E.1: Premixer modelled as an ideal gas reactor

For given equivalence ratio ϕ, both the fuel and oxidizer in the mixture possess a mass fraction. The global equation is given by,

$$\nu_F F + \nu_O O -> PRODUCTS \tag{E.1}$$

Where ν is the stoichiometric coefficient, F and O are the fuel and oxidizer respectively. The mass stoichiometric ratio 's' is calculated from the above equation as,

$$s = \frac{\nu_O W_O}{\nu_F W_F} \tag{E.2}$$

From the definition of equivalence ratio,

$$\phi = \frac{\left(\frac{Y_F}{Y_O}\right)}{\left(\frac{Y_F}{Y_O}\right)_{st}} = s\frac{Y_F}{Y_O} \tag{E.3}$$

So for a given fuel and oxidizer composition and molar mass W, the mass fraction of the fuel and oxidizer can be computed.

$$Y_{oxidizer} = \frac{1}{1 + \frac{\phi}{s} + \frac{\alpha W_{N_2}}{W_{O_2}} + \frac{\beta W_{CO_2}}{W_{O_2}}} \tag{E.4a}$$

$$Y_{fuel} = \frac{\phi Y_{oxidizer}}{s} \tag{E.4b}$$

$$\dot{m}_{fuel} = \frac{Y_{fuel}}{1 - Y_{fuel}} \dot{m}_{oxidizer} \tag{E.4c}$$

In few of the parametric studies such as flame stability and LBO, the set.equivalence.ratio() module has been utilized. This is because the mass flow was not needed to be defined and the equivalence ratio was directly declared as an array. But for all other cases for generating NO_x and CO curves, the premixer has been modelled as an ideal gas reactor. The output data is fed as the input to the flame reactor.

F

Reactor pre-processing

The methodology followed to determine the flame reactor volume was described in section 3.4. Transport properties such as thermal conductivity k, density ρ, heat capacity C_p and laminar flame speed s_L has to be given as input to compute the chemical time scale. Using the obtained data for a series of equivalence ratios, these values were pre-processed to establish the flame volume factor (FVF) and recirculation volume factor (RVF) as a function of ϕ. The pre-processing was done in MS-Excel and the obtained curve was curve fitted to obtain a function. The sample table is described in table F.1.

ϕ	k	C_p	ρ_u	ρ_{PSR}	s_L	ρ_{avg}	T_{chem}	V_{PSR}	FVF
0.5	0.053919	1148.205	5.049	1.943	0.1117	3.496	1.076	6.202	5.38
0.51	0.053963	1149.476	5.047	1.922	0.1192	3.485	0.948	5.523	5.32
0.52	0.054007	1150.746	5.045	1.903	0.1269	3.474	0.838	4.931	5.28
0.53	0.054052	1152.014	5.043	1.883	0.135	3.463	0.743	4.419	5.25
0.54	0.054096	1153.281	5.041	1.865	0.143	3.453	0.66	3.964	5.22
0.55	0.054139	1154.547	5.039	1.847	0.152	3.443	0.589	3.569	5.19
0.56	0.054183	1155.811	5.038	1.829	0.161	3.424	0.526	3.222	5.16
0.57	0.054227	1157.075	5.036	1.812	0.170	3.414	0.472	2.916	5.13
0.58	0.054271	1158.336	5.034	1.795	0.179	3.405	0.424	2.647	5.099
0.59	0.054314	1159.597	5.032	1.778	0.189	3.396	0.383	2.411	5.07
0.60	0.054358	1160.856	5.030	1.763	0.199	3.388	0.346	2.200	5.05

Table F.1: Pre-processing data for finding out FVF for the model

Using the above data, the functions,defined as polynomial or power equations, are described as the model inputs. A sample curve for the flame volume reactor is shown below,

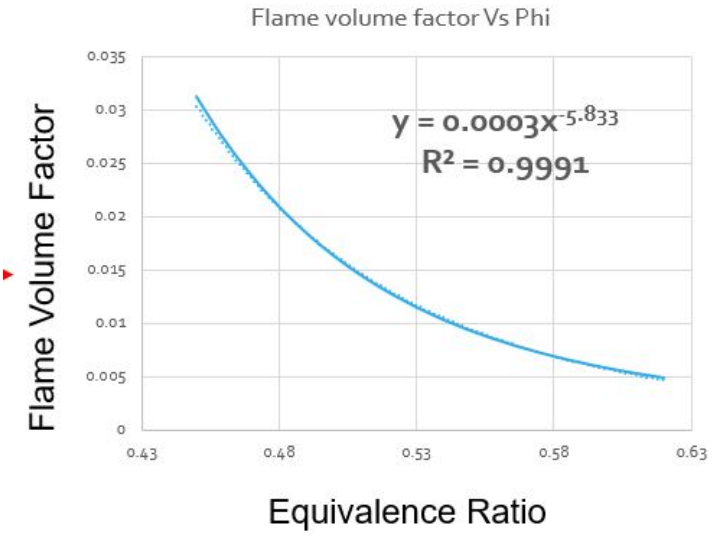

Figure F.1: Flame Volume Factor as a function of equivalence ratio

It can be observed that the FVF reduces with increase in equivalence ratio or flame temperature. This means that at higher flame temperatures, the flame zone becomes narrower and burns without substantial downstream travel. The laminar flame speed correspondingly increase, meaning faster reactions in a shorter volume.

F.1. Recirculation zone length based on momentum ratio

Fuel-Air Momentum ratio: The flame front is defined as a combination of main flame and recirculating zone, in previous investigations on swirl stabilized burners [13, 42**?**]. The flame front position x_F, can be correlated to the momentum ratio of the fuel flow and air flow. The definition of momentum ratio J is shown in equation F.1. When J <= 2 for a fixed inlet flow velocity, the position of the flame front is almost constant and a linear increase is seen for J > 2 as shown in figure F.2a [86].

$$J = \frac{\rho_{fuel} u_{fuel}^2}{\rho_{air} u_{air}^2} \tag{F.1}$$

The dashed lines figure F.2a indicate the variation of the normalized flame front position for methane, at a fixed inlet velocity. From figure F.2b, it can be seen that for a fixed inlet flow velocity, the position of the flame front reduces slightly with increase in equivalence ratio. Hence, the recirculation zone length decreases with higher equivalence ratios.

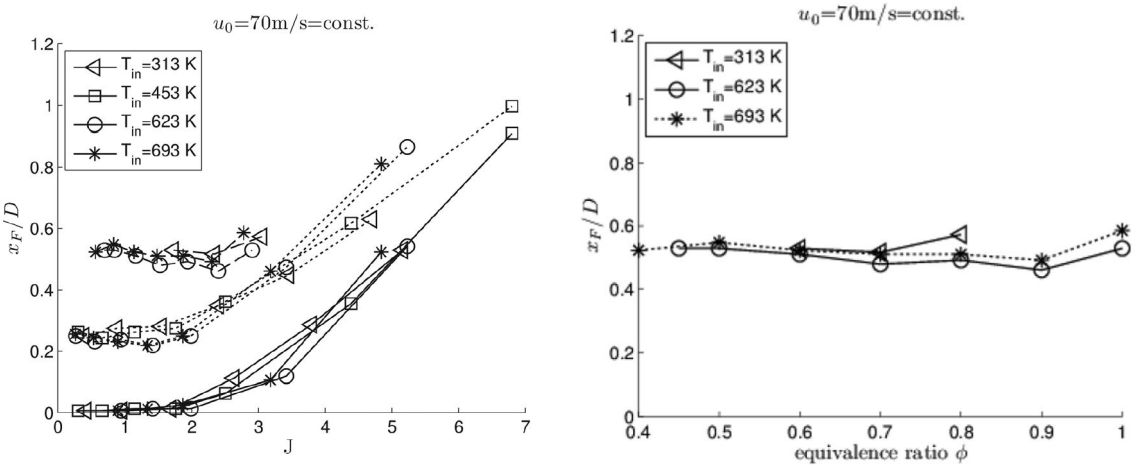

(a) Variation of x_f with J [86]

(b) Variation of x_f with ϕ [86]

Figure F.2: Variation of recirculation zone length x_F with momentum ratio J and equivalence ratio ϕ (P = 1 bar)

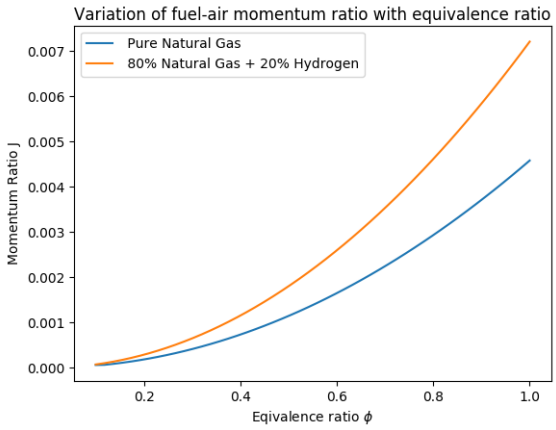

Figure F.3: Variation of momentum ratio J for natural gas- air and 80-20 NG H_2-air with equivalence ratio at P = 10 bar; It is seen that for both cases, J is less than 2 indicating a near-constant recirculation zone length

F.2. Spatial variation of NO_x

The distribution of NO_x between the PSR and PFR at two different flame temperatures is shown in figure F.4. At 1700 K, around 80% of the total NO_x is formed in the PSR zone. Very less spatial variation of NO_x occurs in the PFR zone. This is highlighted in figure F.4a. Lower peak temperature and larger flame zone volume increases the residence time in the flame vector. As the NO_x increases with local residence time, majority of the NO_x is in the PSR zone.

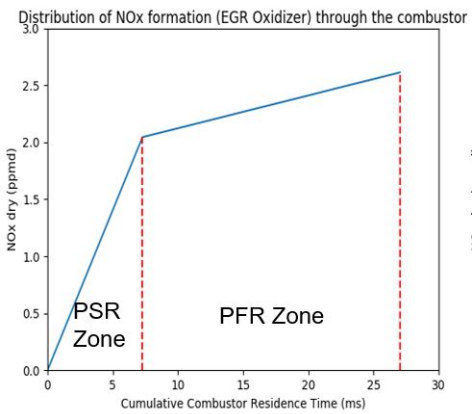

(a) T= 1700 K : NO_x distribution

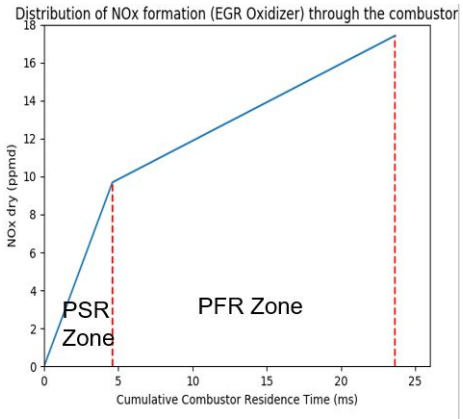

(b) T= 1850 K : NO_x distribution

Figure F.4: Spatial variation of NO_x at 10 bar

On the other hand, at a high flame temperature of 1850 K, the PSR-PFR NO_x split changes to 55%-45% from 80%-20%. The amount of NO_x formed in the post-recirculation region is significant as shown in figure F.4b. As a result of higher peak temperature inside the control volume, the reactivity and flame speed is higher. This leads to enhanced NO_x formation further downstream as well.